

**ANOMALOUS BEHAVIOUR  
OF MOLYBDENUM IN STEEL WELDS**

**Habib Ullah Choudhary  
Churchill College  
Cambridge**

**A dissertation submitted for the degree of  
Doctor of Philosophy  
at the University of Cambridge**

**September 1993**

Dedicated to my parents, my wife, and my children Shiraz and Faraz

---

## PREFACE

This dissertation is submitted for the degree of Doctor of Philosophy at the University of Cambridge. It contains an account of research carried out at the Department of Materials Science and Metallurgy, University of Cambridge between October 1990 to September 1993, under the supervision of Dr. H. K. D. H. Bhadeshia. Except where appropriately referenced, this work is entirely original and is not the result of collaboration and has not been submitted in whole or in part for a degree, diploma or other qualifications at this, or any other, University. This dissertation contains less than 60,000 words.



Habib Ullah Choudhary

September, 1993

## ACKNOWLEDGEMENTS

First of all I express my sincere gratitude to my supervisor, Dr. H. K. D. H. Bhadeshia for his encouragement and enthusiasm during the course of this research work. I wish to thank Professor C. J. Humphreys for the provision of laboratory facilities at the University of Cambridge. Thanks are also extended to the Cambridge Commonwealth Trust, Dr. Wali Mohammad Trust, ESAB AB (Sweden), NEI Parsons and Churchill College for the financial support.

I thank Dr. A. L. Greer for his valuable guidance concerning my research work. I also express my thanks to Dr. L. -E. Svensson of ESAB (Sweden), Dr. G. M. Evans of OERLIKON (Switzerland), Dr. G. Rees, Prof. J. R. Yang, Dr. H. Murakami and members of P. T. Group, Ashraf, Shafiq, Suresh, Hiroshi, Susumu, Kazuaki, Julia, Nikki, Marty, Akihiro, Rachel, Shahriar, Chang, Chou, Howard, Akira, Kouichi, Shinichi, Hsuing, Wei, Phil, Shikila and Atique for creating a very good and encouraging research environment. It gives me great pleasure to acknowledge my friends, Masood, Aslam, Zafar, Arshad, Humayun, Shahid, Anwar, Zahid, Mujahid, Shahab and many others for making my stay at Cambridge memorable one. In addition I would like to thank Abdul Majeed, Dr. Zafar ullah, Jan Nasar, Dr. M. Asif, Masroor Ahmad, Zaheer Ahmad, Arshad Ali, Khalid Butt, Kaleem Anwar, Javid Khan for encouraging me to study at Cambridge.

I greatly acknowledge my wife, Nurgis, for her moral support during the period of my research. I am thankful to my brothers, sisters and especially my parents for their prayers for my success. Finally I acknowledge my sons Shiraz and Faraz for their unfailing support.

## ABSTRACT

The addition of molybdenum to steel welds in quite small concentrations leads to a variety of anomalous microstructural and mechanical property effects. In some cases, the effects manifest even when there are no obvious changes in microstructure at the resolution of a transmission electron microscope. There are two particular discrepancies. A quantitative analysis of molybdenum-containing steel welds indicates that there is a degree of strengthening which cannot be explained by the known solid solution or microstructural effects of molybdenum in steels. Secondly, in multirun welds, the addition of molybdenum appears to make the microstructure which evolves during solidification (*the primary microstructure*) extremely stable. These and other associated phenomena are examined in this thesis.

The molybdenum effects mentioned above have been reproduced in detail, using a series of 'high-purity' multirun welds. Having confirmed that molybdenum increases the fraction of primary microstructure in such welds, an attempt was made to see whether the effect is attributable to a change in the austenitisation characteristics with alloying additions. Extensive work using dilatometric techniques backed by microscopy analysis has demonstrated that molybdenum does not lead to any substantial or unexpected changes in the ability to form austenite. The second hypothesis, that the primary microstructure is stabilised as molybdenum increases the tempering resistance, is proven and provides a good explanation of the observations.

A series of tempering experiments have established that the anomalously high strength of the molybdenum containing welds cannot be attributed to solid solution strengthening or microstructural effects. Indeed, it appears that there is a sub-microscopic secondary hardening type effect which enhances the strength. Even the thermal treatment that occurs as the weld cools from the solidification temperature is shown to be sufficient to induce molybdenum based secondary hardening type effects. Some preliminary atomic resolution effects also lend support to this concept.

Titanium as a trace element is important in steel welds, as an element which promotes the intragranular nucleation of acicular ferrite on titanium-rich phases. It is

demonstrated that the titanium effect is not intrinsically different for molybdenum-containing welds. However, the extra hardenability associated with molybdenum certainly helps to suppress the formation of other grain boundary nucleated phases which might swamp events that occur on the inclusions within the grains. An interesting observation is that titanium has a positive effect in limiting the grain boundary nucleated phases, because the intragranularly nucleated acicular ferrite to some extent stifles the formation of other phases.

# CONTENTS

Preface .....	i
Acknowledgements .....	ii
Abstract .....	iii
Contents .....	v
Nomenclature and Abbreviations .....	ix
<b>Chapter 1: General Introduction .....</b>	<b>1</b>
1.1 Introduction .....	1
1.2 Molybdenum–Chromium Steels .....	2
<i>1.2.1 The Effect of Molybdenum on Weld Metal .....</i>	<i>3</i>
1.3 The Heat Affected Zone .....	4
1.4 Transformation Products from Austenite .....	5
<i>1.4.1 Reconstructive Transformation .....</i>	<i>5</i>
<i>1.4.2 Allotriomorphic Ferrite .....</i>	<i>5</i>
<i>1.4.3 Displacive Transformation .....</i>	<i>6</i>
<i>1.4.4 Widmanstätten Ferrite .....</i>	<i>7</i>
<i>1.4.6 Bainite .....</i>	<i>8</i>
<i>1.4.5 Acicular Ferrite Formation .....</i>	<i>9</i>
<i>1.4.6 Martensite .....</i>	<i>9</i>
1.5 Tempering of Martensite .....	10
<i>1.5.1 Secondary Hardening and Precipitation of Alloy Carbides .....</i>	<i>10</i>
1.6 Time–Temperature Transformation (TTT) Diagrams .....	11
1.7 Austenite Formation .....	11
<i>1.7.1 Effect of Initial Microstructure and Heating Rate .....</i>	<i>12</i>
1.8 Summary .....	13

<b>Chapter 2: Experimental Techniques</b> .....	21
2.1 Introduction .....	21
2.2 Materials .....	21
2.3 Heat Treatment .....	21
2.4 Chemical Composition .....	22
2.5 Dilatometry .....	22
2.6 Thermomechanical Simulator .....	23
2.7 Differential Scanning Calorimetry (DSC) .....	24
2.8 Optical Microscopy .....	24
2.9 Scanning Electron Microscopy (SEM) .....	24
2.10 Transmission Electron Microscopy (TEM) .....	24
2.11 Carbon Replicas .....	25
2.12 Energy Dispersive X-ray Spectroscopy (EDXS) .....	25
2.13 Hardness Testing .....	25
2.14 Thermodynamic Calculations .....	25
<b>Chapter 3: The Effect of Molybdenum on the Microstructure of Steel Welds</b> .....	28
3.1 Introduction .....	28
3.2 Experimental Procedure .....	28
3.3 Results and Discussion .....	29
<i>3.3.1 Calculation of Phase Diagrams and TTT Curves</i> .....	29
<i>3.3.2 Thermodynamic Calculations</i> .....	30
<i>3.3.3 Measurements of the Primary Microstructure</i> .....	30
<i>3.3.4 Calculation of Microstructural Constituents</i> .....	31
<i>3.3.5 Microstructure of As-deposited Weld Metal</i> .....	32
<i>3.3.6 Microstructure of the Reheated Weld Metal</i> .....	33
<i>3.3.7 Hardness Testing</i> .....	34
3.4 Summary and Conclusions .....	35

<b>Chapter 4: The Effect of Molybdenum on the Austenitization Behaviour of Steel Welds</b> .....	52
4.1 Introduction .....	52
4.2 Experimental Procedure .....	54
4.3 Results and Discussion .....	54
4.4 Summary and Conclusions .....	59
<b>Chapter 5: The Excess Strength and Tempering Resistance of Molybdenum-Containing Steel Welds</b> .....	66
5.1 Introduction .....	66
5.2 Experimental Procedure .....	67
5.3 Results and Discussion .....	68
5.3.1 <i>Microstructural Changes</i> .....	68
5.3.2 <i>Microanalysis</i> .....	69
5.3.3 <i>Macrohardness Measurements</i> .....	69
5.3.4 <i>Kinetic Strength</i> .....	70
5.4 Summary and Conclusions .....	72
<b>Chapter 6: AN ATOM PROBE STUDY OF THE EARLY STAGES OF PRECIPITATION</b> .....	84
6.1 Introduction .....	84
6.2 Experimental Procedure .....	85
6.3 Results and Discussion .....	86
6.4 Summary and Conclusions .....	87
<b>Chapter 7: THE EFFECT OF TITANIUM ON THE MICROSTRUCTURE OF STEEL WELDS</b> .....	92
7.1 Introduction .....	92
7.2 Experimental Procedure .....	92
7.3 Results and Discussion .....	93

<i>7.3.1 Microstructural Observations</i> .....	93
<i>7.3.2 Austenite Formation</i> .....	94
<i>7.3.3 Macrohardness Measurements</i> .....	95
<i>7.3.4 Microanalysis</i> .....	96
7.4 Summary and Conclusions .....	96
<b>Chapter 8: Suggestions For Future Research</b> .....	105
<b>References</b> .....	106

## NOMENCLATURE AND ABBREVIATION

$Ae_3$	Upper limiting temperature of the $\alpha + \gamma$ phase field at equilibrium
$Ae'_3$	Upper limiting temperature of the $\alpha + \gamma$ phase field at paraequilibrium
$Ae_1$	Lower limiting temperature of the $\alpha + \gamma$ phase field at equilibrium
$Ae'_1$	Lower limiting temperature of the $\alpha + \gamma$ phase field at paraequilibrium
$B_S$	Bainitic transformation start temperature
CCT	Continuous Cooling Transformation Diagram
CHT	Continuous Heating Transformation
$e_\alpha$	Linear thermal expansion coefficient of ferrite
$e_\gamma$	Linear thermal expansion coefficient of austenite
IPS	Invariant plane strain
$L$	Length of the specimen prior to the transformation, mm
$\Delta L$	Length change due to transformation, mm
$M_S$	Martensitic transformation start temperature
$q$	Half thickness of allotriomorphic ferrite
$Q$	Activation energy
$R$	Universal gas constant
$T_0$	Temperature at which ferrite and austenite of identical composition have the same free energy
$T'_0$	Temperature at which ferrite and austenite of identical composition have the same free energy, taking into account the strain energy of the ferrite
$T_i$	Isothermal heat treatment temperature
TTT	Time-Temperature-Transformation
$T_1$	First isothermal heat treatment temperature
$T_2$	Second isothermal heat treatment temperature
$T_\gamma$	Austenitising temperature
$V_a$	Volume fraction of acicular ferrite
$V_\alpha$	Volume fraction of allotriomorphic ferrite
$V_W$	Volume fraction of Widmanstätten ferrite
$V_m$	Volume fraction of microphases
$W_s$	Widmanstätten ferrite transformation start temperature
$\bar{x}$	Average carbon concentration of the alloy

$x^{\alpha\gamma}$	Paraequilibrium carbon concentration in ferrite
$x^{\gamma\alpha}$	Paraequilibrium carbon concentration in austenite
$x_{T_0}$	Carbon concentration in austenite, as given by the $T_0$ curve
$x_{T'_0}$	Carbon concentration in austenite, as given by the $T'_0$ curve
$\alpha$	Allotriomorphic ferrite
$\alpha_1$	One dimensional parabolic thickening rate constant for paraequilibrium growth of ferrite
$\alpha_a$	Acicular ferrite
$\alpha_b$	Bainitic ferrite
$\alpha_W$	Widmanstätten ferrite
$\gamma$	Austenite

---

# Chapter 1

## GENERAL INTRODUCTION

---

### 1.1 Introduction

This chapter provides a general introduction to the research and contains a summary of what is in reality the vast field of the physical metallurgy of alloyed steels. The ability to control the microstructure of welds relies on a deep understanding of the phase transformation theory governing the microstructural changes which occur as the weld solidifies and cools to ambient temperatures. The microstructure which thus evolves is called the as-deposited or *primary* microstructure. In multi-run welds, some of the regions of the original primary microstructure are reheated to temperatures high enough to cause reverse transformation into austenite, which during the cooling part of the thermal cycle retransforms into a variety of somewhat different products. Other regions may simply be tempered by the deposition of subsequent runs. The microstructure of the reheated regions is called the *reheated* or *secondary* microstructure.

Most of the work involving the use and development of phase transformation theory for welds has focused on the as-deposited or *primary* microstructure, which usually consists of a mixture of allotriomorphic ferrite ( $\alpha$ ), Widmanstätten ferrite ( $\alpha_w$ ), acicular ferrite ( $\alpha_a$ ), bainite ( $\alpha_b$ ), martensite, retained austenite, pearlite, contained within the columnar austenite grains typical of the solidification structure of low-alloy steel weld deposits [Davies and Garland, 1975; Savage, 1980; Alberry and Jones, 1982; Bhadeshia *et al.*, 1985; Bhadeshia, 1989, 1990; David and Vitek, 1993; Easterling, 1993].

A weld model has been developed to permit the estimation of microstructure and properties of a wide variety of welds of different chemistries (currently accounting for C, Mn, Si, Ni, Mo, Cr, V as solute elements) and fabrications using any of a number of welding processes [Bhadeshia *et al.*, 1985]. It works rather well for the as-deposited weld metal. The model is able to predict the size, shape, distribution, chemical composition, growth rate, *etc.* as a function of time and temperature dur-

ing cooling, taking account of interference between particles growing from different sites. When such welds consist of several layers deposited sequentially on top of each other, this existing model is able to crudely estimate the fractions of primary and secondary (*i.e.* reheated) microstructures in each case. These fractions are of vital importance in determining the weld mechanical properties.

However, as the molybdenum concentration is increased, experimental data [Evans, 1986, 1988] indicate that more of the primary microstructure is preserved than is indicated theoretically, with much of the prior deposit being apparently unaffected by the multiple thermal cycles associated with multirun welds. In multirun steel welds, the heat input associated with the deposition of successive layers of weld metal causes some or all of the underlying structure to be reheated to temperatures where austenite formation occurs [Yang and Bhadeshia, 1987a]. It could be the case that molybdenum retards the reaustenitization in steel welds, therefore enabling more of the primary microstructure to be preserved. It has also been noticed that the calculated strength is underestimated as the molybdenum concentration is increased [Sugden and Bhadeshia, 1988]. The present research project was initiated to explain these anomalies observed in the prediction of microstructure in Fe–C–Mo steel welds.

The purpose of this investigation was to examine systematically a series of molybdenum containing weld deposits, using analysis techniques such as differential scanning calorimetry and dilatometry, accompanied by detailed microstructural characterisations. An overview of the research programme is shown in Fig. 1.1.

## 1.2 Molybdenum–Chromium Steels

Molybdenum–chromium steels have been used in the petroleum industry reactor vessels mainly to reduced corrosion by sulphur and its compounds which are present in crude oil. The improved oxidation resistance and high temperature strength extend their applications to other areas, like steam generators and heaters. The range of applications includes chemical reactor vessels, nuclear power generation components and also superheaters of steam generators. They have recently been used in hydrotreating vessels in the petroleum industry, where they are exposed to high temperatures and also high pressures of hydrogen. The operating temperature is usually in the range 500 °C to 600 °C; the temperature range re-

duces to between 400 °C and 500 °C for high pressure applications [Lundin *et al.*, 1986].

The molybdenum–chromium steels are used in service in two states, namely in the quenched and tempered condition but mostly in the normalised condition. The most widely used Mo–Cr steel is the so-called 2.25Cr–1Mo wt.% alloy. The microstructure can be a mixture of allotriomorphic ferrite and bainite or more usually completely bainitic, with some retained austenite [Kar and Todd, 1982].

Use of high–strength quenched and tempered steels is a result of the general trend to save weight and costs and to increase service life [Musgen, 1985]. The molybdenum and chromium form relatively stable carbides which go into solution during austenitization and are precipitated again during tempering. In addition, molybdenum has a solid solution hardening effect. Typical applications are: pressure vessels for transport and storage, submarines, heavy road vehicles *etc.*

### *1.2.1 The Effect of Molybdenum on Weld Metal*

There is a microstructural effect which is especially prominent in molybdenum and chromium steels which have relatively high concentrations of molybdenum (> 0.5 wt.%) or chromium (> 1.5 wt.%). The columnar austenite grains of steel weld deposits transform into bainite instead of acicular ferrite. It appears therefore, that at relatively high concentrations of molybdenum or chromium, acicular ferrite is in increasing proportions replaced by classical bainite until eventually the microstructure becomes almost entirely bainitic. The bainite is in the form of classical sheaves emanating from the austenite grain surfaces, often with layers of austenite left untransformed between the individual platelets of bainitic ferrite. This is in spite of the presence of non–metallic inclusions, which usually serve to intragranularly nucleate the plates of acicular ferrite.

Some interesting quantitative data have been reported by Evans (1988), he found that as the molybdenum concentration of low carbon weld deposits is increased, the amount of allotriomorphic ferrite decreases. The volume fraction of the remainder of the microstructure, which is described as ‘ferrite with aligned second phase’ therefore increases with concentration (Fig. 1.2). This ferrite with aligned second phase really refers to packets of parallel plates of Widmanstätten ferrite or to sheaves of bainitic ferrite. There is some evidence [Bhadeshia *et al.*,

1986b] that in typical weld deposits of the type studied by Evans, the fraction of Widmanstätten ferrite decreases to very small values (0.04–0.1) as the Cr or Mo concentration increases, so that most of the increase in the volume fraction of the ‘ferrite with aligned second phase’ can be ascribed to an increase in the volume fraction of bainite. This fact is also consistent with the observation that Fe–2.25Cr–1Mo wt.% weld deposits used in the power generation industry exhibit a bainitic microstructure in the as-deposited condition in spite of the presence of nonmetallic inclusions [Klueh, 1974b; Wada and Eldis, 1982; Kar and Todd, 1982; Lundin *et al.*, 1986]. The large alloy concentration in this steel prevents the growth of allotriomorphic ferrite under normal heat treatments condition.

The effect of molybdenum content on the mechanical properties and microstructure of low alloy weld metal has also been investigated [Pacey *et al.*, 1982; Kayali *et al.*, 1983; Raiter and Gonzalez, 1988]. An increase in the toughness at low temperatures has been observed when the molybdenum content is increased from 0.24 to 0.48 wt.%, but the molybdenum had little effect in the ductile regime. These investigations were carried out on Mo–Zr–Ti submerged arc weld metal deposits. This beneficial effect of molybdenum was mainly due to an increase in the fraction of acicular ferrite at the expense of allotriomorphic ferrite and Widmanstätten ferrite. Acicular ferrite is considered to have a high toughness, because of its fine grained interlocking structure which resists crack propagation by cleavage. An increase in the yield and tensile strength have also been observed for both as deposited and stress-relieved welds. A preliminary study of the effect of molybdenum on the microstructure is described in Chapter 3.

### 1.3 The Heat Affected Zone

When base plates are joined by fusion welding, the material of the plates near the fusion boundary is heated to its melting point and then cooled rapidly under conditions of restraint imposed by the geometry of the joint. As a consequence of this severe thermal cycle the original microstructure and properties of the base metal in a region close to the weld are changed. This region is called the heat affected zone (Fig. 1.3). The microstructural change that usually occurs depends on the type of alloy system and the prior heat treatment practice of the metal or alloy welded. On moving from the fusion line toward the original base metal structure, distinct regions

can be observed within the HAZ, depending on the peak temperature to which it is heated. These are crudely classified into the coarse austenite grain region ( $\sim 1300\text{--}1100^\circ\text{C}$ ), fine austenite grain region ( $\sim 1100\text{--}900^\circ\text{C}$ ), partially austenitised region ( $\sim 900\text{--}700^\circ\text{C}$ ) and tempered region ( $\sim 500\text{--}700^\circ\text{C}$ ) [Reed and Bhadeshia, 1990]. In order to obtain a reasonable understanding of the HAZ it is necessary to consider how the microstructure of the base metal reacts to the complete thermal cycle, the time held at temperature and, finally, the cooling cycle and its effect on the phase transformations and precipitation reactions.

## 1.4 Transformation Products from Austenite

The final microstructure of the low alloy steel weld evolves during the  $\gamma \rightarrow \alpha$  transformation when a variety of microstructural constituents may form, depending upon the chemical composition and cooling rate. However, the most important phases are allotriomorphic ferrite, Widmanstätten ferrite, acicular ferrite, bainite, and martensite. The transformation products formed by the decomposition of austenite are: (a) reconstructive transformation products (i) allotriomorphic ferrite, and (b) displacive transformation products (i) Widmanstätten ferrite (ii) bainite (iii) acicular ferrite; and (iv) martensite.

### 1.4.1 Reconstructive Transformation

Reconstructive transformations are those in which the interface advances by the thermally activated uncoordinated movement of atoms across the interface. The atoms move independently of each other and in an apparently random manner. Here the original austenite grain structure will be destroyed by the transformation. There is much mixing up of atoms during transformation and there is no atomic correspondence between the parent and product lattices.

### 1.4.2 Allotriomorphic Ferrite

Allotriomorphic ferrite ( $\alpha$ ) is the first phase to form on cooling below the  $A_{e3}$  (upper temperature limit of the  $\alpha + \gamma$  phase field at equilibrium) temperature and nucleates heterogeneously at the boundaries of the columnar austenite grains (Fig. 1.4). The details of the thermodynamics and kinetics of the allotriomorphic ferrite transformation have recently been reviewed [Bhadeshia *et al.*, 1985]. The growth is usually assumed to involve a paraequilibrium mechanism. Paraequilibrium

growth is considered to be controlled by carbon diffusion only. It is a constrained equilibrium in which the ratio of iron to substitutional alloying element remains constant everywhere, but subject to that condition that the carbon attains equality of chemical potential [Hillert, 1952; Bhadeshia *et al.*, 1985].

It is generally accepted that the presence of substantial quantities of allotriomorphic ferrite can lead to poor toughness in low alloy steel weld deposits [Calvo *et al.*, 1963; Savage *et al.*, 1966; Underwood, 1970; Widgrey *et al.*, 1975; Rodrigues *et al.*, 1977 and Cochrane *et al.*, 1982]. This can be attributed to its relatively coarse grain size, and also its morphology, the continuous layers of which provide minimal resistance to crack propagation [Levine and Hill, 1977].

#### 1.4.3 Displacive Transformation

During displacive transformation, the atoms move less than an interatomic distance and retain their relationships with their neighbours. In this type of transformation the iron or substitutional atoms do not move more than a lattice spacing, similar to martensitic transformation (often called shear transformation or military transformation). But the above transformation can be controlled by the diffusion of interstitial alloying elements like carbon.

Two of the most important characteristics of the transformation are that it is diffusionless for the substitutional species and that the change in crystal structure is obtained by a physical deformation of the parent lattice. In a martensitic transformation, labelled rows of atoms in the parent crystal remain in the correct sequence in the martensitic lattice, despite deformation. As there is no mixing up of atoms during transformation, it is possible to suggest that a particular atom of the martensite originated from a corresponding particular atom in the parent crystal. This property may be expressed by stating that there exists an atomic correspondence between the parent and product lattices. The difference between the displacive and reconstructive transformation is illustrated in Fig. 1.5. In the case of a reconstructive transformation, the atoms are able to move about (in any uncoordinated manner) in such a way that there is no macroscopic change in shape other than due to any density changes. In addition there may be a composition change during diffusional reactions since some atoms may have a preference for a particular phase. Hence there is no atomic correspondence between the parent and

product lattices during diffusional transformations, the sequence of labelled atoms in Fig. 1.5 has therefore changed on transformation.

Microstructures like allotriomorphic ferrite and pearlite form in the reconstructive transformation temperature range; Widmanstätten ferrite, bainitic ferrite and martensite form in the displacive transformation temperature range during conventional heat treatment practice.

#### 1.4.4 *Widmanstätten Ferrite*

Widmanstätten ferrite is a phase formed by the transformation of austenite below  $A_{e_3}$ . It forms in a temperature range where reconstructive transformations become relatively sluggish and give way to displacive transformations. Widmanstätten ferrite which grows by a displacive transformation mechanism, maintains an atomic correspondence between the parent and product phases. On an optical scale, Widmanstätten ferrite has the shape of a thin wedge, the actual shape being somewhere between that of a plate and a lath.

Widmanstätten ferrite can nucleate either directly from austenite grain boundaries, in which case it is called 'primary Widmanstätten ferrite' or it can nucleate from previously formed grain boundary allotriomorphic ferrite, when it is designated to be a 'secondary Widmanstätten ferrite' [Dubé, 1948]. All Widmanstätten ferrite grows as sets of parallel plates separated by thin regions of austenite which may subsequently be retained to ambient temperature or which might transform to martensite and/or pearlite.

Widmanstätten ferrite cannot be put into the group of reconstructive transformation products, because there is no diffusion involved in the actual lattice change; iron and substitutional elements do not diffuse during transformation.

#### 1.4.5 *Bainite*

Bainite forms by the decomposition of austenite at a higher undercooling relative to the Widmanstätten ferrite and grows in the form of sheaves originating from austenite grain boundaries. The overall morphology of sheaf is illustrated in Fig. 1.6. The sheaf consists of much smaller platelets (sub-units) of ferrite. The mechanism is believed to be displacive with no diffusion during transformation [Bhadeshia and Edmonds, 1980; Bhadeshia and Waugh, 1982; Stark *et al.*, 1987]. The excess carbon trapped in bainitic ferrite is removed by a combination of diffusion into the

residual austenite, and by the precipitation of carbides between the ferrite. The retained austenite eventually decomposes by a diffusional transformation into a mixture of more carbides and ferrite [Bhadeshia, 1987].

The sheaf itself has a wedge shaped plate morphology on a macroscopic scale. The initial nucleation event takes place at the prior austenite grain boundaries and subsequently, sub-units nucleate and grow from the tips of the previous sub-units. The kinetics of bainite are also shown to be consistent with the proposed diffusionless, displacive transformation mechanism [Christian and Edmonds, 1984; Bhadeshia, 1987, 1988; Bhadeshia and Christian, 1990].

It has long been believed that bainite occurs in two morphologies, upper and lower bainite, with only the latter containing carbide particles inside the ferrite plates. Matas and Hehemann (1961) proposed a qualitative model to explain this (Fig. 1.7). The plates of bainite grow without diffusion but at high temperatures the excess carbon rapidly partitions into the residual austenite so that upper bainite is obtained with carbide precipitation from the austenite only. When diffusion rates slow down at lower temperatures, carbides have an opportunity to precipitate from the supersaturated ferrite, giving the lower bainite microstructure.

#### 1.4.6 Acicular Ferrite Formation

Acicular ferrite ( $\alpha_a$ ) apparently nucleates intergranularly at inclusions within the large columnar austenite grains. It is like a needle as shown in Fig. 1.8 and is generally recognised that  $\alpha_a$  has in three dimensions the morphology of thin lenticular plates. It is a phase most commonly observed as austenite transforms during the cooling of low-alloy steel weld deposits. It is of considerable commercial importance because it provides a relatively tough and strong microstructure. It forms in a temperature range where reconstructive transformations become relatively sluggish and gives way to displacive reactions such as Widmanstätten ferrite, bainite and martensite. The volume fraction  $v_a$  of acicular ferrite is usually estimated by difference:

$$v_a = 1 - v_\alpha - v_W - v_M$$

where  $v_M$  is the volume fraction of microphases, which in turn can be estimated as given by Bhadeshia *et al.* (1985).

There are several reviews [Grong and Matlock, 1986; Abson and Pargeter,

1986] which highlight the mechanism of acicular ferrite formation and its effect on properties. There appears to be a strong dependence of the transformation on intragranular inclusions in the austenite. Fundamental studies indicate that acicular ferrite is similar to bainitic transformation [Yang and Bhadeshia, 1987; Strangwood and Bhadeshia, 1987]. The acicular ferrite plates form by a diffusionless and displacive transformation mechanism immediately after which, carbon is partitioned into the residual austenite. Its detailed morphology differs from classical sheaf-like bainite simply because the former nucleates intragranularly at inclusions within large  $\gamma$  grains whereas in wrought steels which are relatively free of nonmetallic inclusions, bainite nucleates initially at  $\gamma/\gamma$  grain surfaces and continuous growth by the repeated formation of sub-units, to generate the classical sheaf morphology. Acicular ferrite does not normally grow in sheaves because the development of sheaves is stifled by hard impingement between plates nucleated independently at adjacent sites

#### 1.4.7 Martensite

Martensite is a product of diffusionless displacive transformation and can occur in the form of thin, lenticular plates, which often extend right across  $\gamma$  grains, or as packets of approximately parallel, fine laths, whose size is generally less than of the  $\gamma$  grains. Martensite forms due to rapid quenching of austenite to room temperature. The martensite in normal low alloy steel weld deposits occurs only in small quantities, mostly limited to the regions which are called as microphases, which also contain some retained austenite. In high strength weld deposits (high alloy content) the microstructure consists only of mixtures of martensite and bainite [Svensson and Bhadeshia, 1988]. There is now an increased use of these alloys for high strength applications.

### 1.5 Tempering of Martensite

Tempering is the process of heating martensitic steels to elevated temperature so that they become more ductile. It describes how the microstructure and mechanical properties change as the metastable sample is held isothermally at temperature ( $\sim 150\text{--}700\text{ }^\circ\text{C}$ ) below  $Ae_1$  (lower temperature limit of the  $\alpha + \gamma$  phase field at equilibrium). It involves the segregation of carbon, the precipitation of carbides, the

decomposition of retained austenite, and the recovery and recrystallization of the martensite structure.

The processes that occur during the tempering of martensite are usually categorised as follows. Stage 1 primarily influences any carbon that may be in solid solution; the excess carbon first tends to segregate to defects or cluster within the solid solution. It eventually precipitates, either as cementite for low carbon steels, or as transition carbides for relatively high carbon alloys. The carbon concentration that remains in solution may be quite large if the precipitate is a transition carbide. Further annealing leads to stage 2, in which almost all the excess carbon is precipitated, and the carbides all convert into the stable cementite form. Any retained austenite may also decompose during this stage. Continued tempering then leads to the spheroidisation of carbides, extensive recovery of the dislocation structure, and finally to the recrystallisation of the new ferritic plates into equiaxed grains.

#### *1.5.1 Secondary Hardening and Precipitation of Alloy Carbides*

Secondary hardening is usually associated with the tempering of martensite in steels containing strong carbide forming elements like Cr, V, Mo, Nb, *etc.* The stage of tempering is accompanied by a drop in the hardness at first, but the alloy carbides, when they eventually form at the expense of cementite, often pose formidable obstacles to dislocation motion and lead to an increase in hardness with tempering time. This is the phenomenon commonly referred to as secondary hardening. Eventually, the usual growth and coarsening reactions make even these carbides less effective in hindering dislocation motion and the hardness then drops with tempering time.

The structure, composition, morphologies and occurrence of many carbide phases have been studied [Kuo, 1956; Smith and Nutting, 1957; Baker and Nutting 1959; Irvine and Pickering, 1960; Woodhead and Quarrell, 1965; Thomson, 1990]. It is usual to refer to the carbides by the general formulae, *e.g.*  $M_2C$ ,  $M_7C_3$ ,  $M_{23}C_6$ ,  $M_6C$ , where M indicates a mixture of metal atoms.

The first carbide to form on the tempering of low alloy steel is cementite  $M_3C$ ; the conventional precipitation sequence in low alloy steels as equilibrium is approached is well established [Baker and Nutting, 1959]. Cementite will dissolve rapidly at high temperatures, to be replaced by cementite +  $M_2C$ , then  $M_{23}C_6$  or

$M_6C$  and finally  $M_{23}C_6$ . The exact nature of the precipitation sequence and the kinetics of the process depend on the alloy composition and heat treatment.

## 1.6 Time–Temperature Transformation (TTT) Diagrams

Time–temperature transformation diagrams are very useful in representing the transformation characteristics of steels, and in revealing the role of alloying elements in influencing the microstructure of steels. The method developed by Bhadeshia (1982), involves the calculation of two separate ‘C’ curves representing the initiation of diffusional and displacive transformations respectively (Fig. 1.9). The positions of the curves in the time/temperature domain are determined using a semi–empirical thermodynamic approach capable of taking account of C, Mn, Si, Ni, Cr, Mo and V in any reasonable combination, as long as the steel can be classified as a low–alloy steel.

The upper ‘C’ curve refers to the time taken for the initiation of the allotriomorphic ferrite transformation and the lower ‘C’ curve refers to the initiation of displacive transformations, such as the Widmanstätten ferrite and bainite reactions [Bhadeshia, 1981a, 1982]. It is assumed that the lower ‘C’ curve also describes the formation of acicular ferrite. The thermodynamically calculated martensite start temperature ( $M_s$ ) is also presented, as a horizontal line [Bhadeshia, 1981c, 1981d].

The calculation of the TTT, phase diagrams including  $Ae_3$ ,  $Ae'_3$  (upper temperature limit of the  $\alpha + \gamma$  phase field at paraequilibrium),  $W_s$  (Widmanstätten ferrite start temperature),  $B_s$  (bainite start temperature) and  $M_s$  temperatures will be presented later in Chapter 3.

## 1.7 Austenite Formation

Austenite formation is very important in many fabrication processes involving multipass welding but has not been widely investigated. It is consequently quite important to study the process of austenite formation in low alloy steels, especially given the increasing tendency of steel manufacturers and users to rely on microstructure and property prediction models. Phase transformation theory plays a key role in such models. The austenite formation process is influenced by starting microstructure, heating rate and chemical composition.

In multirun welds, the heat input associated with the deposition of successive

layers of weld metal causes some or all of the underlying structure to be reheated to temperatures where austenite formation occurs [Yang and Bhadeshia, 1987]. The final layer deposited is expected to exhibit a true primary microstructure. The remaining regions of the welds may have undergone transient temperature rises high enough to cause partial or complete reverse transformation into austenite. The new austenite then transforms during cooling to a microstructure which is very different from the solidification structure associated with weld deposits and can seriously affect the mechanical properties of the final weld. The volume fraction of the reheated zone depends on the number and the size of the beads deposited [Easterling, 1983]. The reheated microstructure typically has a higher toughness and a lower strength than the as-deposited microstructure. However most research involving the modelling of microstructure in the reheated regions has been concerned with the prediction of austenite grain size and microstructure [Reed and Bhadeshia, 1989].

#### *1.7.1 Effect of Initial Microstructure and Heating Rate*

The kinetics of austenitization and the nature of the transformation products depend strongly on alloy chemistry, the initial microstructure and heating rate. Some research dealing with the initial microstructure effect on the morphology of austenite, has already been done [Speich *et al.*, 1969; Law and Edmonds, 1980; Speich *et al.*, 1981; Garcia *et al.*, 1981; Souza *et al.*, 1982; Lenel and Honeycombe, 1984; Cal *et al.*, 1985; Yang and Bhadeshia, 1987, 1989, 1990]. Many investigators have examined in detail the formation of austenite from martensitic low carbon steels. [Kinoshita and Ueda, 1974; Matsuda and Okamura, 1974; Homma, 1974; Watanabe and Kunitake, 1976]. It has been found there are two types of austenite morphology, acicular and globular austenite, dependant on the condition of the prior microstructure, austenitizing temperature and heating rate. If the initial microstructure consists of ferrite laths for example bainite or martensite, the austenite adopts an acicular morphology otherwise grow in a globular morphology. It is generally agreed that acicular austenite is inherited initially from the elongated nature of prior martensitic laths or packets, and is favoured by slow heating rates and low austenitizing temperatures. Globular austenite can also occur directly, favoured by the opposite conditions to those described above. Some workers have further

characterized the austenite as grain boundary allotriomorphic, grain boundary idiomorphic and Widmanstätten morphologies similar to the terminology common to the decomposition of austenite [Plichta and Aaronson, 1974; Lenel and Honeycombe, 1984a].

Law and Edmonds (1980) have studied the austenite transformation start ( $Ac_1$ ) and finish ( $Ac_3$ ) temperatures as a function of heating rate for the ferritic, bainitic, and martensitic microstructures. Throughout the range of heating rates, the  $Ac_1$  temperature was lowest in the case of the martensitic specimens. The temperature increased for the bainitic structure and also for the ferrite. In addition the transformation was completed first in the martensitic structure, and then in the bainite and the ferritic structure. They found that nucleation of acicular austenite on lath boundaries is governed by austenitizing temperature and heating rate, but this transitional form is eventually replaced by the globular morphology as regions of acicular austenite coalesce. Yang *et al.* (1990) studied the effect of heating rates on the reaustenitisation from martensitic microstructure in Fe–C–Si–Mn alloy. They found that the transformation start temperature is raised as the heating rate increases.

## 1.8 Summary

A literature review of some of the basic concepts of phase transformation in steel has been presented. At lower temperatures, decomposition of austenite in steel gives rise to characteristic microstructure consisting of allotriomorphic ferrite, Widmanstätten ferrite, acicular ferrite and bainite. The significance of tempering of martensite and reaustenitization in controlling the microstructure of multirun steel weld deposits is emphasized.

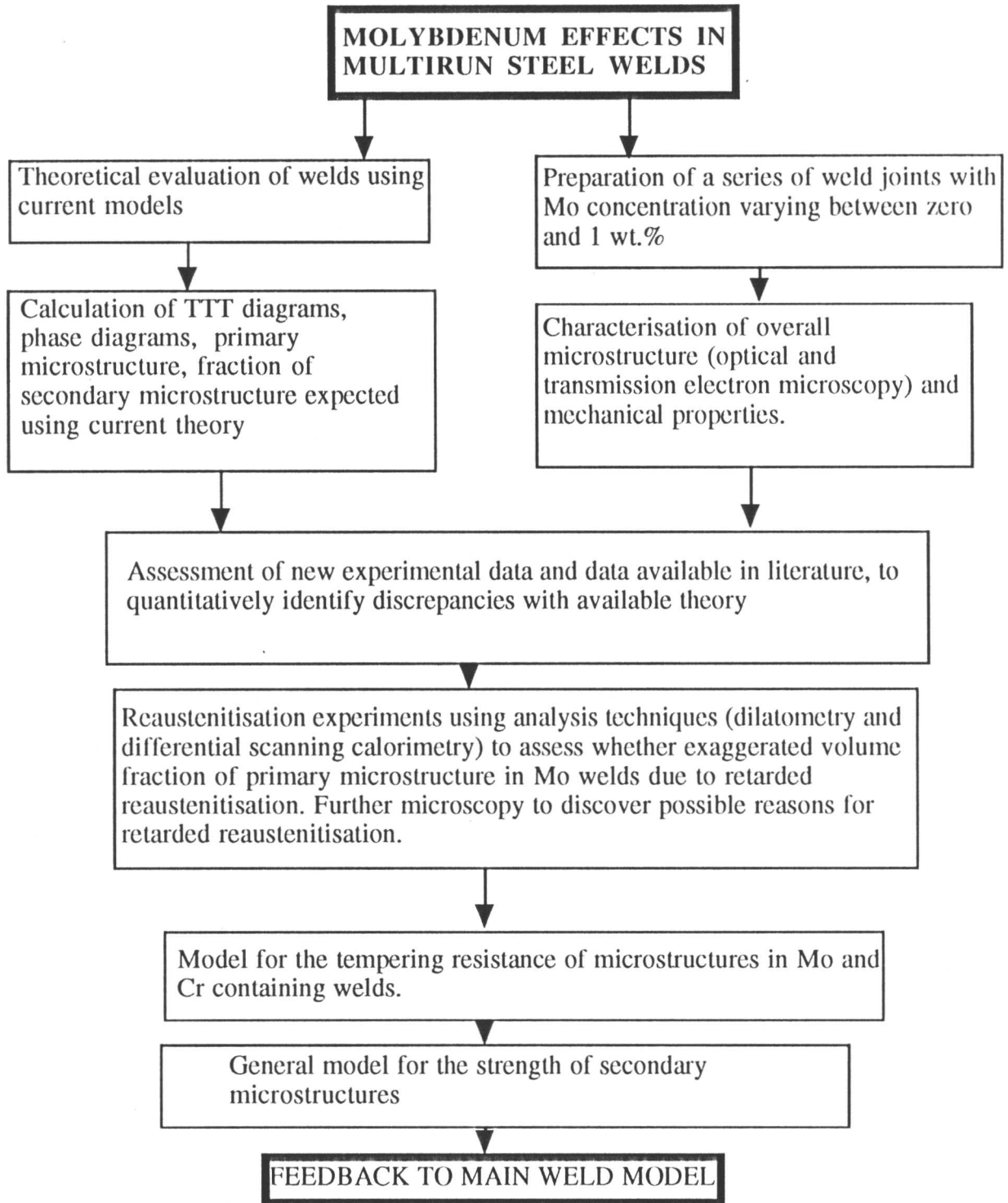


Fig. 1.1: Flow chart for the molybdenum effect programme.

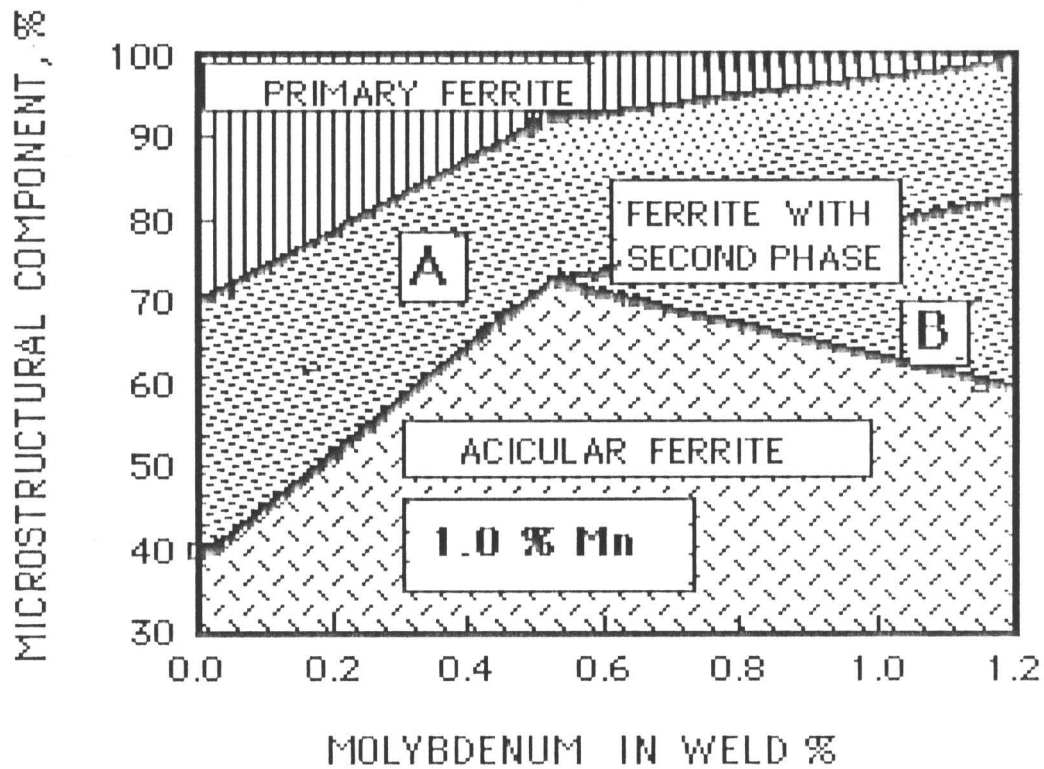


Fig. 1.2: Changes in the as-deposited microstructure of steel welds as a function of molybdenum concentration [After Evans]. The region labelled 'ferrite with aligned second phase' by Evans has been subdivided into regions A and B, to represent the Widmanstätten ferrite and bainite microstructure respectively.

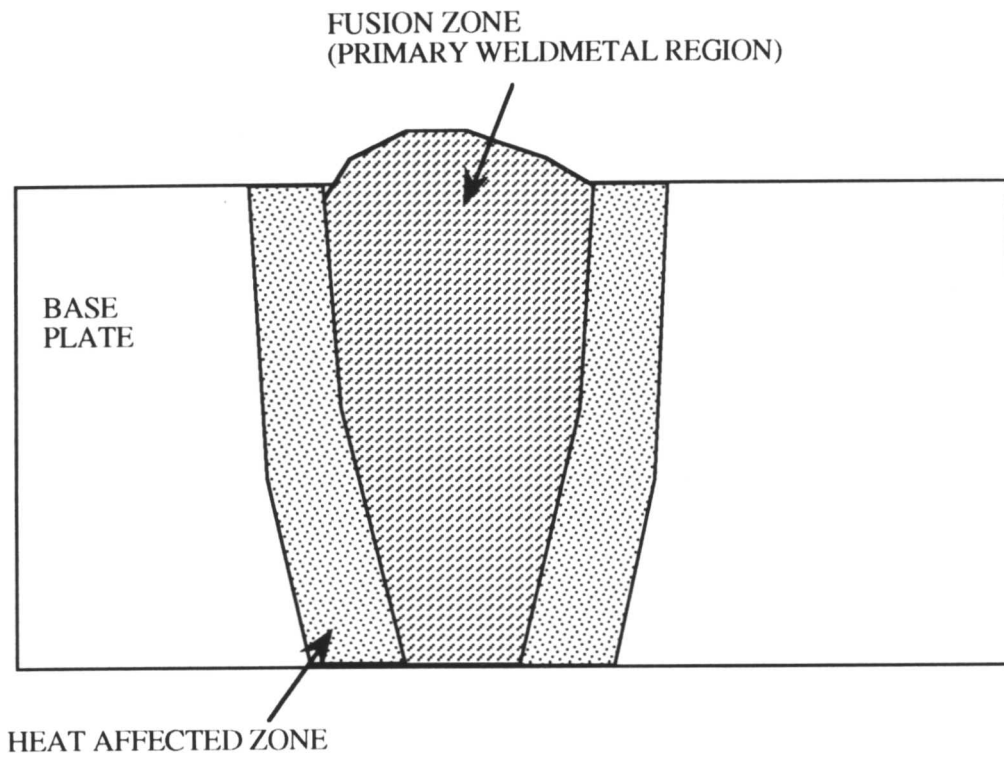


Fig. 1.3: Schematic illustrating heat effected zone, fusion zone or primary weld metal region in multipass steel weld deposits.

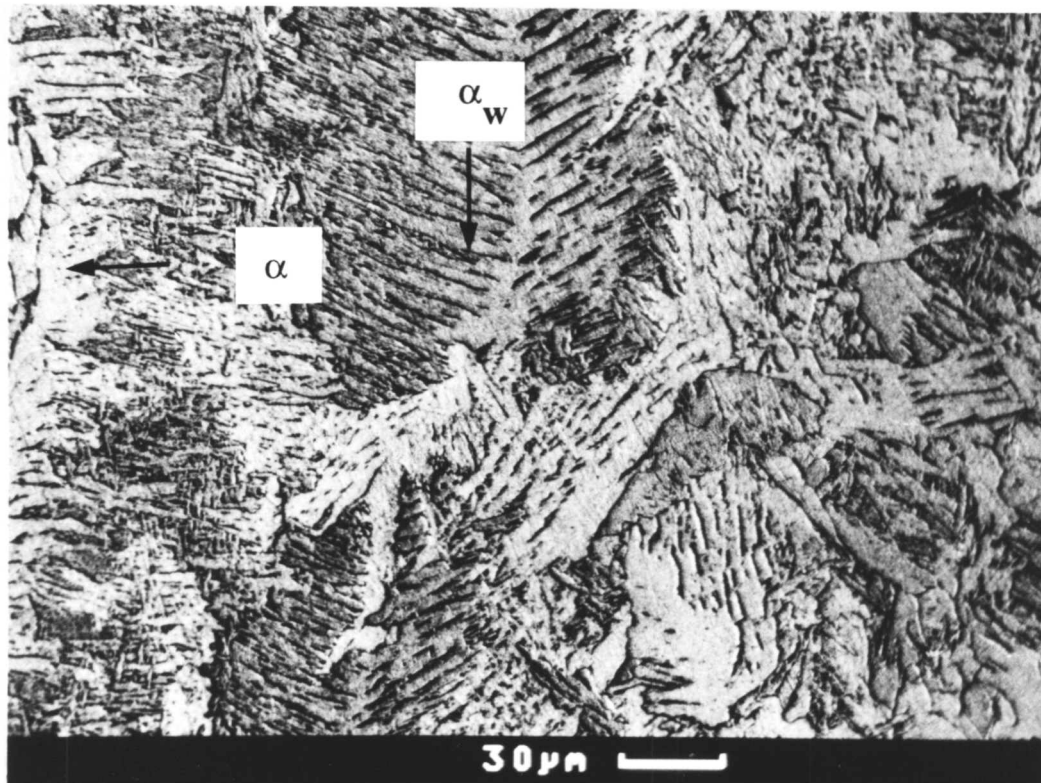


Fig. 1.4: SEM (Scanning Electron Microscopy) micrograph of allotriomorphic ferrite and Widmanstätten ferrite in a Fe-0.078C-0Mo wt.% steel welds.

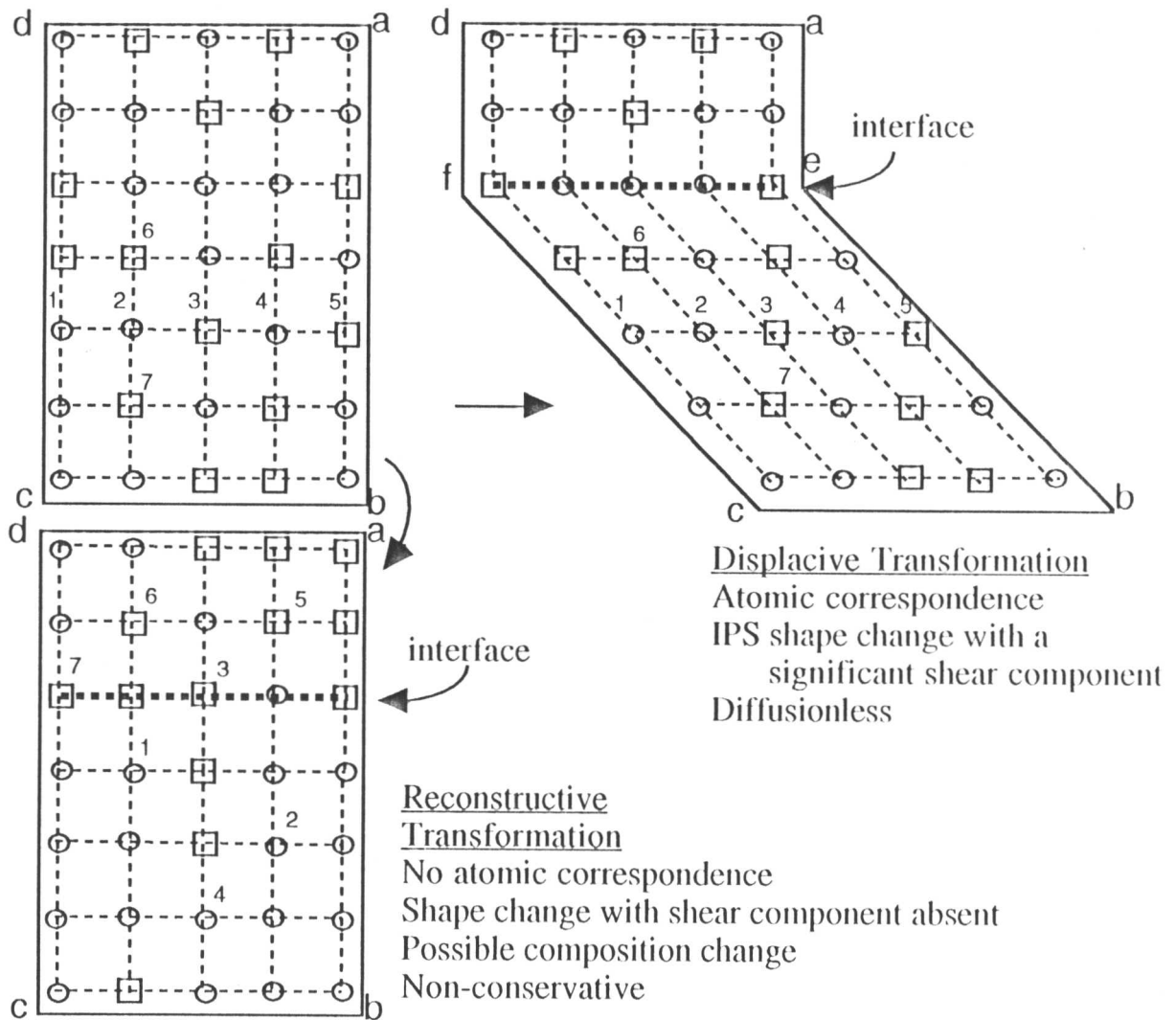


Fig. 1.5: Schematic illustration of the difference of the mechanism between reconstructive and displacive transformation [Bhadeshia, 1987].

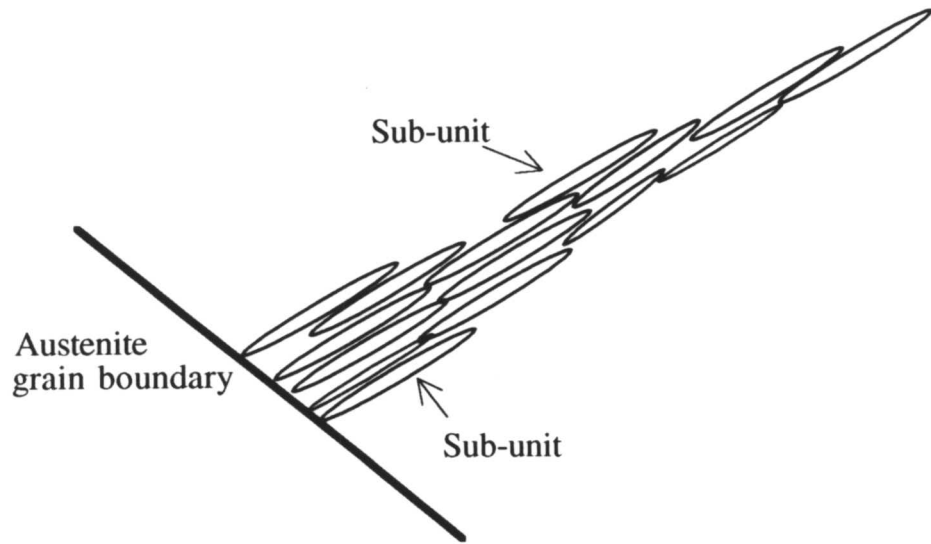


Fig. 1.6 (a): Schematic illustration of a sheaf of bainite.

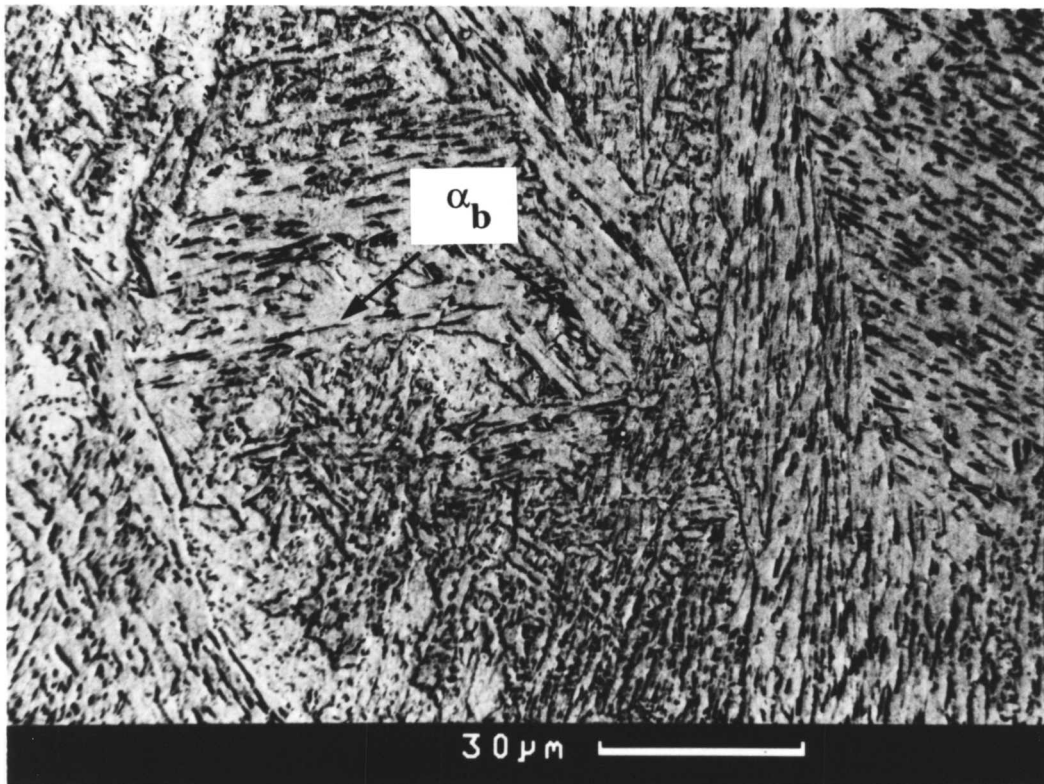


Fig. 1.6 (b): SEM micrograph of bainite in a Fe-0.078C-1Mo wt.% steel welds.

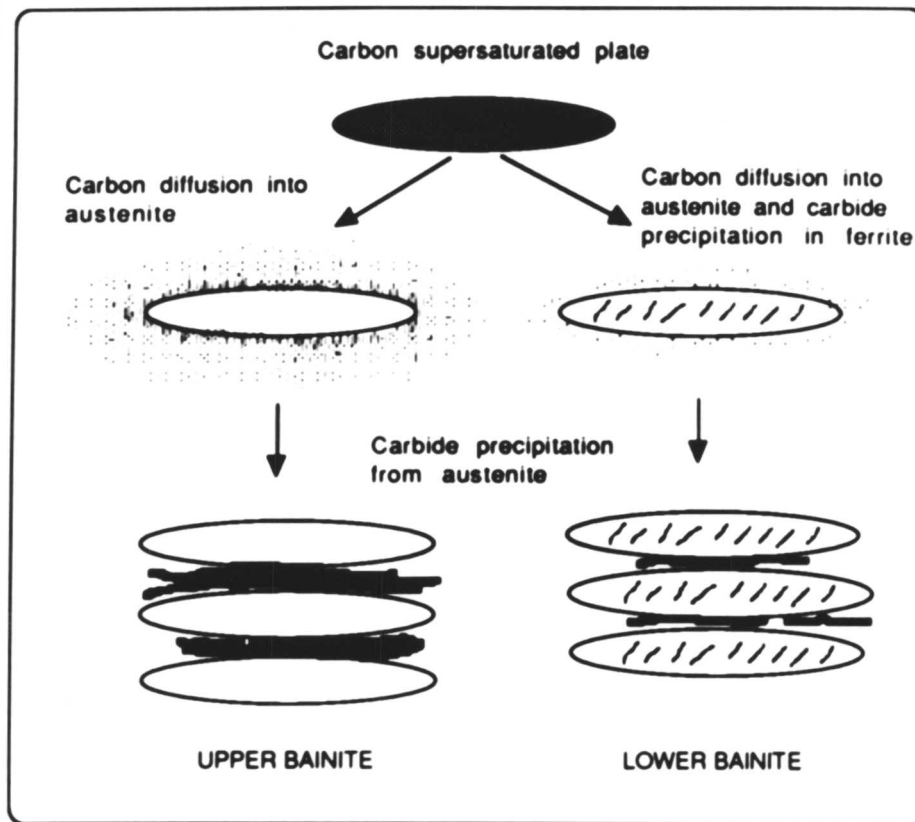


Fig. 1.7: Schematic representation for the upper to lower bainite transition in steel, as modelled by Takahashi and Bhadeshia (1990).

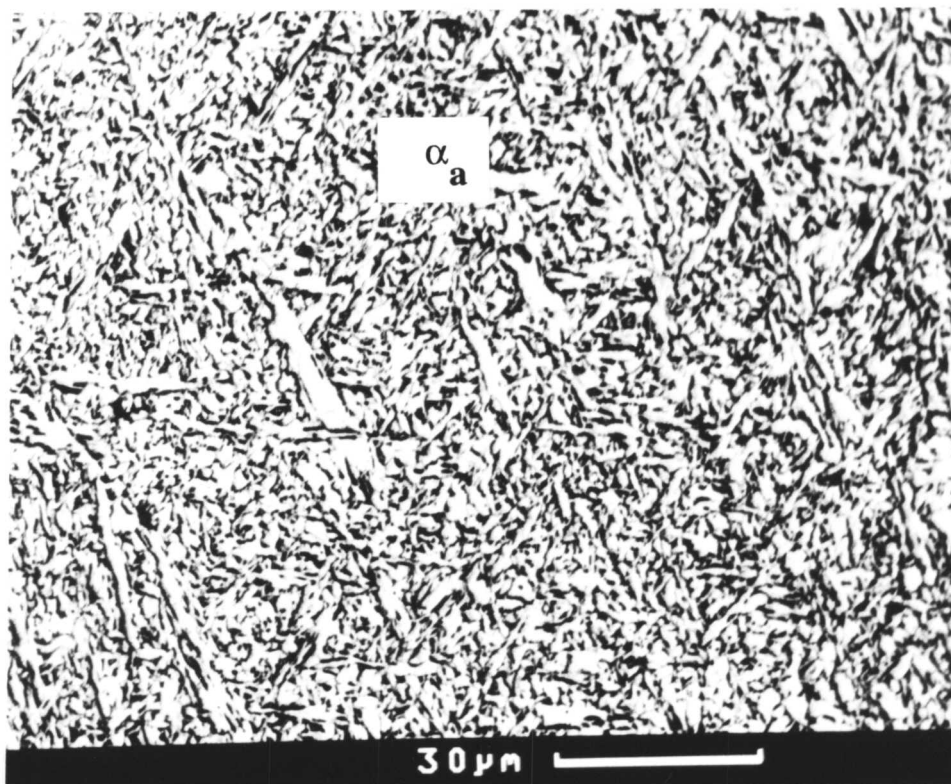


Fig. 1.8: SEM micrograph of acicular ferrite in a Fe-0.078C-1Mo-0.0025Ti wt.% steel welds.

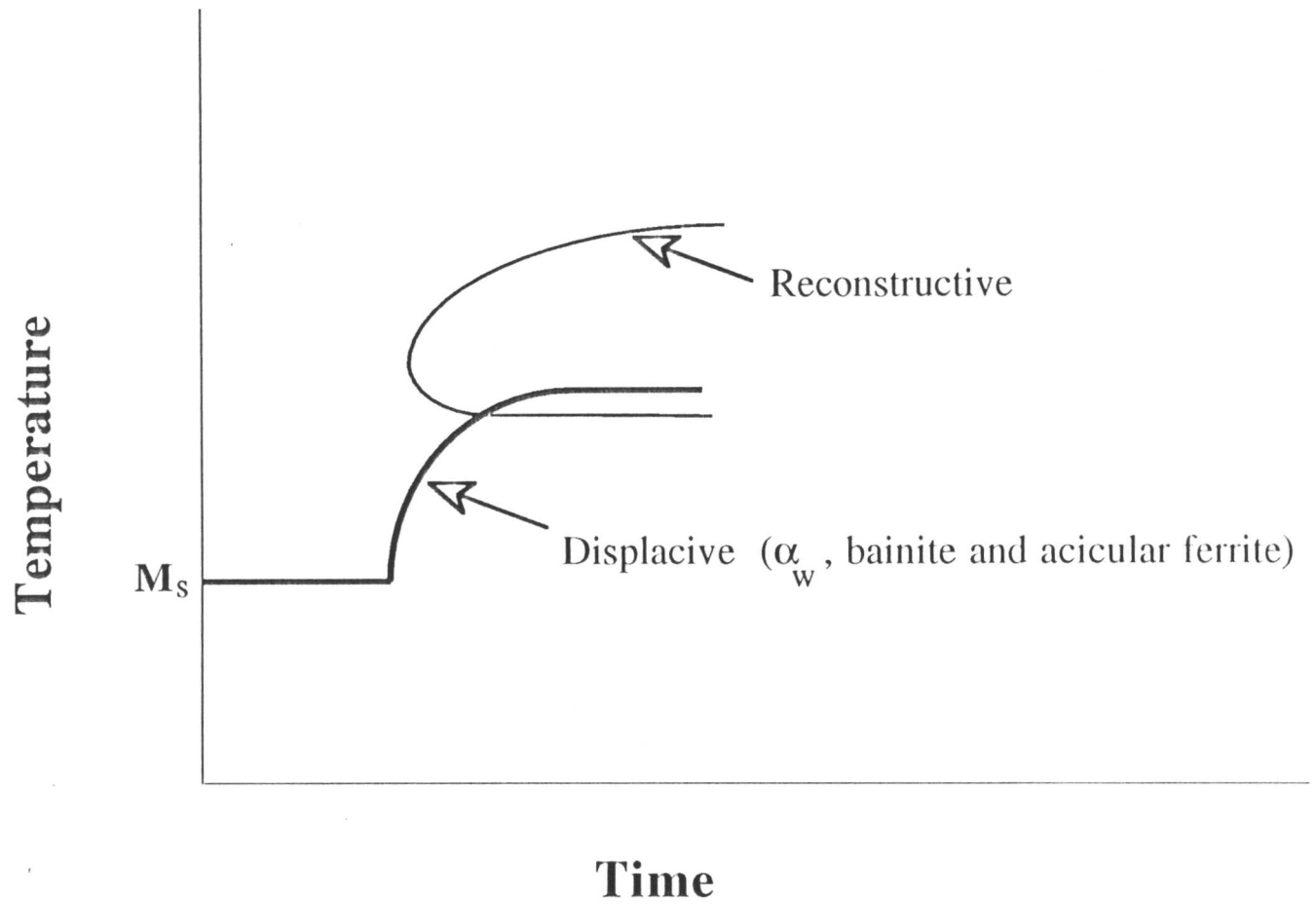


Fig. 1.9: Schematic TTT diagram illustrating the two C curves.

---

# Chapter 2

## EXPERIMENTAL TECHNIQUES

---

### 2.1 Introduction

This chapter includes a brief description of the alloys studied, and the heat treatment and other experimental procedures employed, as summarised in Fig. 2.1.

### 2.2 Materials

Low hydrogen iron powder type electrodes were prepared by Oerlikon Welding Industries, Switzerland, for fabricating joints using the manual metal arc welding technique. The ferro-manganese content of the coating was varied to compensate for changes in molybdenum, rather successfully since all four welds ended up with more or less the same manganese concentrations at 1.05, 1.15, 1.13 and 1.09 wt.%. Different amounts of ferro-molybdenum were also added to the coatings to produce deposits with molybdenum concentrations of 0.005, 0.21, 0.42 and 1.16 wt.% respectively. A small amount of titanium was also added to the alloys. The chemical compositions of the alloys are given in Table 2.1.

Welding was carried out in the flat position; a total of 27 beads constituted the weld, with three beads per layer. The parent plate thickness was 20 mm. The welding variables were:

- welding voltage: 21 Volts,
- welding current: 170 Amps.
- welding speed:  $0.004 \text{ m s}^{-1}$  and
- interpass temperature:  $200^\circ\text{C}$ .

### 2.3 Heat Treatment

Thin rods of 3 mm diameter and bars  $1 \times 1 \times 4$  cm were machined from the original samples. The specimens for heat treatment were sealed in silica tubes containing a partial pressure of argon. The heat treatment studies were carried out using an electric resistance furnace (accuracy  $\pm 5^\circ\text{C}$ ). Some of the rapid heat

treatments were carried out using high speed dilatometry. The heat treatment cycles are illustrated in Fig. 2.2.

## 2.4 Chemical Composition

The chemical compositions (wt.%) were determined spectroscopically except for oxygen and nitrogen, which were measured using Leco furnaces, with 50 g of material for each determination to ensure representative results. The alloy compositions are given in Table 2.1.

Table 2.1: Weld metal composition in wt.%.

Alloy	C	Si	Mn	Ni	Mo	Cr	V	Ti	O	N
Fe-0Mo wt.%	0.079	0.30	1.05	0.027	0.005	0.035	0.001	0.0005	0.0435	0.0060
Fe-0.21Mo wt.%	0.042	0.31	1.15	0.03	0.21	0.03	0.013	0.0005	0.0321	0.0077
Fe-0.42Mo wt.%	0.049	0.30	1.13	0.03	0.42	0.03	0.014	0.0005	0.0312	0.0074
Fe-1Mo wt.%	0.078	0.34	1.09	0.028	1.16	0.036	0.003	0.0005	0.0391	0.0083

## 2.5 Dilatometry

All kinetic measurements were carried out using a Theta Industries high speed dilatometer, equipped with water cooled induction furnace. This enables rapid heating or cooling experiments. The temperature is monitored continuously via a Pt/Pt-10 wt.% Rh thermocouple spot-welded to the centre of the specimen. The cooling of the specimen during dilatometry was carried out using helium gas. The whole arrangement was sealed under a vacuum of better than  $10^{-3}$  atmospheres during operation. The dilatometer has been interfaced with a BBC/Acorn microcomputer which is used for programming the thermal cycles and automatically recording length change, time and temperature information at millisecond intervals, and the data are stored for further analysis. The set up of the sample is explained schematically in Fig. 2.3. The specimens for dilatometry were in the form of rods 3 mm in diameter and 15 mm in length, machined from the weld deposits with the cylinder axes parallel to the welding direction. The specimens were machined from regions far from the fusion line of the parent plate and are not affected by dilution

from the parent material. A transverse section of the weld was cut, such that the surface itself was normal to the welding direction. The 3 mm rods were produced by swaging, involving a successive reduction in the diameter by approximately 1 mm in each step. After swaging, the 3 mm diameter rods were homogenized at 1200 °C for 3 days while sealed in quartz tubes containing a partial pressure of high purity argon. The homogenization treatments were carried out in a resistance-heated horizontal tube furnace.

To avoid surface nucleation and surface degradation, all specimens were electroplated with nickel and all heat treatments were carried out in a helium gas environment. The nickel plating was carried out in two stages. In the first stage, an adherent but non-uniform layer of nickel was plated on the surface by a striking treatment. The striking was carried out at a temperature of 50 °C in a solution of 250 g of nickel sulphate, 27 ml of concentrated sulphuric acid and distilled water, amounting to 1 litre in all. The current density applied was 7.75 mA mm<sup>-2</sup>. The time for striking was 3 minutes. In the second stage the specimens, after striking, were plated in a solution containing 140 g nickel sulphate, 140 g anhydrous sodium sulphate, 15 g of ammonium chloride and 20 g boric acid which was made up to 1 litre with distilled water. The current density applied was 0.4 mA mm<sup>-2</sup>. The plating was carried out at a temperature of 50 °C for 15 minutes. The approximate plating thickness was around 0.08 to 0.1 mm.

## 2.6 Thermomechanical Simulator

A thermomechanical simulator ('Thermecmaster' manufactured by Fuji Electric Industrial Co. Ltd.) was also used. It has a high frequency induction heating system, allowing heating of the specimen to within  $\pm 5$  °C, and is computer controlled. Rapid heating and cooling at specified rates are also possible, with gases (Ar, He, or N<sub>2</sub>) being used for quenching. The samples were cylinders of 8 mm diameter and 12 mm length, made from the weld metal by machining. Heating was performed in an argon atmosphere and quenching was done with nitrogen gas.

Temperature is measured using a Pt/Pt-13 wt.% Rh thermocouple resistance welded to the specimen. The dilation of the specimen in a radial direction during transformation is measured using a laser beam. In order to prevent surface oxidation and nucleation effects, the specimens were nickel plated [Strangwood and Bhadeshia,

1987c] before use in simulator.

## 2.7 Differential Scanning Calorimetry (DSC)

High temperature DSC was used to study and compare the continuous heating transformation behaviour of the steel welds. It is a specially designed high temperature, heat flux DSC with computer control and data acquisition. The sample was in the form of a small disc of diameter approximately 5–6 mm and thickness between 0.5 and 1 mm. The sample and reference are placed in thermally balanced alumina crucibles. All the experiments were carried out using an argon atmosphere in the DSC chamber.

## 2.8 Optical Microscopy

Samples were prepared for microstructural characterization by hot-mounting in acrylic moulding powder, followed by grinding on SiC paper to 1200 grit and polishing to 1  $\mu\text{m}$  cloth coated with diamond paste. Specimens were etched in 2 % nital. The microstructures were examined using an OLYMPUS optical microscope, fitted with a 35 mm camera.

## 2.9 Scanning Electron Microscopy (SEM)

Some samples were imaged in a scanning electron microscope operated at 20 kV and equipped with an energy dispersive X-ray analyser. SEM is the ideal instrument for recording microstructures at sufficiently high resolution for quantitative evaluation of the microstructural components. Conventional SEM images are difficult to interpret, but the use of the image inversion feature on the CAMSCAN S2 microscope enables a more easily recognisable microstructure to be seen. The reason for the image inversion is that by etching in nital it gives the appearance of raised acicular ferrite plates surrounded by any other microstructure.

## 2.10 Transmission Electron Microscopy (TEM)

Specimens for TEM were prepared by both the twin jet electropolishing of thin foils and by the carbon extraction replica technique. The discs were thinned to 50  $\mu\text{m}$  by abrasion on silicon carbide paper and then electropolished in a twin jet electropolisher using a 5% perchloric acid, 25 % glycerol and 70 % ethanol mixture

at an applied voltage of 60 V, with the solution being cooled to  $-10^{\circ}\text{C}$  using liquid nitrogen. The microscopy was carried out using a Phillips EM400T TEM, operated at 120 kV.

### 2.11 Carbon Replicas

Carbon extraction replicas were prepared by deposition of an amorphous layer of carbon on specimen surfaces which had been prepared for optical microscopy. The carbon film was removed by electrolytic etching in a solution of 5 % hydrochloric acid in methanol at +1.5 V, washing in industrial methylated spirits, and then floating the film off in distilled water and collecting on copper grids. The replicas were examined in a Phillips EM400T TEM, operated at 120 kV.

### 2.12 Energy Dispersive X-ray Spectroscopy (EDXS)

Microanalyses were carried out both on matrix and particles using thin foils and the carbon extraction replicas. A LINK series 860 energy dispersive X-ray spectrometer attached to PHILLIPS 400T TEM was used for all the analyses. X-ray spectra were recorded at a specimen tilt of 35 degree and live times of at least 200 seconds were used. The dead time was not allowed to exceed 25 %. The data were analysed using the LINK RTS2-FLS software.

### 2.13 Hardness Testing

Macrohardness tests were carried out using a Vickers hardness tester. The specimens were polished and etched with 2 % nital before hardness testing. The hardness values at a load of 5 kg were obtained from the mean of three indentations on each sample.

### 2.14 Thermodynamic Calculations

Thermodynamic calculations were performed using a computer package (called MTDATA) in which the equilibria in multicomponent, multiphase systems are determined using critically assessed thermodynamic data (developed by National Physical Laboratory, U. K.). The phase chemistries and proportions can be calculated by minimising the Gibbs free energy of the system.

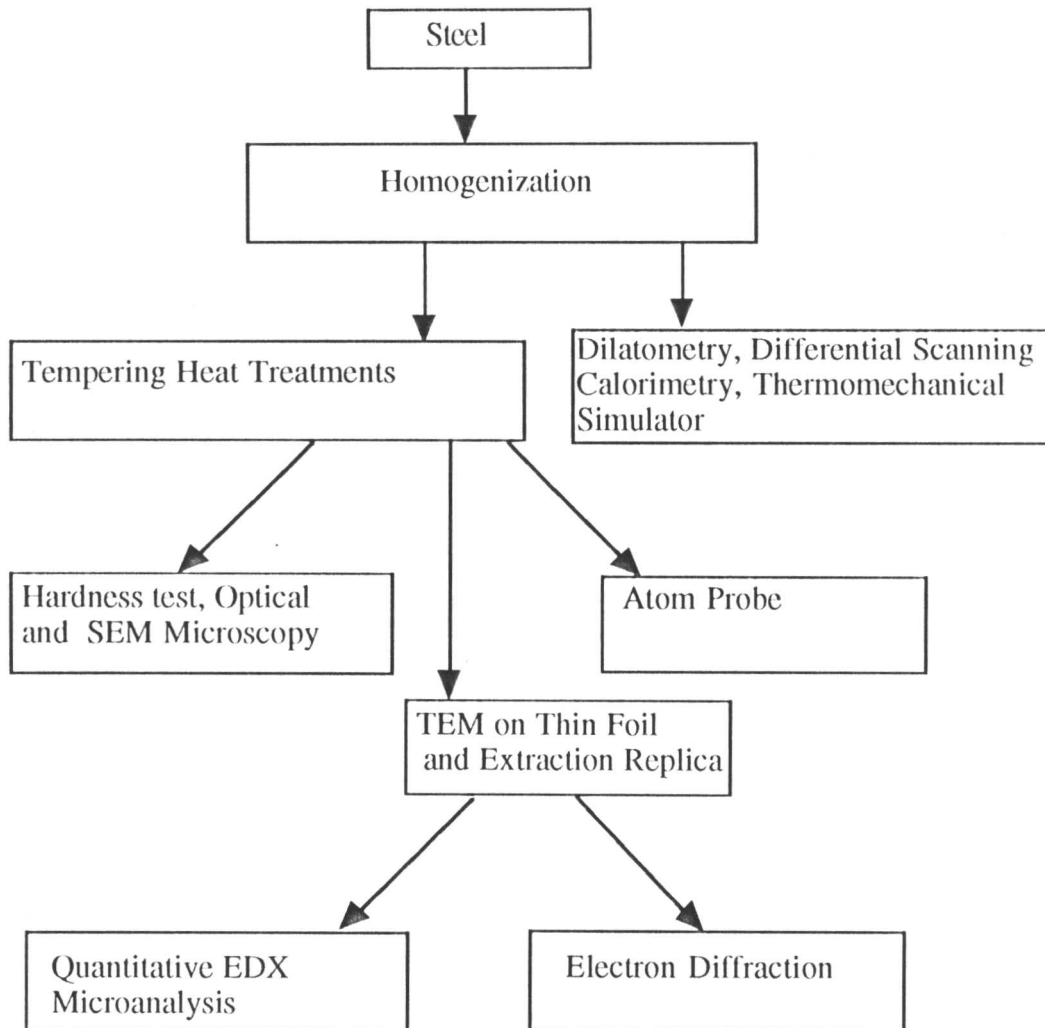


Fig. 2.1: Flow chart illustrating the experimental methods used.

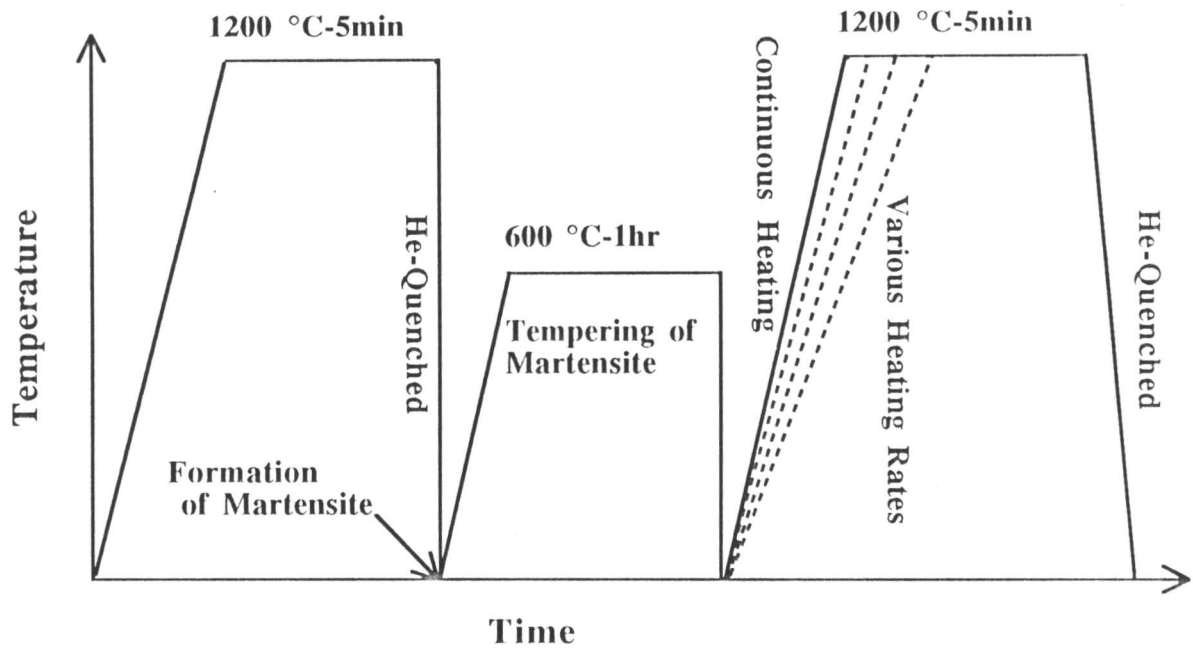


Fig. 2.2: Schematic illustration of the heat treatments cycles used.

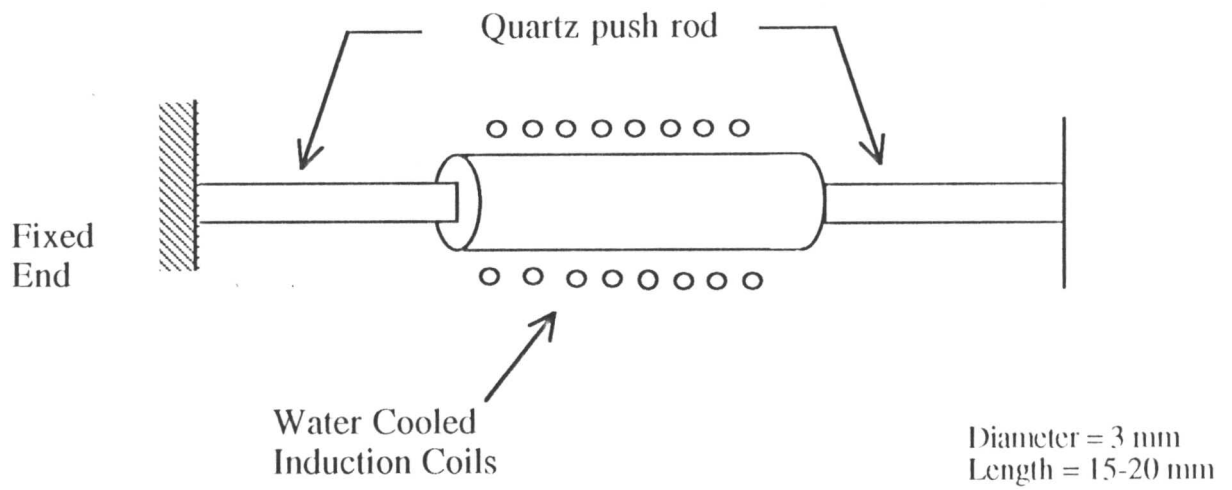


Fig. 2.3: Schematic illustration of the specimen set up in the dilatometer.

---

## Chapter 3

# THE EFFECT OF MOLYBDENUM ON THE MICROSTRUCTURE OF STEEL WELDS

---

### 3.1 Introduction

An investigation was carried out to determine the effect of molybdenum content on the microstructure and mechanical properties of multipass steel weld deposits. An examination of the weld metals in the as-deposited, reheated and tempered conditions was performed using optical and scanning electron microscopy. Observations of the primary weld metal microstructure using transmission electron microscopy are also presented. The effect of molybdenum on the microstructure and mechanical properties of low alloy steel welds has been investigated previously [Pacey *et al.*, 1982; Kayali *et al.*, 1983; Lundin *et al.*, 1986; Evans, 1988; Raiter and Gonzalez, 1988]. Generally, the addition of molybdenum has been found to increase the amount of acicular ferrite and decrease the volume fraction of allotriomorphic ferrite. The toughness can be significantly improved at low temperatures by increasing the percentage of fine grained acicular ferrite [Kayali *et al.*, 1983].

As the molybdenum concentration is increased, experimental data [Evans, 1988] indicate consistently that more of the primary microstructure is preserved than is indicated theoretically, both in the primary and reheated regions in multi-run steel welds. The aim of this investigation has been to reproduce the behaviour reported by Evans (1988) and also to find out the possible reasons for the increase in primary microstructure due to molybdenum in multirun steel welds. This chapter summarises the results of a microstructural study of a series of welds containing molybdenum.

### 3.2 Experimental Procedure

Transverse sections were machined from the all-weld metal test assemblies to perform the metallographic studies on the top beads, the high and the low temper-

ature reheated zones. The sectioned specimens were mechanically polished down to a  $1\mu\text{m}$  finish and etched in 2 % nital. The chemical compositions of the steels used are listed in chapter 2. Optical and scanning electron microscopy were used to characterise the microstructure of the welds. Measurements of the microstructure of the as-deposited weld metal were carried out using point counting on an optical microscope. The austenite grain size was measured by drawing test lines normal to the major axes of the columnar grains, consistent with the approach of Svensson *et al.* (1986). Specimens of the primary microstructure, were also prepared as thin foils for transmission electron microscopy.

### 3.3 Results and Discussion

#### 3.3.1 Calculation of Phase Diagrams and TTT Curves

Calculations of phase diagrams and TTT curves were carried out using a model developed by Bhadeshia (1981, 1982a). The results are presented in Figs. 3.1–3.2. The phase diagram shows three distinct curves [Bhadeshia and Edmonds, 1980]. The  $T_0$  curve is the locus of all points where austenite and ferrite of identical composition have equal free energies. The  $T'_0$  is a modification of the  $T_0$  curve to allow for  $400\text{ J mole}^{-1}$  of strain energy associated with the transformation. The  $Ae'_3$  curve represents the  $(\alpha + \gamma)/\gamma$  paraequilibrium phase boundary.

The TTT diagram consists of two separate ‘C’ curves in which one represents reconstructive and the other displacive transformations. The positions of the curves in the time/temperature domain are determined using a semi-empirical thermodynamic approach capable of taking account of C, Mn, Si, Ni, Cr, Mo and V in any reasonable combination, as long as the steel can be classified as a low-alloy steel [Bhadeshia, 1982].

The upper ‘C’ curve refers to the time taken for the initiation of the allotriomorphic ferrite transformation and the lower ‘C’ curve refers to the initiation of displacive transformations, such as the Widmanstätten ferrite and bainite reactions [Bhadeshia, 1981a, 1982]. It is assumed that the lower ‘C’ curve also describes the formation of acicular ferrite. The thermodynamically calculated martensite start temperature is also presented, as a horizontal line [Bhadeshia, 1981c, 1981d]. The weld metals studied in this investigation were especially designed in order to eluci-

date any molybdenum effect. The calculated phase and TTT diagrams for all the alloys are presented in Fig. 3.3. The effect of increasing molybdenum retards the displacive transformation and also depress the diffusional transformation. The calculated phase diagrams illustrate that the molybdenum lowers the transformation temperature from austenite to ferrite. This shows that calculated volume fraction of ferrite is decreased with the molybdenum concentration. It lowers  $T'_0$ ,  $T_0$  and  $Ae'_3$  curves with the molybdenum concentration.

The calculated  $Ae_3$ ,  $Ae'_3$ ,  $W_s$ ,  $B_s$  and  $M_s$  temperatures are given in Table 3.1. The calculation of  $Ae_3$  was carried using a program developed by Sugden and Bhadeshia (1988). There is not much difference between the  $W_s$ ,  $B_s$  and  $M_s$  temperatures of the variety of alloys, but the  $Ae_3$  and  $Ae'_3$  temperatures differ by some 30 °C as a function of the molybdenum concentration.

---



---

Table 3.1: Calculated transformation data for different alloys.

---

Alloy	$Ae_3$ °C	$Ae'_3$ °C	$W_s$ °C	$B_s$ °C	$M_s$ °C
Fe-0Mo wt.%	842	830	720	601	488
Fe-0.21Mo wt.%	859	843	720	607	497
Fe-0.42Mo wt.%	860	844	740	605	493
Fe-1Mo wt.%	875	855	740	593	490

---



---

### 3.3.2 Thermodynamic Calculations

The purpose was to investigate the different phases including  $Mo_2C$ ,  $Fe_3C$ ,  $\alpha$  and  $\gamma$  using MTDATA package for the alloys listed in Table 2.1. The results are presented in Fig. 3.4. The calculations have been done for the alloys in the temperature range of 500–1000 °C. The volume fraction of  $Mo_2C$  carbides were increases as a function of molybdenum. The austenite formation temperatures  $Ae_1$  and  $Ae_3$  were higher for the Fe-1Mo wt.% when compared against the Fe-0Mo wt.%.

### 3.3.3 Measurements of the Primary Microstructure

The primary microstructure refers to that which is unaffected by the deposi-

tion of other weld metal— it is the as-deposited microstructure. It was determined quantitatively by tracing the appropriate regions from micrographs onto a paper and then cutting and weighing. The ratio of the weight of the primary regions to the total weight is then assumed to reflect the volume percentage of primary microstructure. The results are shown in Table 3.2. The standard error of the weighted means,

$$\frac{\sigma}{\sqrt{n}}$$

are calculated as in Topping (1961). It is found that the error is approximately  $\pm 7\%$ .

The macrostructures of the welds are shown in Fig. 3.5, and illustrate the observed differences in etching response on alloying. Each weld deposit contained 27 runs in total with 3 beads per layer. Further detail is presented in Fig. 3.6, where ‘P’ refers to the primary microstructure, ‘R’ the reaustenitised regions and ‘T’ the tempered regions. The fraction of primary microstructures is clearly larger in the high molybdenum alloys, consistent with the results of Evans (1988).

### 3.3.4 Calculation of Microstructural Constituents

There exists a method for estimating the fraction of primary microstructure in a welded joint of the type concerned here [Bhadeshia *et al.*, 1985]. It is this method which originally indicated that there is something peculiar about molybdenum in welds. It is therefore instructive to use Bhadeshia’s method for the present alloys. The alloy composition and the measured austenite grain size together with welding conditions were the input parameters. The austenite grain size was measured in the transverse section of the weld by the mean lineal intercept technique. The intercept lines were drawn normal to the major axes of the columnar grains. The austenite grain structures are shown in Fig. 3.7 and the quantitative data in Table 3.3. It is found that there is no significant increase in the austenite grain size with molybdenum concentration.

Table 3.2: Quantitative data on the as-deposited microstructure.

ALLOY	Percentage of Primary microstructure
Fe-0Mo wt.%	40
Fe-0.21Mo wt.%	45
Fe-0.42Mo wt.%	55
Fe-1Mo wt.%	75

Table 3.3: Comparison of austenite grain structure. The calculations were carried out according to the model developed by Bhadeshia *et al.* (1985) and modified by the work of Svensson *et al.* (1986).

ALLOY	Mean Linear Intercept $\bar{L}_{tn}$ in $\mu\text{m}$		
	Experiment	Standard Deviation	Calculated
Fe-0Mo wt.%	87	32	97
Fe-0.21Mo wt.%	103	29	97
Fe-0.42Mo wt.%	82	17	92
Fe-1Mo wt.%	81	35	90

### 3.3.5 Microstructure of As-deposited Weld Metal

The aim here was to identify the key microstructural constituents of the weld metals in their as-deposited state (Fig. 3.8). Four major microstructural components could be identified:

- allotriomorphic ferrite;
- bainite;
- Widmanstätten ferrite;
- acicular ferrite.

Point count measurements of allotriomorphic ferrite, Widmanstätten ferrite, acicular ferrite and bainite are presented in Table 3.4. It is noted that Widmanstätten ferrite forms as thin wedge shape nucleated from austenite grain boundaries and also develops from the grain boundary allotriomorphic ferrite. While bainite forms as sheaves of fine plates originating from austenite grain boundaries. The

sheaf grows by the repeated nucleation and growth of new sub-units. The initial nucleation event takes place at the prior austenite grain boundaries and subsequently, sub-units nucleate and grow from the tips of the previous sub-units [Christian and Edmonds, 1984; Bhadeshia and Christian, 1990]. The point count measurements were in each case based on 1000 observations. The standard error of the observations is calculated as in Topping (1961). It is found that the error is approximately  $\pm 4\%$ . The results indicate a continuous trend of decreasing allotriomorphic ferrite content with increasing molybdenum concentration. It was found that the calculated volume fraction of allotriomorphic ferrite [Bhadeshia *et al.*, 1985] was greater than that measured, the discrepancy increasing with the molybdenum concentration. A comparison of the data is presented in Figs. 3.9–3.10. It is evident that as the molybdenum concentration increases, the amount of acicular ferrite increases at the expense of allotriomorphic ferrite. It is well known that alloying elements such as Mn, and especially molybdenum, delay the precipitation of grain boundary components and they promote the appearance of acicular ferrite [Pacey *et al.* 1982; Evans, 1988]. However, at 1 wt.% molybdenum acicular ferrite replaced by bainite. This is also supported by the fact that Fe–2.25Cr–1Mo wt.% weld deposits used in the power generation industry exhibit a bainitic structure in the as-deposited condition in spite of the presence of inclusions [Klueh, 1974b; Wada and Eldis, 1982; Kar and Todd, 1982; Lundin *et al.*, 1986; Vitek *et al.*, 1986; Mcgrath *et al.*, 1989]. The amount of Widmanstätten ferrite also decreased with increasing Mo concentration.

Further detailed microscopy was carried out using SEM. The results essentially confirmed the optical metallography (Fig. 3.11–3.12). Transmission electron microscopy confirmed that the Fe–1Mo wt.% contain a bainitic microstructure (Fig. 3.13). Note the parallel sub-units which are in identical crystallographic orientation in space, and the light grey regions of retained austenite between the sub-units of bainite.

### *3.3.6 Microstructure of the Reheated Weld Metal*

SEM examination of the high and low peak temperature reheated regions (coarse and fine  $\gamma$ -grained regions) showed an important change in the microstructure as the molybdenum concentration increased. A grain boundary ferrite network

Table 3.4: Microstructural constituents in the welds containing molybdenum.

ALLOY	Microstructural component in %						
	$\alpha$ exp.	calc.	$\alpha_w$ exp.	calc.	$\alpha_a$ exp.	$\alpha_b$ exp.	$\alpha_a + \alpha_b$ calc.
Fe-0Mo wt.%	35	35	40	26	20	05	39
Fe-0.21Mo wt.%	40	43	30	40	25	05	17
Fe-0.42Mo wt.%	24	40	20	31	46	10	29
Fe-1Mo wt.%	05	41	05	27	30	60	32

exp. → experimental determination (point count analysis),  
 calc. → calculated using Bhadeshia *et al.*, (1985) model.

was found in the high temperature reheated region of the molybdenum free weld metal. As the molybdenum content increased the amount of the allotriomorphic ferrite was progressively reduced. The microstructure is bainite and acicular ferrite in high molybdenum alloys (Fig. 3.14).

The microstructure of the low temperature reheated region was markedly influenced by molybdenum additions (Fig. 3.15). SEM studies of the reheated zone showed that the microstructure is the mixture of acicular ferrite and bainite in the high molybdenum weldments and allotriomorphic ferrite and Widmanstätten ferrite in the low molybdenum weldments.

Thus, the microstructure has been verified to consist of a mixture of acicular ferrite and bainite in the high molybdenum welds. Widmanstätten ferrite and allotriomorphic ferrite are found in extremely small quantities.

### 3.3.7 Hardness Testing

Hardness tests were carried out in the as-deposited, reheated and tempered regions of the weld deposits using Vickers hardness testing machine. The results along the the centre-line of the weld deposit are plotted in Fig. 3.16. The molybdenum additions produced a hardness difference of 60–70 HV5 in the top bead, and this occurred also in the upper half. In the lower part, a divergence occurred, repeated thermal cycling causing softening in the molybdenum free weld and hardening in

the weld containing 1 wt.% molybdenum. The hardness of the different zones of the weld deposits are presented in Fig. 3.17. It was also found that the reheated regions of the Fe-1Mo wt.% have a larger value of hardness when compared against the Fe-0Mo wt.% alloy. The results also illustrate that there are smaller fluctuations in the hardness for the alloys rich in molybdenum.

### 3.4 Summary and Conclusions

The primary microstructure of the fusion zone of all weld deposits has been characterised. It is found that the fraction of primary microstructure in the multirun welds increased with the molybdenum concentration. A possible reason is that molybdenum somehow retards the reaustenitization. This hypothesis is investigated in detail in chapter 4. It is also found that the microstructure tends to become rich in bainite and acicular ferrite as the molybdenum concentration increases, at the expense of allotriomorphic ferrite and Widmanstätten ferrite. The microstructure in the reheated zones also show similar trends. No significant changes in the columnar austenite grain size were observed as a function of the alloy chemistry.

The addition of molybdenum to the weldments increased the hardness of the as-deposited metal. The hardness of the high and low temperature reheated regions also increased with increasing molybdenum. It will be shown later that the changes in hardness due to molybdenum are considerably larger than would be expected from solid solution hardening effects alone.

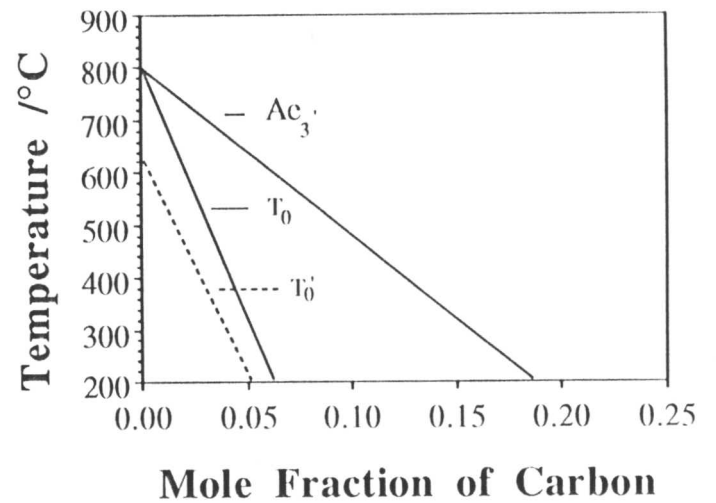
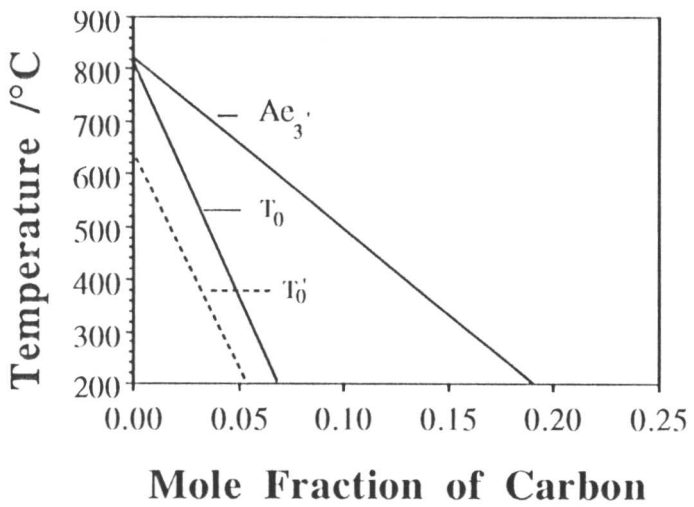
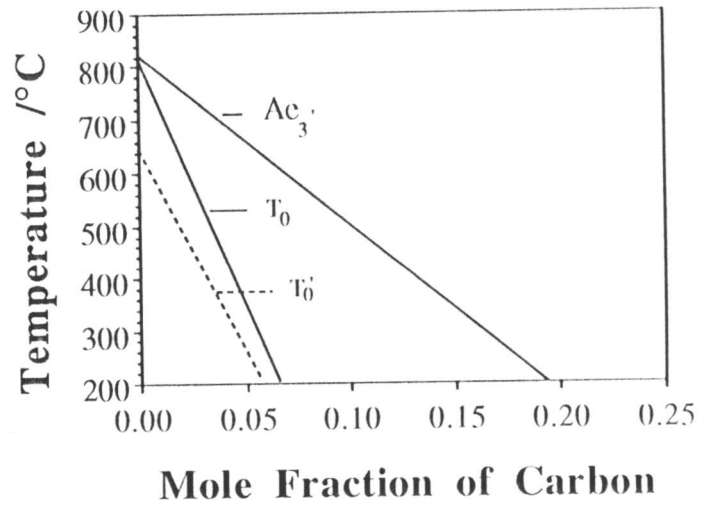
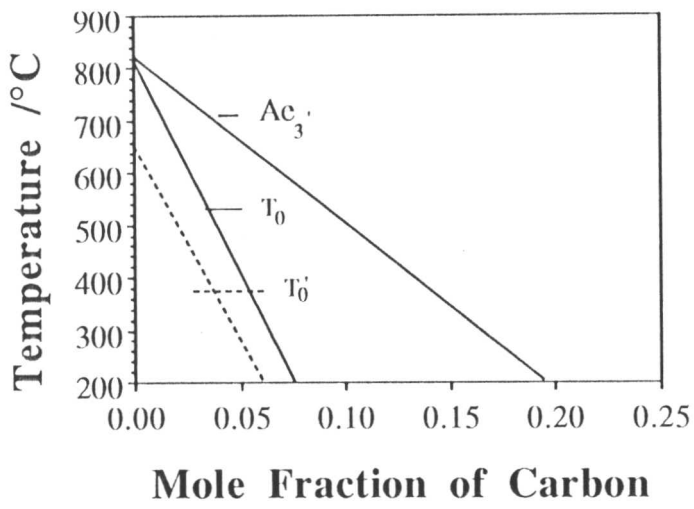
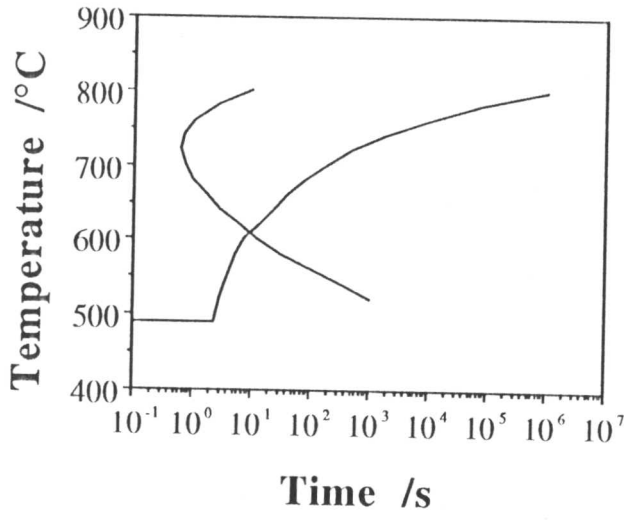
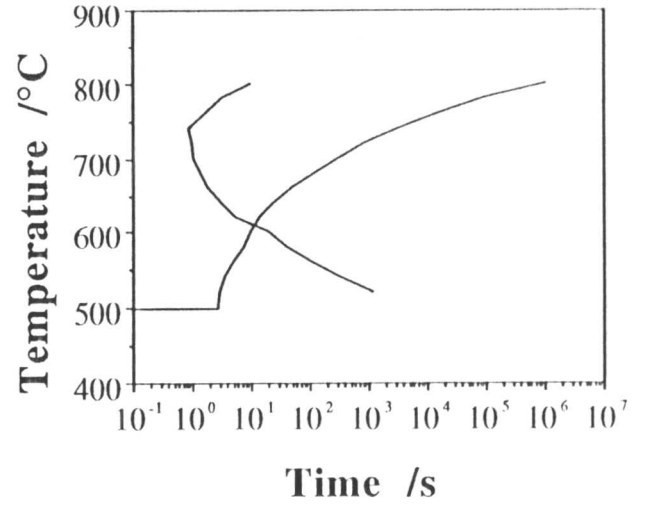


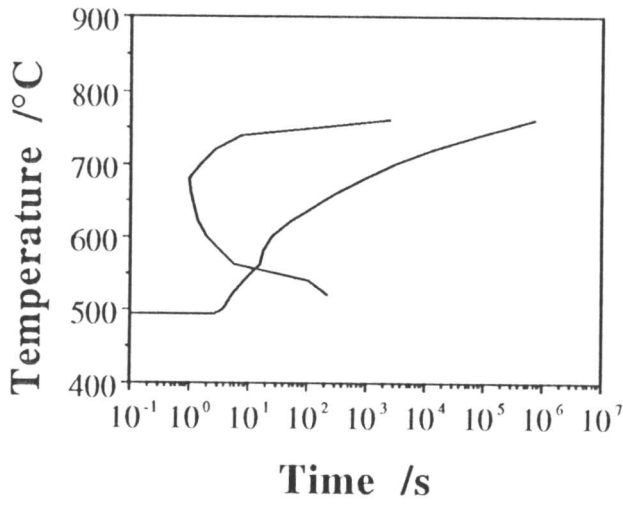
Fig. 3.1: Calculated phase diagrams for weld metals.



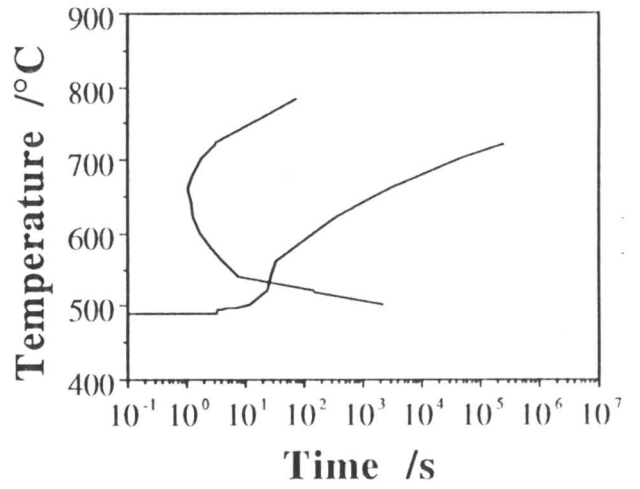
Fe-0Mo wt. %



Fe-0.21Mo wt. %

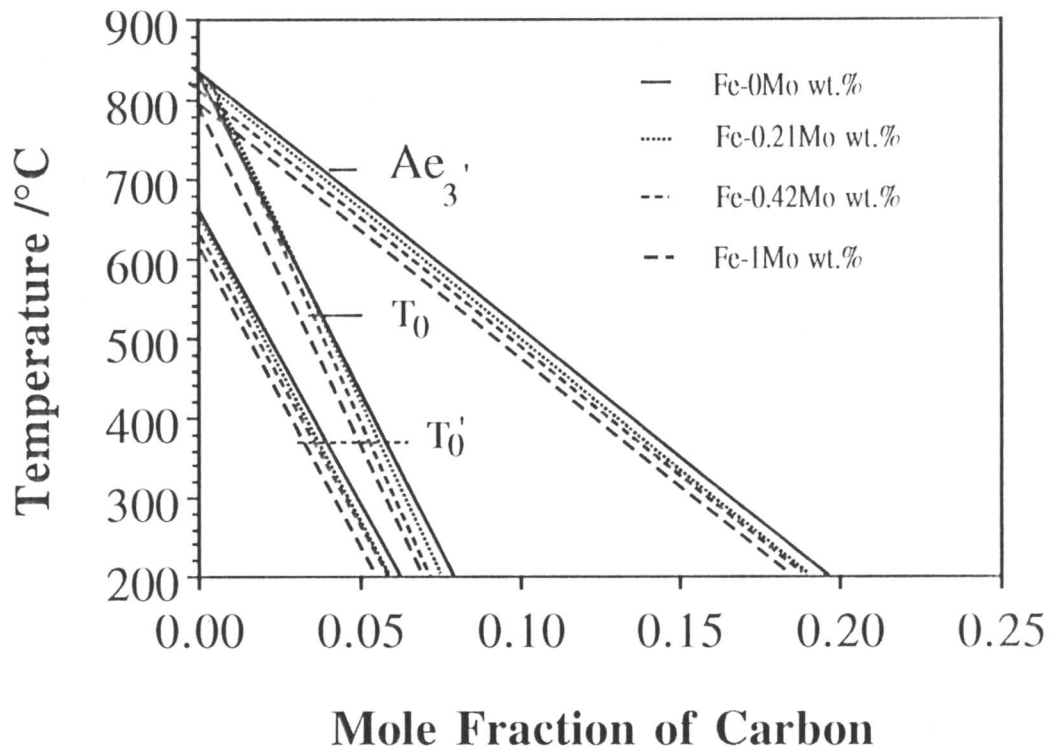


Fe-0.42Mo wt. %

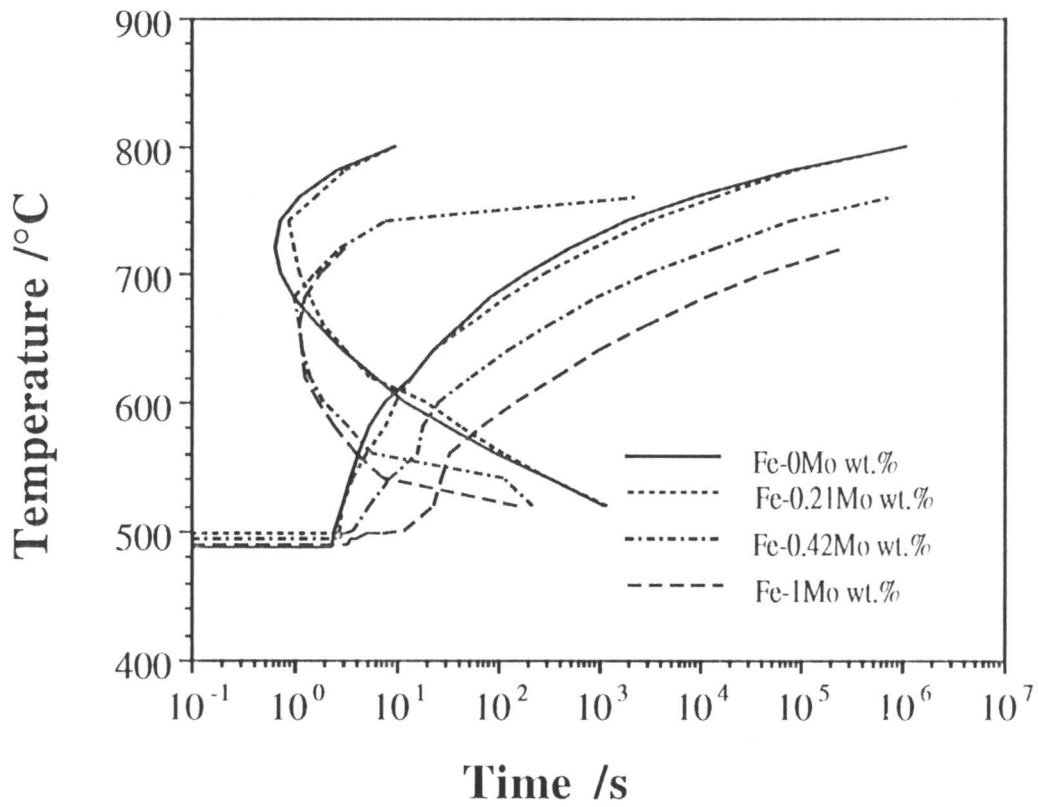


Fe-1Mo wt. %

Fig. 3.2: Calculated TTT diagrams for weld metals

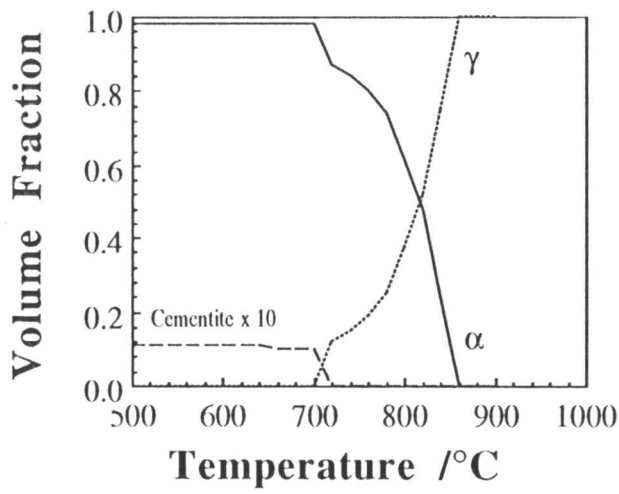


(a)

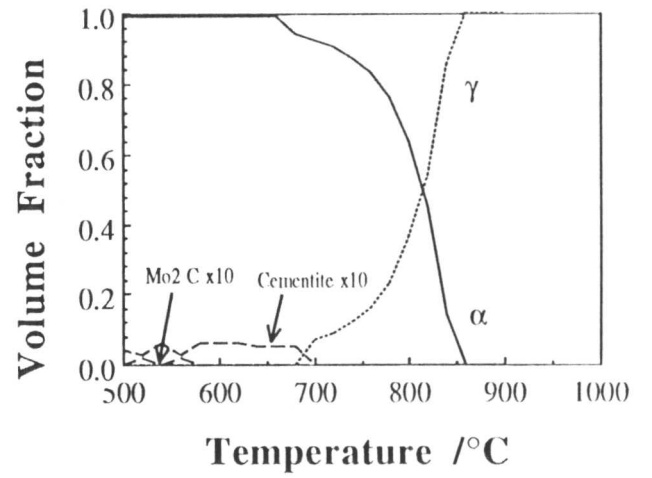


(b)

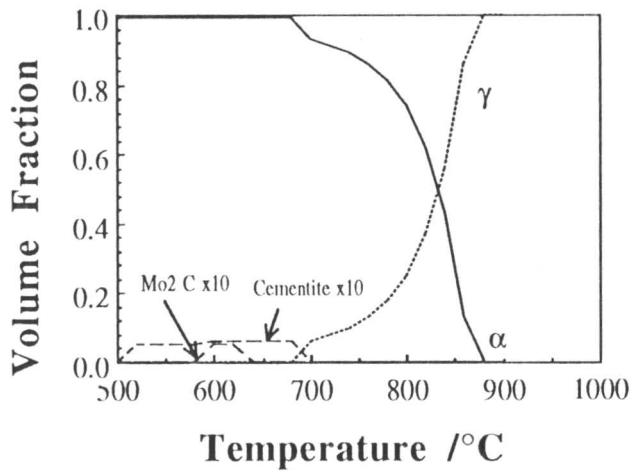
Fig. 3.3: A comparison of calculated phase and TTT diagrams for all the alloys.



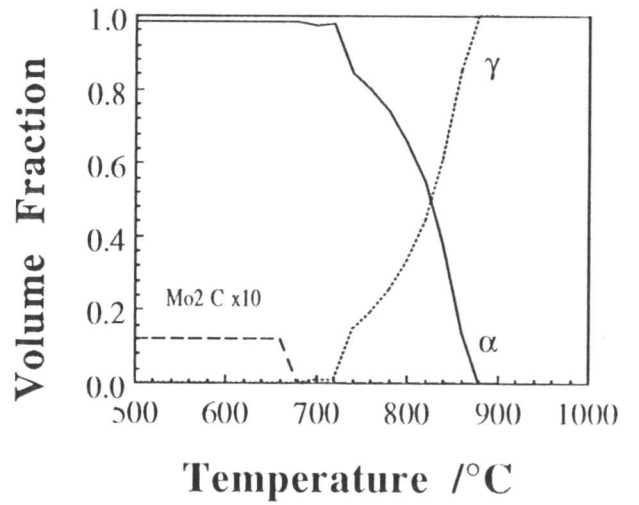
Fe-0Mo wt. %



Fe-0.21Mo wt. %

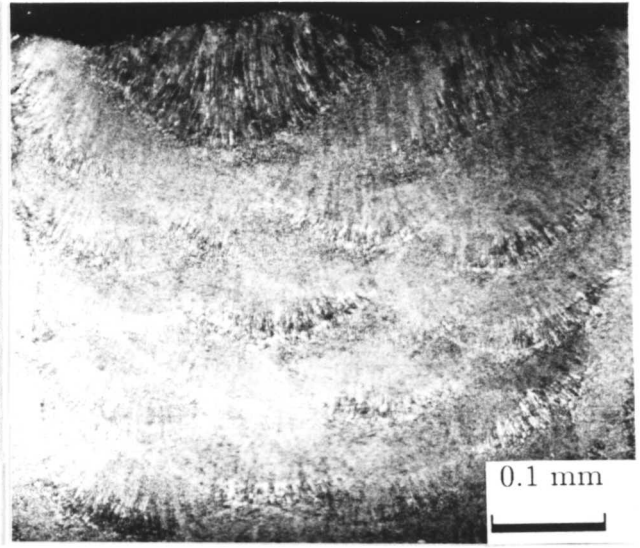
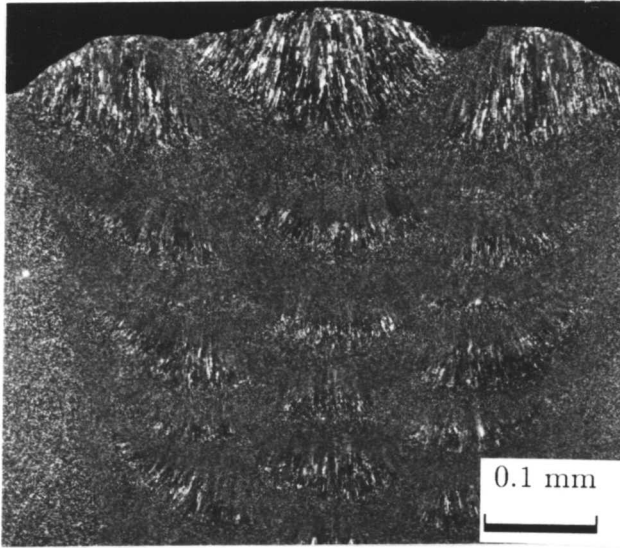


Fe-0.42Mo wt. %



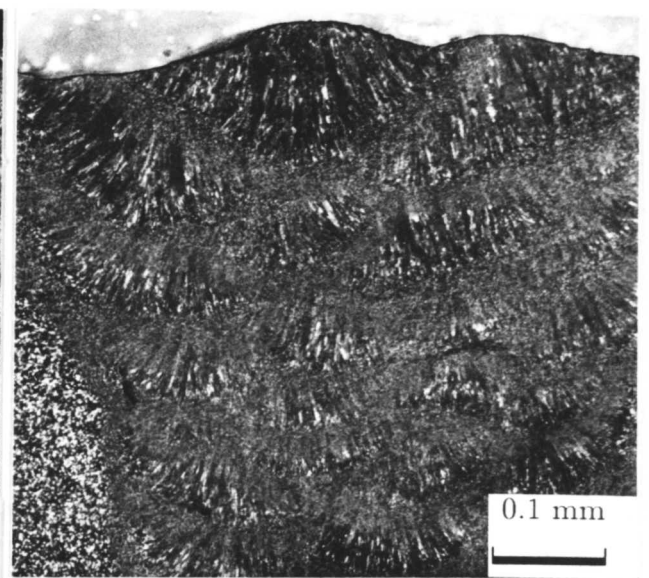
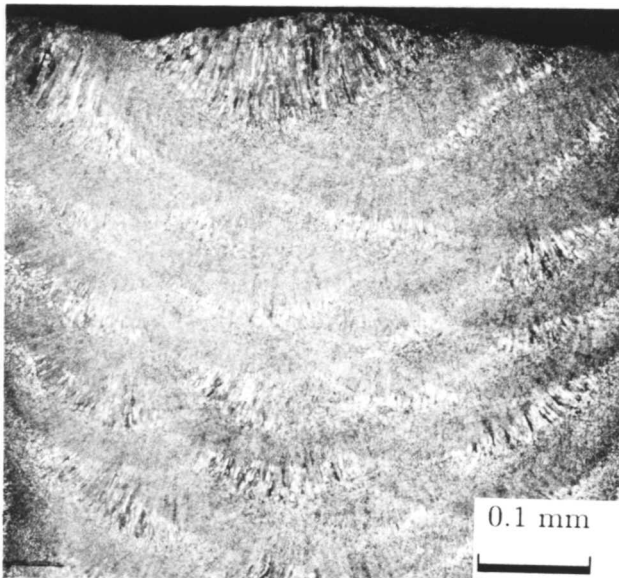
Fe-1Mo wt. %

Fig. 3.4: Showing the calculated equilibrium volume fractions of different phases as a function of temperature.



Fe-0Mo wt.%

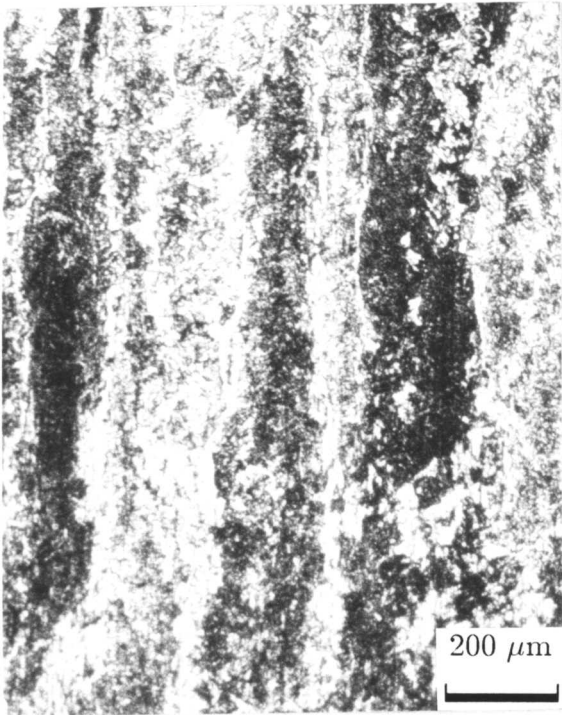
Fe-0.21Mo wt.%



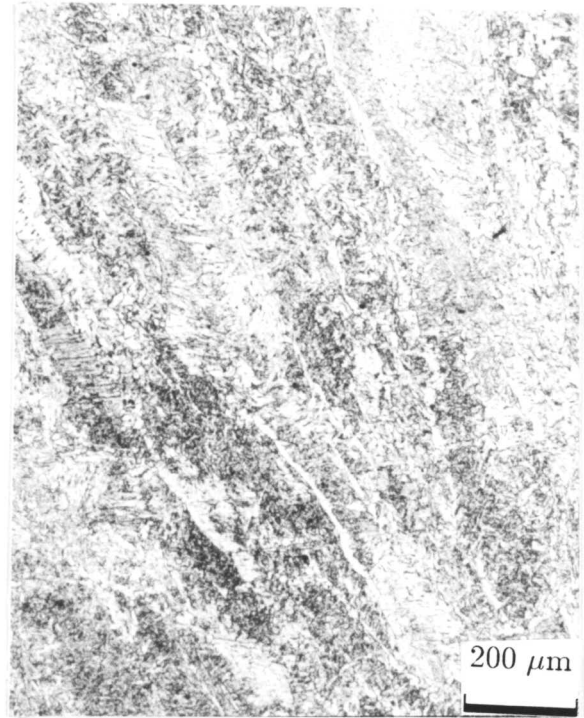
Fe-0.42Mo wt.%

Fe-1Mo wt.%

Fig. 3.5: Macrographs of the typical manual metal arc weld deposits.



Fe-0Mo wt.%



Fe-0.21Mo wt.%

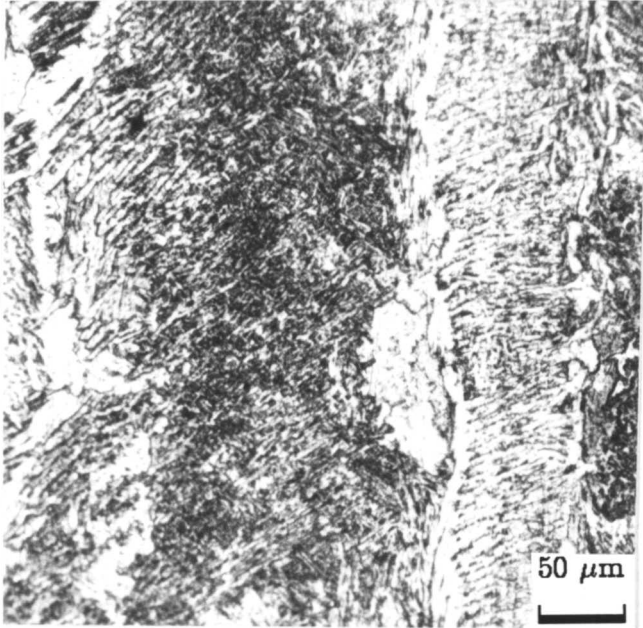


Fe-0.42Mo wt.%

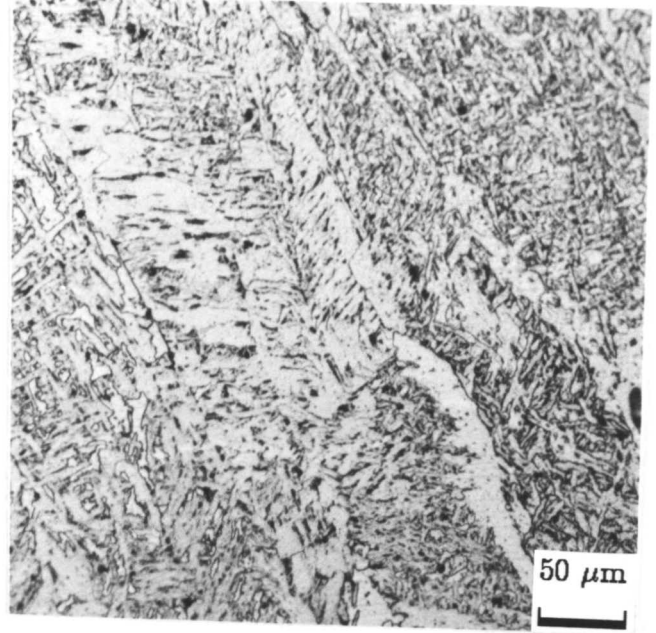


Fe-1Mo wt.%

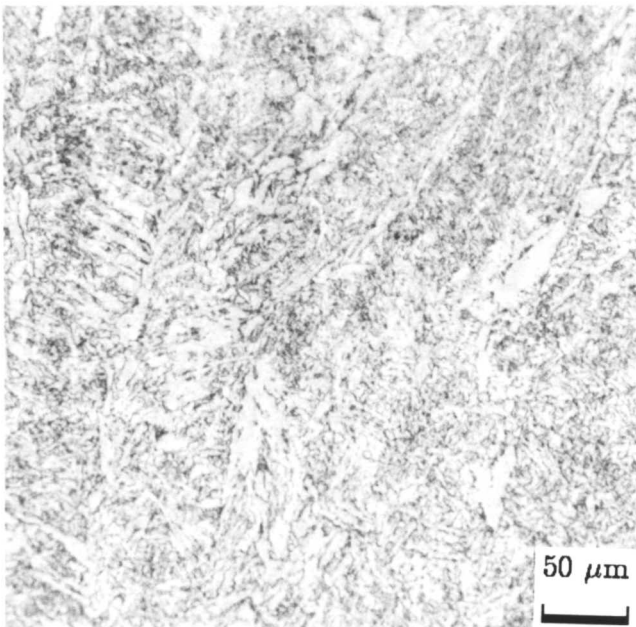
Fig. 3.7: The austenite grain structures in the as-deposited weld metal regions.



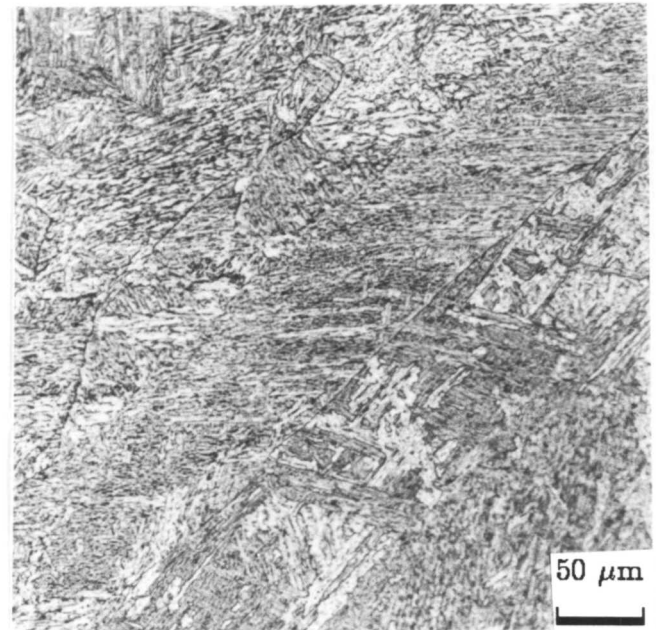
Fe-0Mo wt.%



Fe-0.21Mo wt.%



Fe-0.42Mo wt.%



Fe-1Mo wt.%

Fig. 3.8: Optical micrographs of the as-deposited weld metal regions.

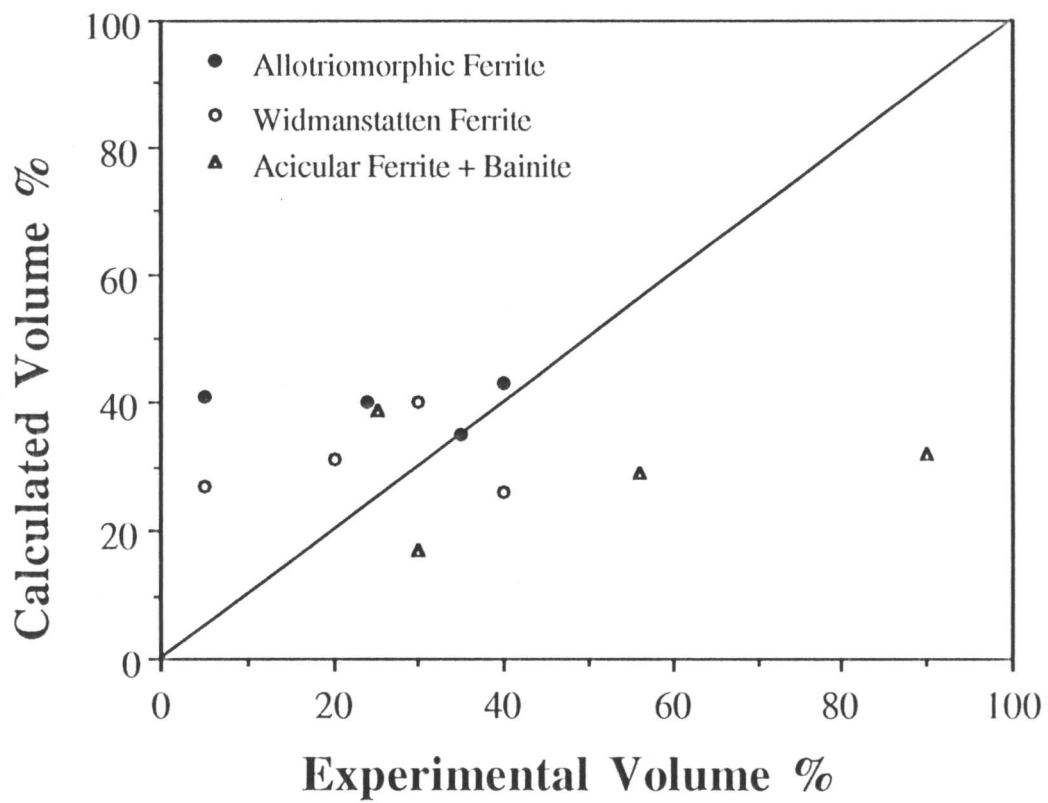
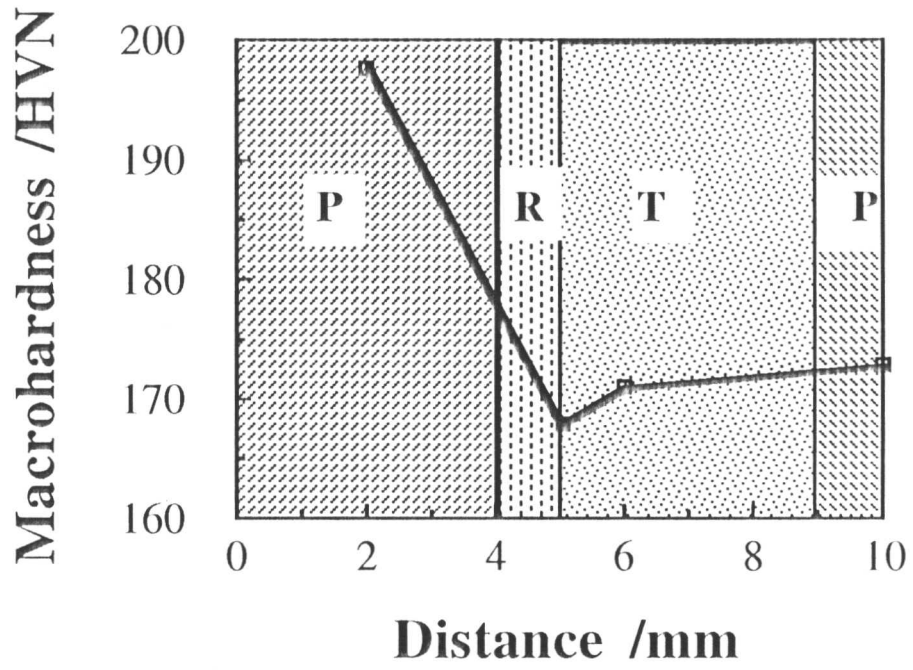
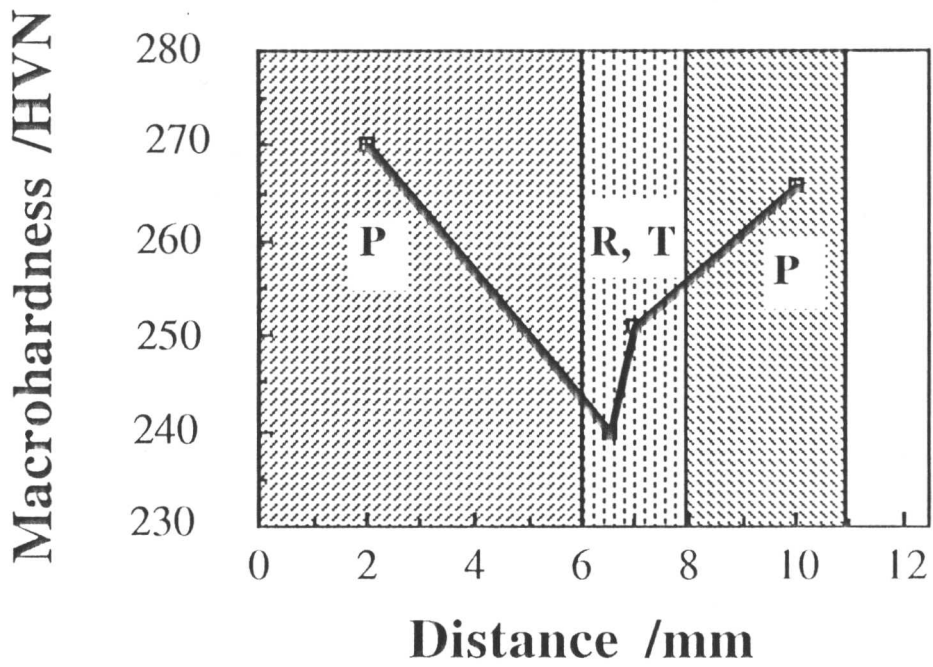


Fig. 3.9: A comparison of the calculated [Bhadeshia *et al.*, 1985] and measured microstructures of the experimental alloys.

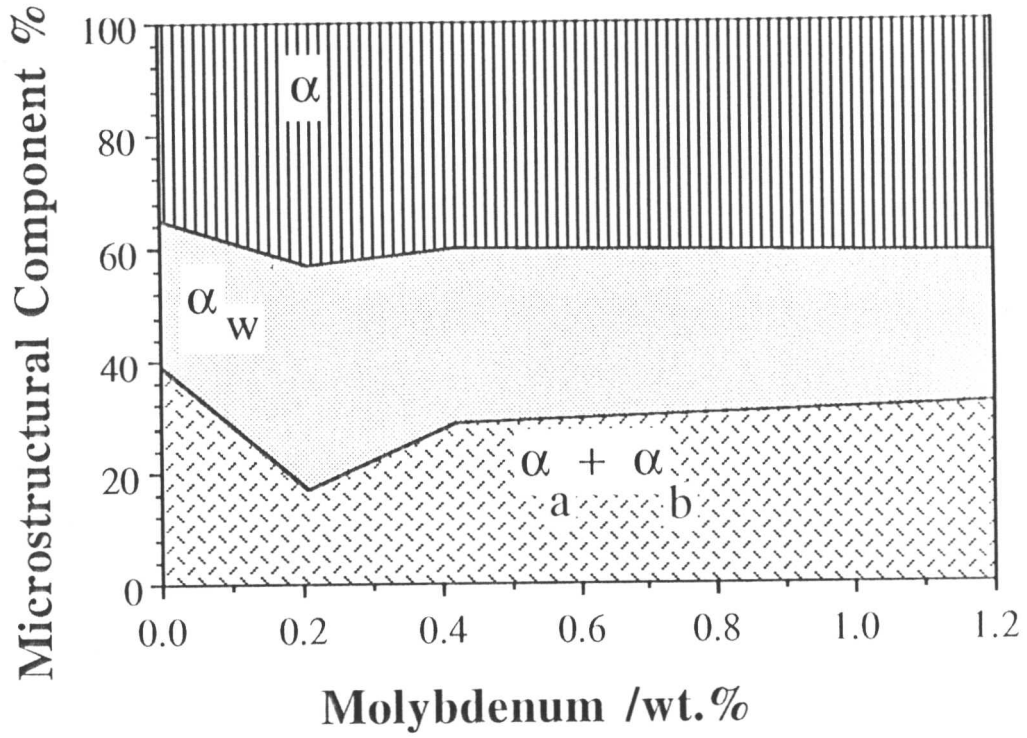


(a)

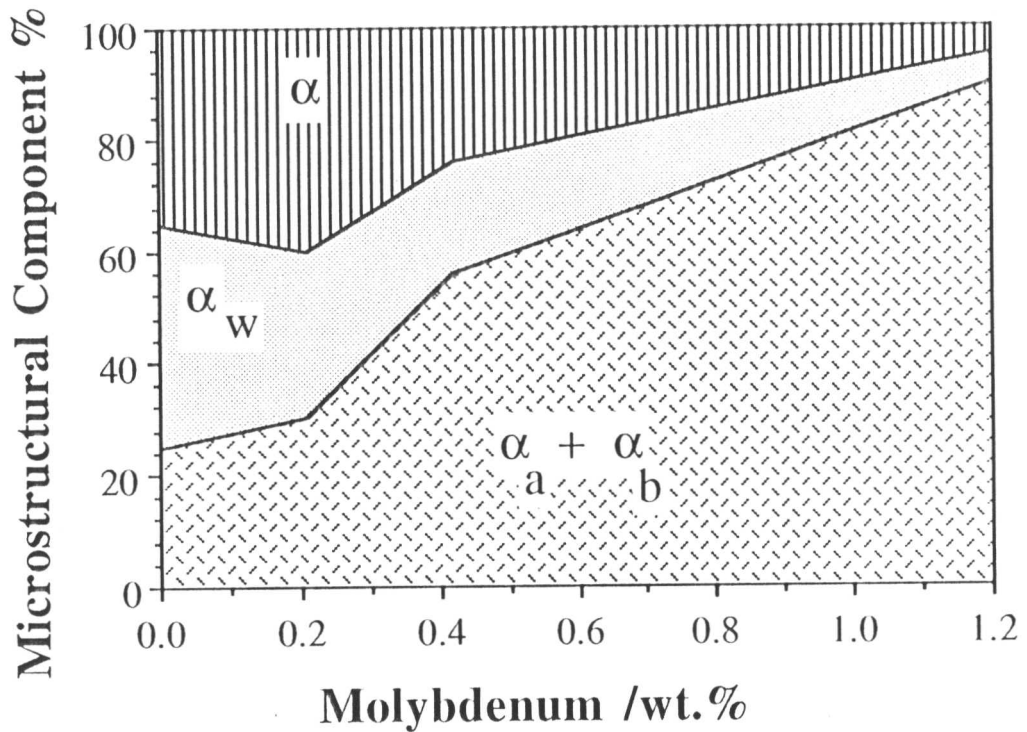


(b)

Fig. 3.6: Showing different weld metals zones. (a) Fe-0Mo wt.% (b) Fe-1Mo wt.%.



(a)



(b)

Fig. 3.10: The effect of molybdenum on the microstructure of the as-deposited weld metal. (a) Calculated microstructure (b) Experimentally observed microstructure.

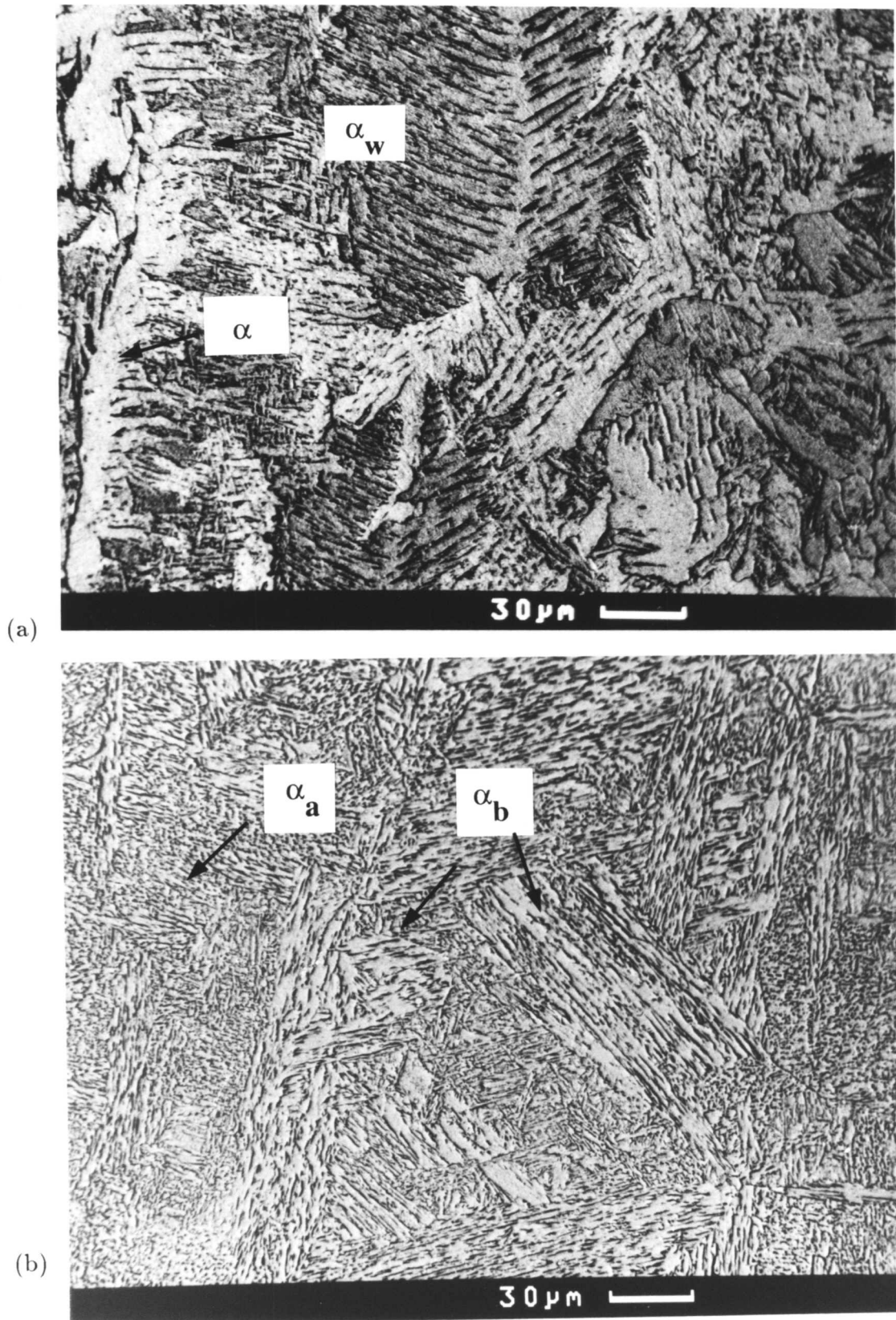


Fig. 3.11: SEM micrographs showing primary microstructure. (a) Showing allotriomorphic ferrite and Widmanstätten ferrite for the Fe-0Mo wt.%. (b) Showing a mixture of bainite and acicular ferrite for the Fe-1Mo wt.%.

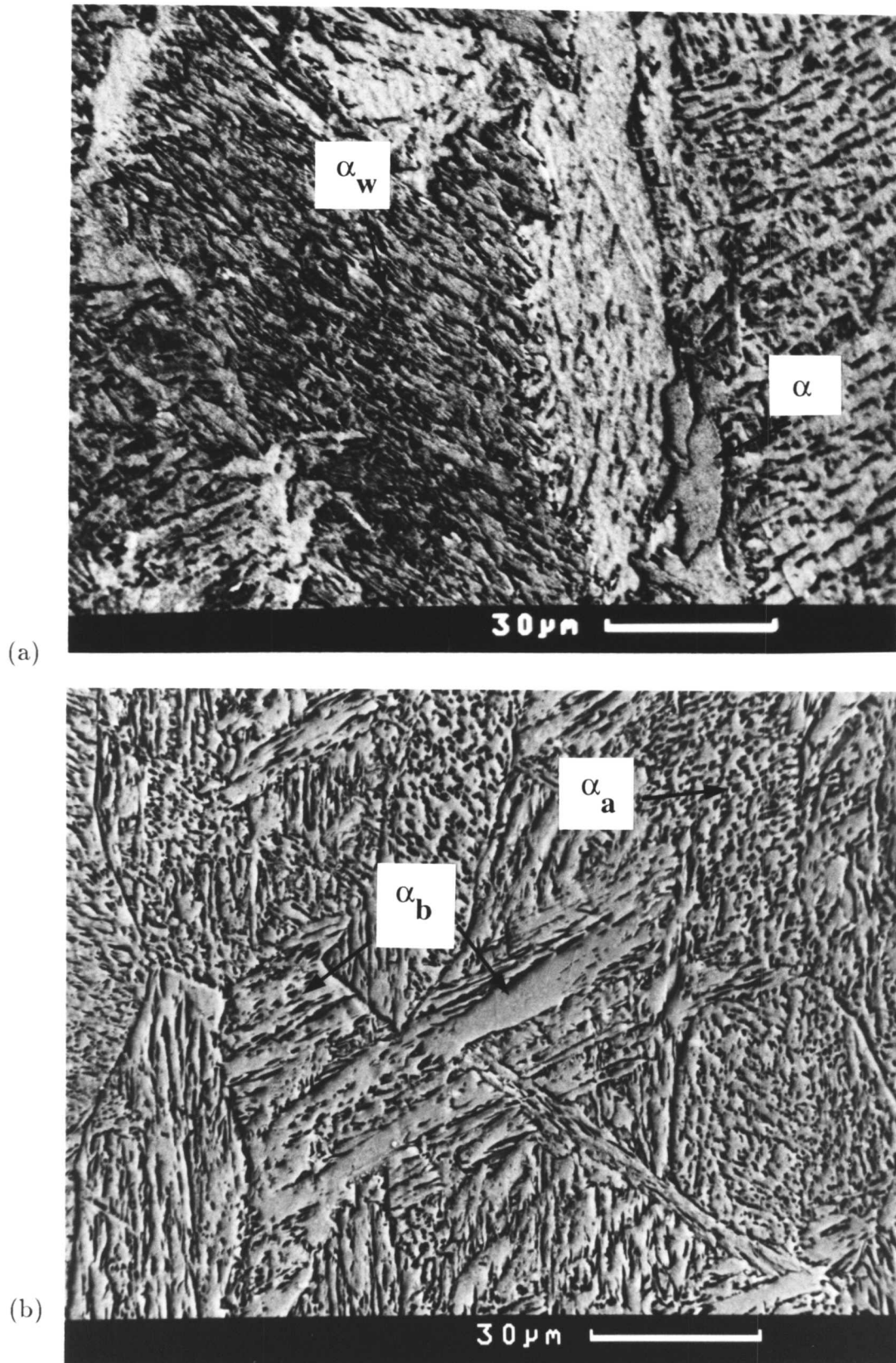


Fig. 3.12: SEM micrographs on high magnification showing primary microstructure.  
(a) Showing allotriomorphic ferrite and Widmanstätten ferrite for the Fe-0Mo wt.%.  
(b) Showing a mixture of bainite and acicular ferrite for the Fe-1Mo wt.%.

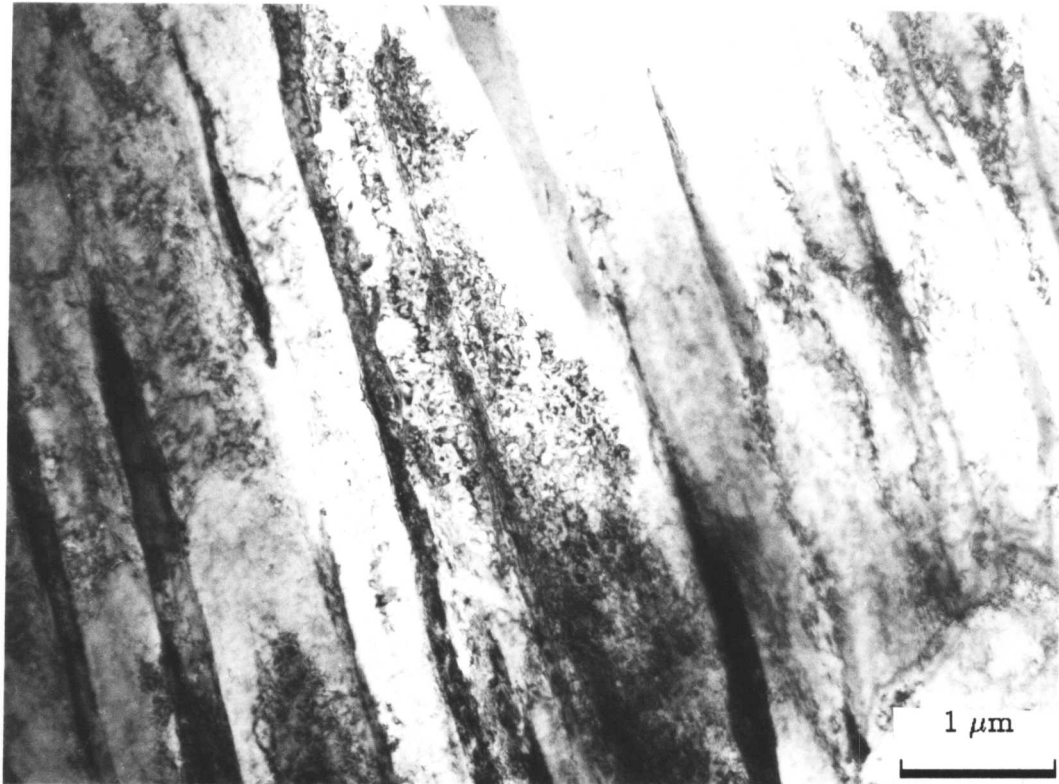
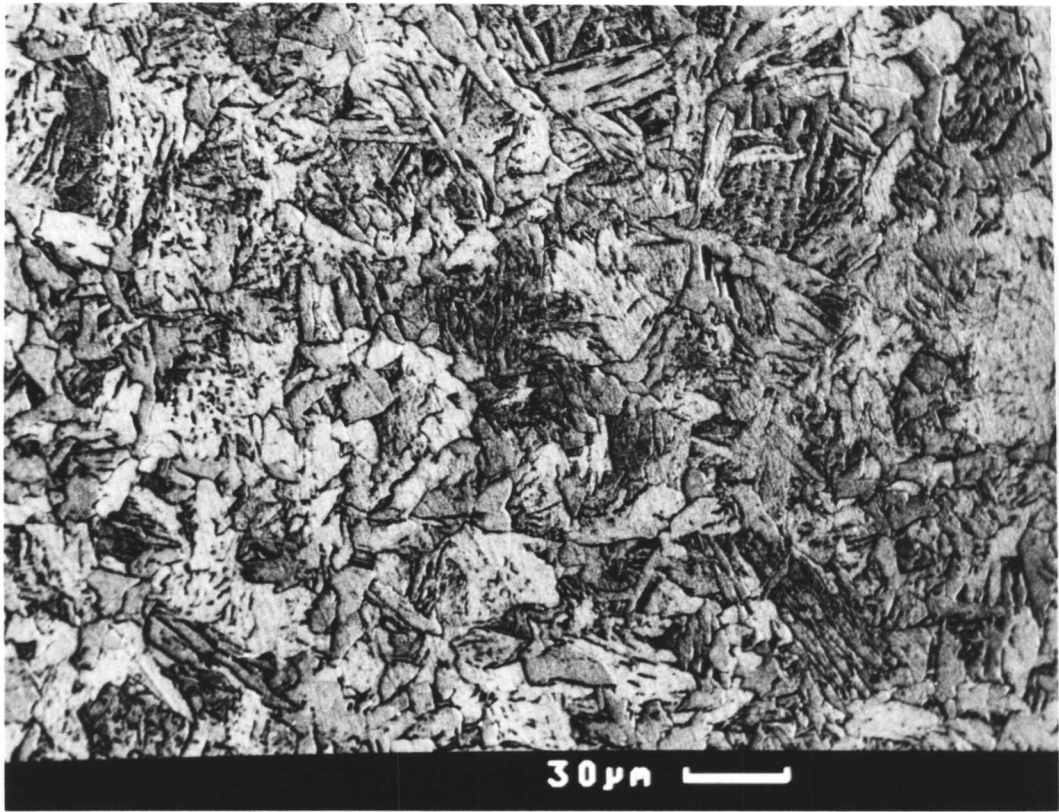
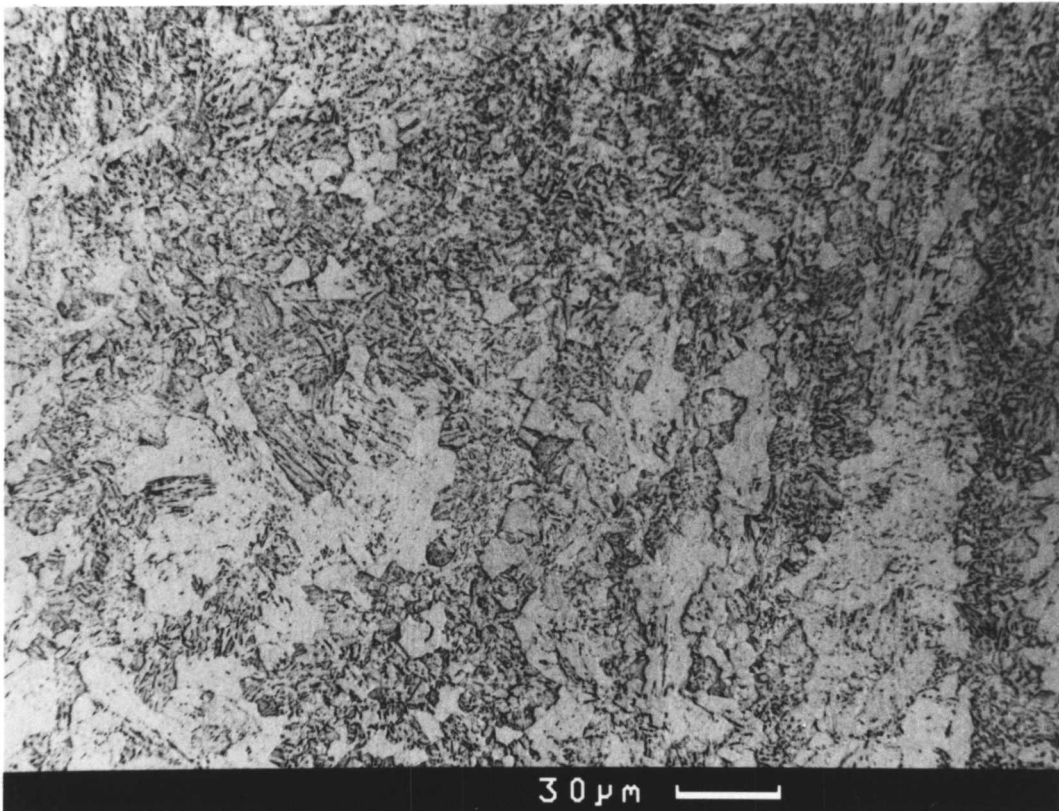


Fig. 3.13: Bright field transmission electron micrograph of the bainitic microstructure in Fe-1Mo wt.%. Note the parallel sub-units which are in identical crystallographic orientation in space, and the light grey regions of retained austenite between the sub-units of bainite.

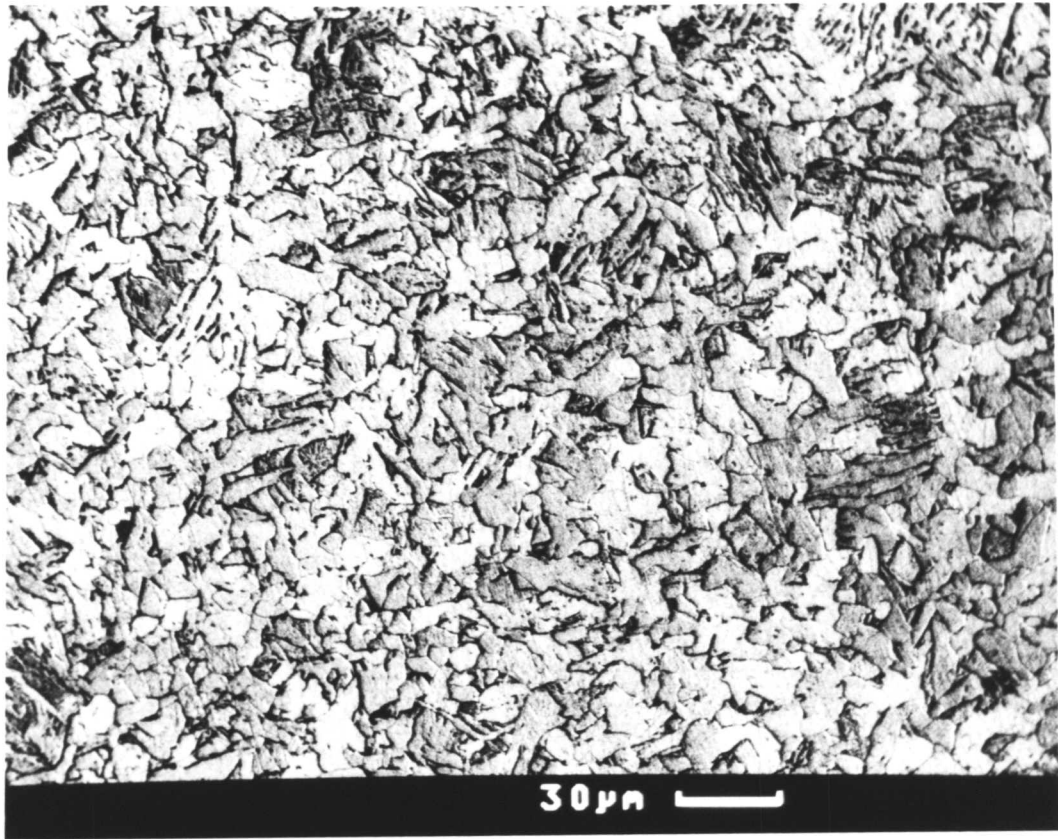


(a)

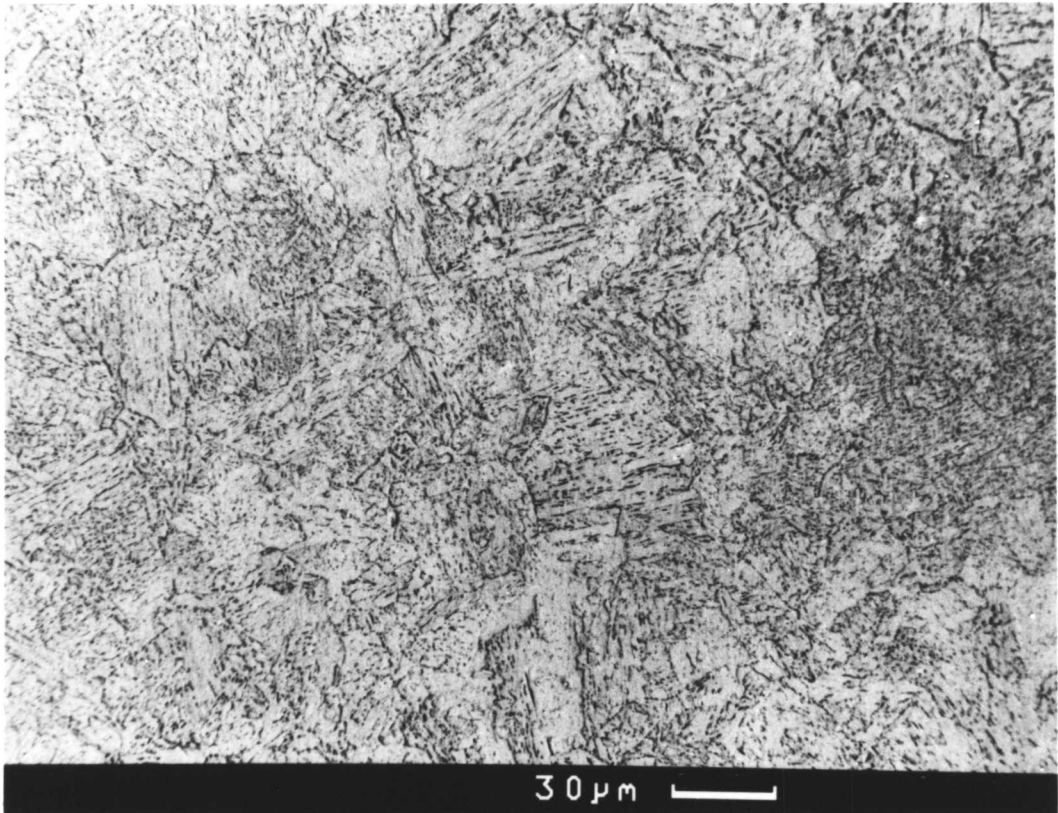


(b)

Fig. 3.14: SEM micrographs showing microstructure of the reheated zone in weld metal deposits. (a) Fe-0Mo wt.% (b) Fe-1Mo wt.%.



(a)



(b)

Fig. 3.15: SEM micrographs showing microstructure of the low temperature reheated zones. (a) Fe-0Mo wt.% (b) Fe-1Mo wt.%.

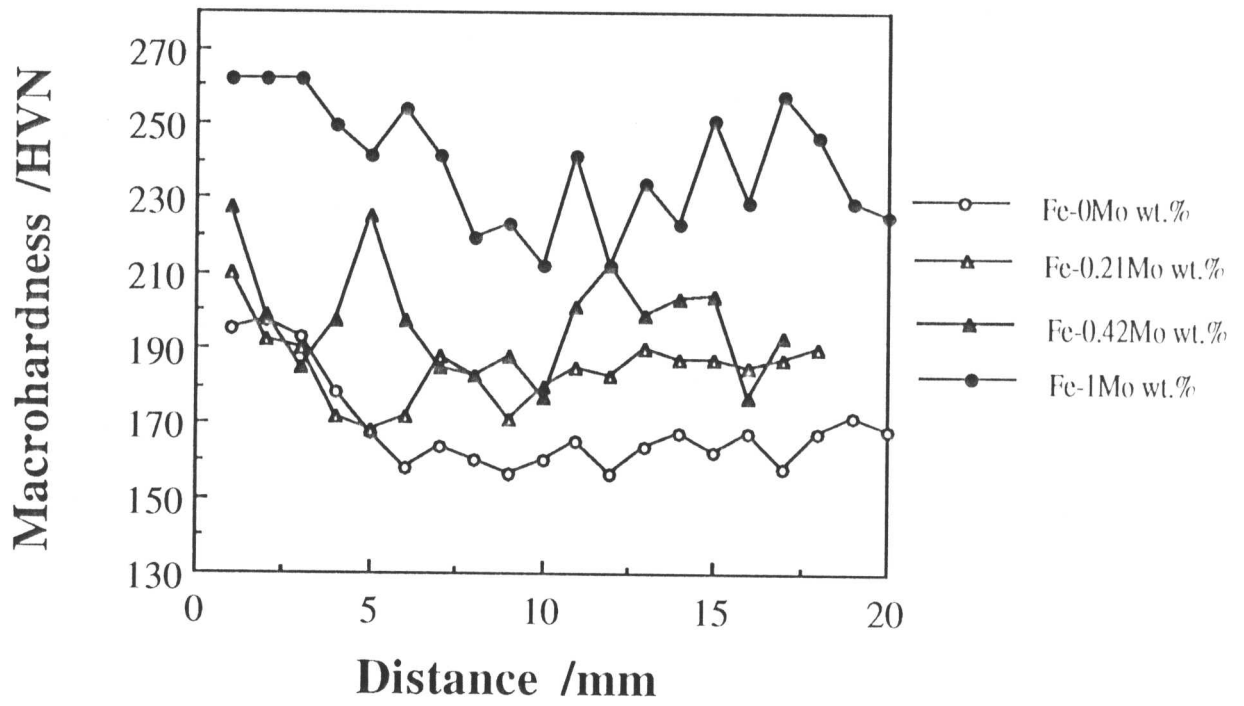


Fig. 3.16: Typical hardness variations across a multipass weld metal regions.

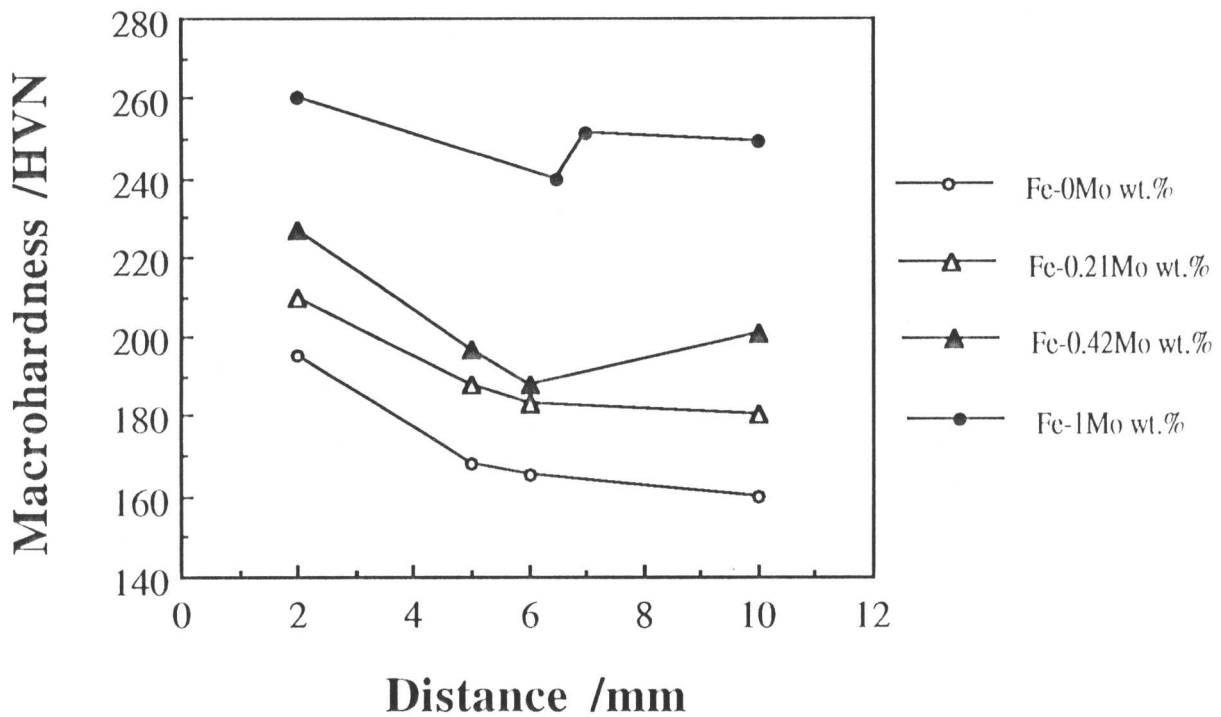


Fig. 3.17: The hardness of the different zones of the weld metal deposits.

---

## Chapter 4

# THE EFFECT OF MOLYBDENUM ON THE AUSTENITISATION BEHAVIOUR OF STEEL WELDS

---

### 4.1 Introduction

Molybdenum-containing multipass steel welds exhibit anomalous microstructures. It is possible that some of the anomalies may be attributed to the influence of molybdenum on the austenitisation behaviour. An investigation has been carried out to study the effect of molybdenum on the austenitisation behaviour of multipass steel weld deposits. The kinetics of austenitisation were investigated for alloys with different molybdenum contents, initially with starting microstructures of tempered martensite. The effect of molybdenum in multipass steel welds has been investigated by Evans (1988) who observed an increase in the amount of primary microstructure with rising molybdenum concentration. The preliminary microstructure study shows the retention of primary microstructure in 1 wt.% molybdenum containing alloy (Fig. 4.1). It has also been noticed that predicted strength is underestimated as molybdenum concentration increases in the weld (Fig. 4.2). The strength calculation for manual metal arc welds, were carried out from the model developed by Bhadeshia *et al.* (1985). There could be two reasons for this, first that the reaustenitisation temperature is raised by molybdenum and second could be the tempering resistance of the microstructure is raised.

The present work is an attempt to understand this phenomenon starting with the hypothesis that the molybdenum effect has something to do with the kinetics of austenite formation during multipass welding. It is believed, for example, that the fraction of primary microstructure depends on how alloy chemistry influences the austenitisation process. The kinetics of austenitisation were investigated for alloys with different molybdenum contents, initially with starting microstructures of tempered martensite. The major purpose of tempering is to avoid transient tempering effects during heating, which would otherwise complicate analysis.

Of course, a tempered martensite microstructure is only one of the many kinds of microstructures present in a multirun weld, but there is a particular reason for choosing tempered martensite. It is speculated that the molybdenum effect arises because very fine clusters or precipitates (of the kind not easily observed using conventional transmission electron microscopy) of molybdenum hinder austenite growth. Thus, the heat input as one layer of weld metal is deposited onto another has a lesser effect on the underlying microstructure, so that more of the primary microstructure is preserved. The heat treatment at 650 °C was supposed to induce the molybdenum clustering /precipitation prior to austenitisation. On the other hand, 350 °C temperature was used to form a control sample since no substantial diffusion of substitutional solutes can be expected at such a low temperature.

The continuous heating transformation (CHT) behaviour of weld metals is also investigated in order to understand the kinetics of austenitisation as a function of heating rate, alloy composition and other variables. Some research dealing with the initial microstructure effect on the morphology of austenite, has already been done [Speich *et al.*, 1969; Law and Edmonds, 1980; Speich *et al.*, 1981; Garcia *et al.*, 1981; Souza *et al.*, 1982; Lenel and Honeycombe, 1984; Cal *et al.*, 1985; Yang and Bhadeshia, 1987, 1989, 1990]. Many investigators have examined in detail the formation of austenite from martensitic low carbon steels. [Kinoshita and Ueda, 1974; Matsuda and Okamura, 1974; Homma, 1974; Watanabe and Kunitake, 1976]. It has been found there are two types of austenite morphology, acicular and globular austenite, dependant on the condition of the prior microstructure, austenitizing temperature and heating rate. The reaustenitisation process has been studied for two starting microstructures [Yang and Bhadeshia, 1987, 1989, 1990], one consisting of a mixture of bainitic ferrite and austenite, and the other of acicular ferrite and austenite. These investigations were carried out to provide a basis for the development of a model for reaustenitisation and subsequently to explain the differences in the observed reaustenitisation behaviour of bainite and acicular ferrite.

The key aim of this investigation is to study the effect of molybdenum on the austenitisation behaviour of multipass steel welds.

## 4.2 Experimental Procedure

All kinetic measurements were carried out using a Theta Industries high speed dilatometer. Chemical compositions of the experimental alloys were described in Chapter 2. The 3 mm rods were produced by swaging, involving a successive reduction in the diameter by approximately 1 mm in each step. After swaging, the 3 mm diameter rods were homogenized at 1200 °C for 3 days while sealed in quartz tubes containing a partial pressure of high purity argon. All specimens were electroplated with nickel and all heat treatments were carried out in a helium gas environment. High temperature DSC was also used to study and compare the CHT behaviour of the steel welds. The specimen preparation techniques have been discussed in Chapter 2.

Thin foil specimens were prepared for TEM as 0.25 mm thick discs slit from specimens used in the dilatometric experiments. Two types of specimens were used for TEM; a specimen tempered at 350 °C for one hour and a second specimen tempered at 650 °C for one hour. The discs were thinned to 50  $\mu\text{m}$  by abrasion on silicon carbide paper and then electropolished in a twin jet electropolisher using a 5% perchloric acid, 25 % glycerol and 70 % ethanol mixture at an applied voltage of 60 V, with the solution being cooled to  $-10$  °C using liquid nitrogen. The microscopy was carried out using a Phillips EM400T TEM, operated at 120 kV.

## 4.3 Results and Discussion

Macrohardness measurements on the as-deposited specimens of all the alloys are presented in Fig. 4.3. The alloy containing 1 wt.% molybdenum has a much higher hardness as compared to the alloy without molybdenum. Transmission electron micrograph for the Fe-1Mo wt.% specimen tempered at 350 °C showing a typical lath martensite and some amount of retained austenite (Fig. 4.4). Electron micrograph for the specimen tempered at 650 °C shows lath of martensite and carbides precipitation within the lath of martensite (Fig. 4.5).

High speed dilatometry was used to study and compare the CHT behaviour of the weld alloys containing different amounts of molybdenum. The  $A_{c1}$ , and  $A_{c3}$  temperatures were determined by continuous heating in the dilatometer. The temperature at which austenite first begins to form ( $A_{c1}$ ) and the temperature at

which the sample has completely austenitic ( $Ac_3$ ) were measured (Table 4.1, 4.2).

The specimens for these alloys were first tempered at 350 °C for 60 minutes at the reaction temperature and then quenched to ambient temperature using helium gas. This was followed by continuous heating to 1200 °C at a variety of heating rates. [The heating rates chosen were respectively 2, 100, 200, 300, 350, 400, and 480 °C min<sup>-1</sup>]. The specimens were again quenched to ambient temperature. The same experiments were repeated for the 650 °C temperature. The relative length change as a function of temperature for the dilatometric experiments carried out at a heating rates of 100 °C min<sup>-1</sup> for alloys Fe-1Mo wt.% (Fig. 4.6). The results (Table 4.1, 4.2) show that there is at most a 20 °C difference in  $Ac_1$  and  $Ac_3$  for both the alloys.

In multirun welds, all the layers other than the final one, experience heating and cooling cycles after the melt has cooled to the interpass temperature, as a consequence of the heat input which leads to the deposition of successive layers. In terms of the influence on microstructure, the thermal cycle experienced as an adjacent layer deposited is expected to be most important, since it will be associated with the highest peak temperature. A multirun weld will, of course, contain a whole range of complex microstructures since many regions of the weld can have experienced a whole series of thermal cycles by the time the point is filled. The results demonstrate that in some cases the relative length change vs temperature curves deviate (> 700 °C temperature) from linearity during heating before the process of austenitisation begins. The volume fraction of austenite as a function of temperature is calculated as follows; consider a schematic diagram of variation of  $\Delta L/L$  with temperature as shown in Fig. 4.7. It is noted that the slope of a plot of  $\Delta L/L$  versus temperature will until  $Ac_3$  be equal to  $e_\alpha$  and slope of  $\Delta L/L$  with T after  $Ac_3$  is  $e_\gamma$ . The volume percentage of  $\gamma$  varies from 0 to 100 from  $Ac_1$  to  $Ac_3$ . It can be calculated by a geometrical method. Let us consider a temperature  $T_1$  between  $Ac_1$  and  $Ac_3$ . The volume fraction of  $\gamma$  from the geometrical method is given by (AX/AB) and this procedure can be repeated for whole range of temperatures and volume fractions of  $\gamma$ .

The specimen for the alloy Fe-1Mo wt.%, was also used in the DSC experiments. The specimen was first transformed at 650 °C for 60 minutes at the reaction

temperature and quenched to ambient temperature using argon gas. It was then continuously heated to 1200 °C at slow heating rate (2 °C min<sup>-1</sup>). The specimen was again quenched to ambient temperature. The temperature difference vs temperature for the experiment carried out at slow heating rate is shown in Fig. 4.8. The experimentally observed temperature of  $A_{c_3}$  was 930 °C . It is consistent with the results of the dilatometry experiments.

Table 4.1: Transformation temperatures observed during continuous heating experiments.

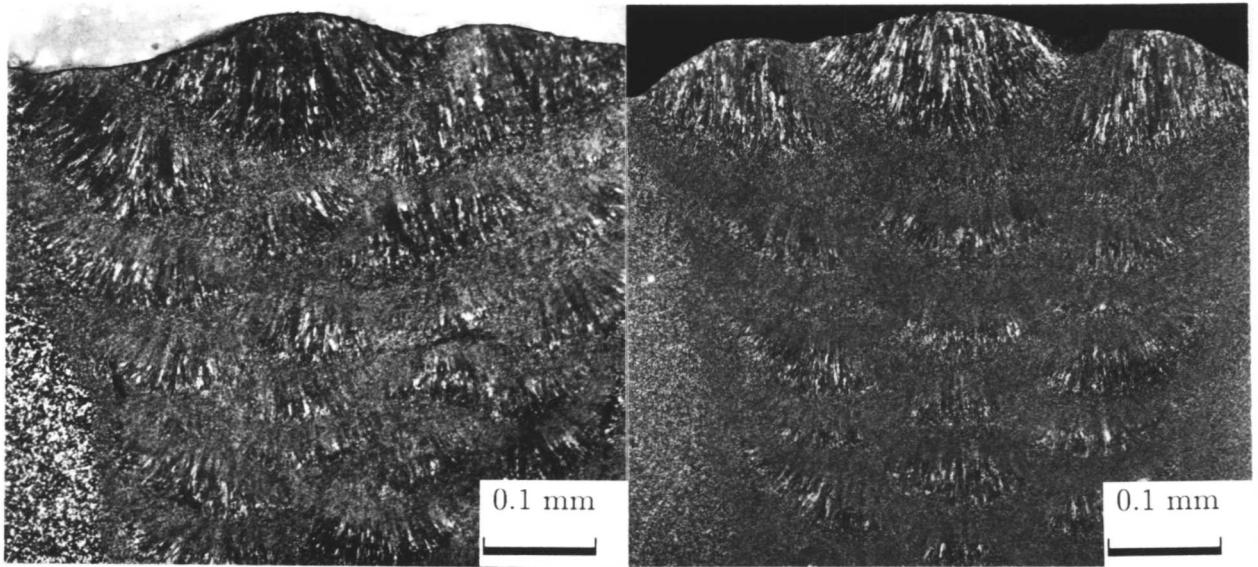
Alloy	Tempering °C	Heating Rate °C min <sup>-1</sup>	$A_{c_1}$ °C	$A_{c_3}$ °C
Fe-0Mo wt.%	350	2	740	920
		100	750	890
		200	740	880
		300	750	860
		350	750	870
		400	740	880
		480	740	890
	650	2	760	920
		100	740	860
		200	740	880
		300	750	880
		350	740	880
		400	740	880
		480	740	880
Fe-0.21Mo wt.%	350	2	750	880
		100	780	880
		200	790	910
		300	780	900
		350	780	900
		400	780	910
		480	780	910
	650	2	750	910
		100	750	910
		200	770	900
		300	780	890
		350	780	900
		400	780	900
		480	780	890

Table 4.2: Transformation temperatures observed during continuous heating experiments.

Alloy	Tempering °C	Heating Rate °C min <sup>-1</sup>	$A_{c_1}$ °C	$A_{c_3}$ °C
Fe-0.42Mo wt.%	350	2	760	930
		100	780	910
		200	790	900
		300	790	890
		350	790	910
		400	790	880
		480	790	900
	650	2	770	930
		100	780	910
		200	780	910
		300	800	910
		350	800	900
		400	800	900
		480	800	890
Fe-1Mo wt.%	350	2	760	940
		100	770	910
		200	780	910
		300	780	900
		350	780	910
		400	780	910
		480	780	910
	650	2	750	940
		100	760	880
		200	760	900
		300	760	900
		350	760	900
		400	760	900
		480	760	900

## 4.4 Summary and Conclusions

The growth of austenite has been studied during the heating of a microstructure containing tempered martensite. It is found that molybdenum in the concentrations studied does not significantly alter the kinetics of austenite formation. Further work is needed to analyse the effect of molybdenum on the primary microstructure, using TEM and an atom probe field ion microscopy.



Fe-1Mo wt.%

Fe-0Mo wt.%

Fig. 4.1: Optical macrographs showing retention of primary microstructure for Fe-1Mo wt.%.

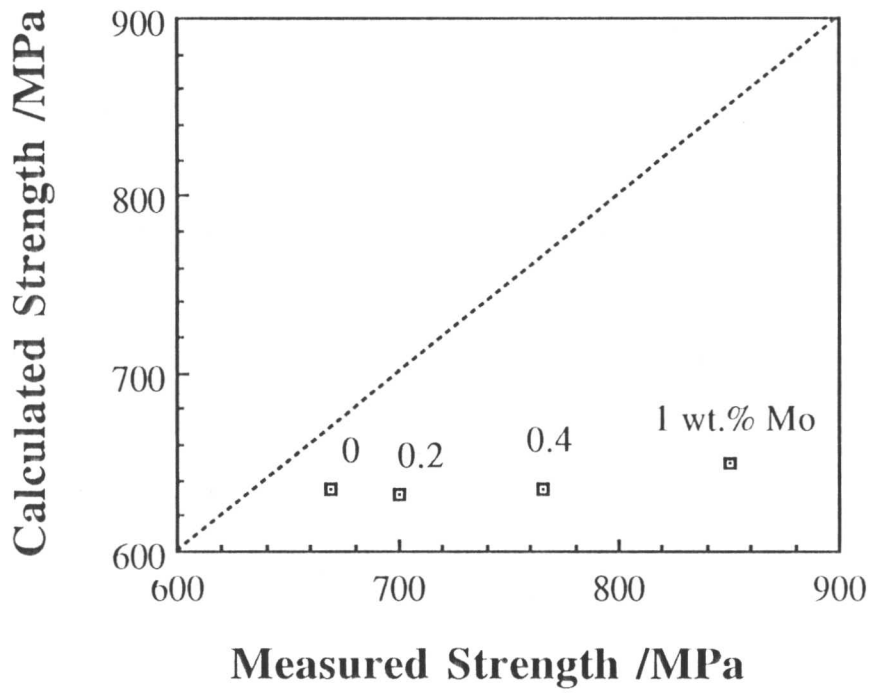


Fig. 4.2: Graph showing calculated and measured strength.

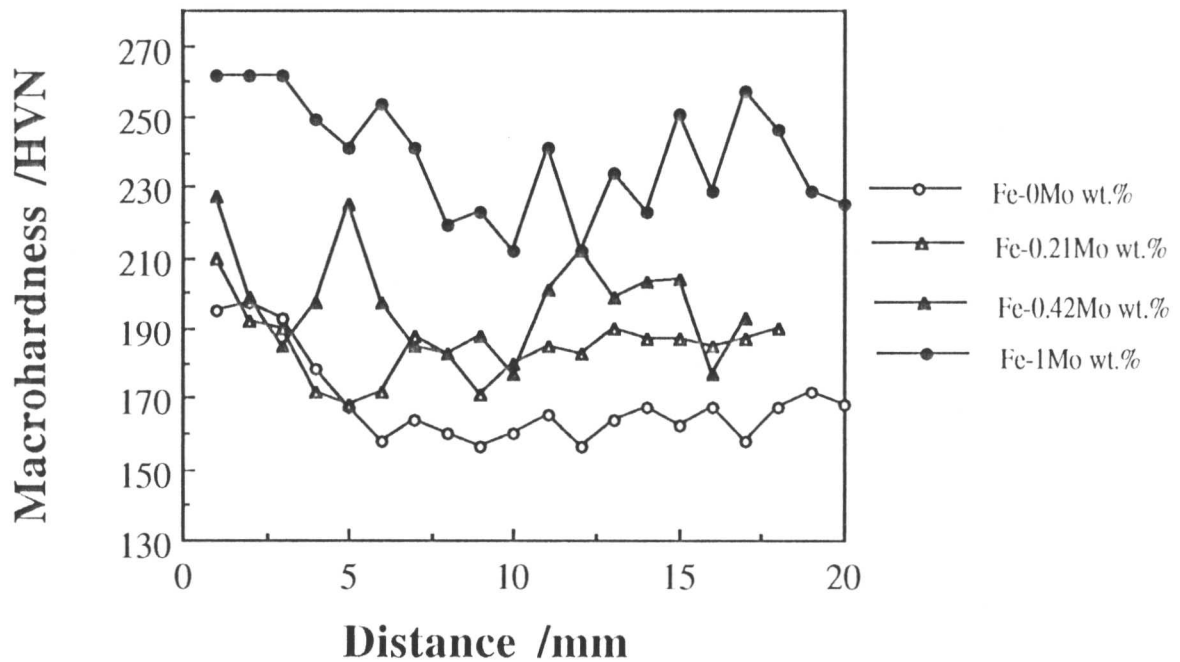


Fig. 4.3: Typical hardness variations across a multipass weld metal regions.

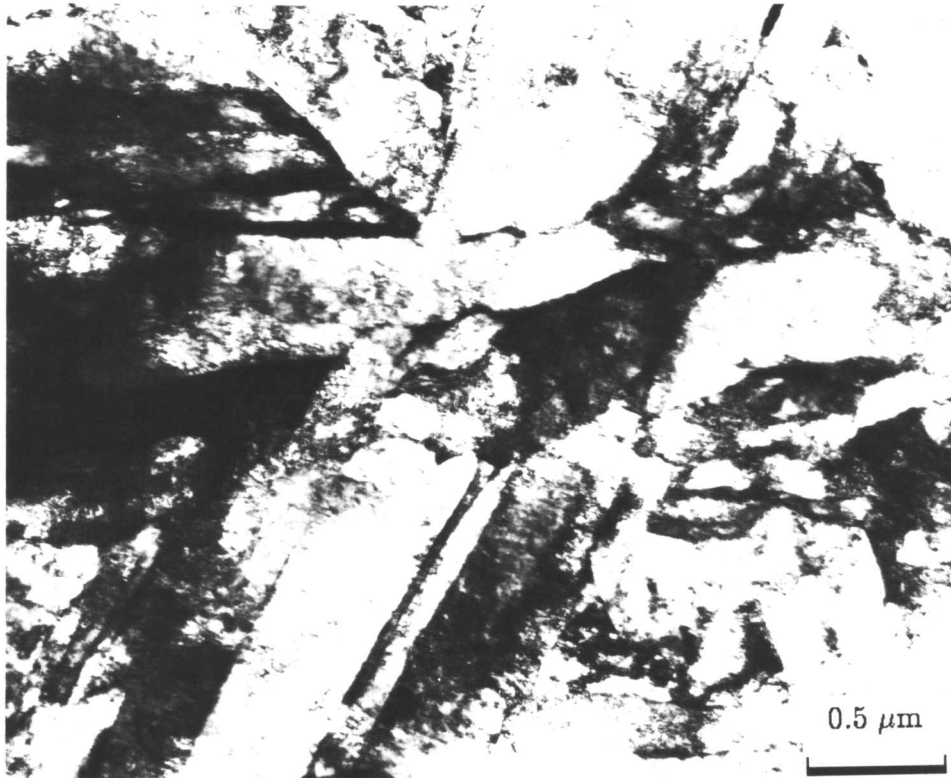


Fig. 4.4: Transmission electron micrograph for the Fe-1Mo wt.% specimen tempered at 350 °C showing a typical lath martensite and retained austenite.

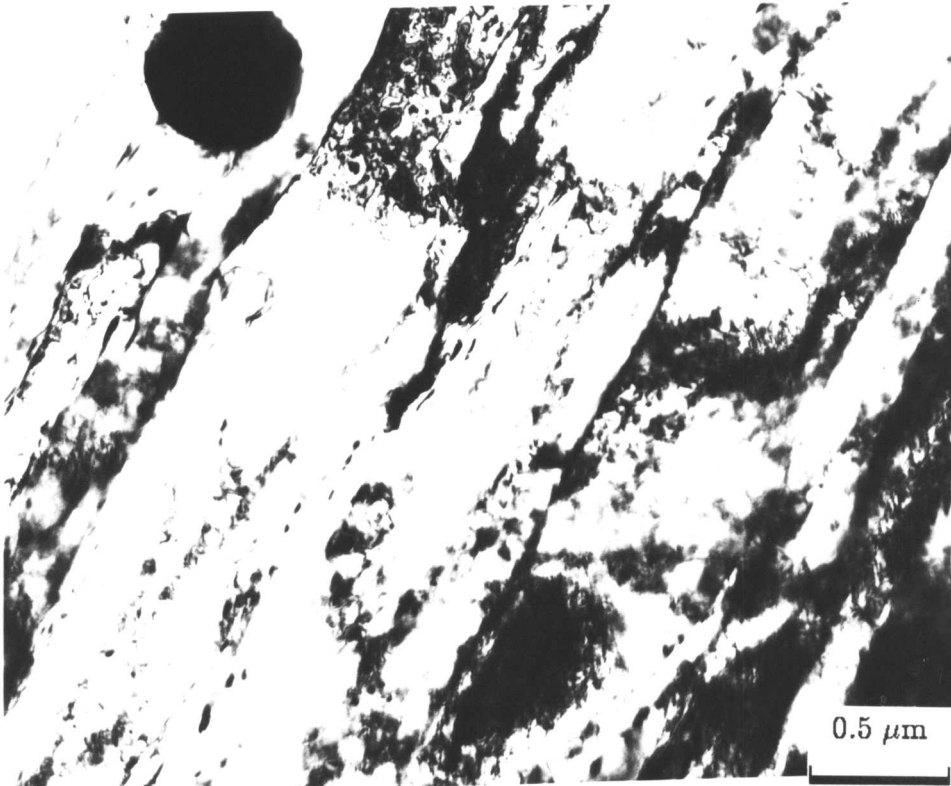


Fig. 4.5: Transmission electron micrograph for the specimen tempered at 650 °C showing lath of martensite and carbides precipitation within the lath of martensite.

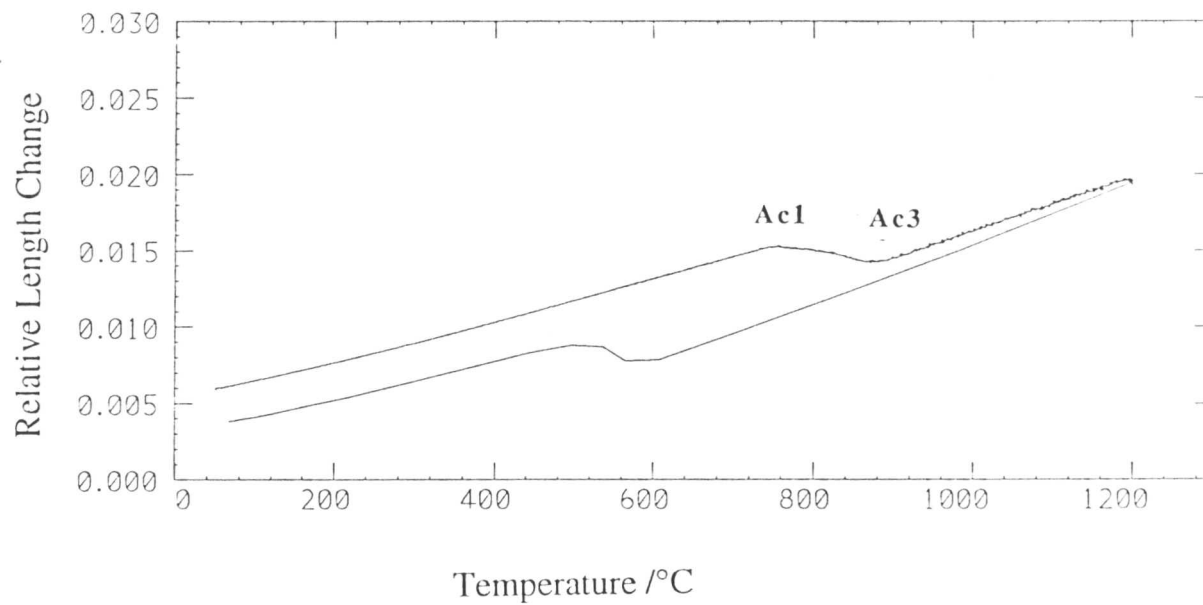


Fig. 4.6: The relative length change vs temperature at a heating rate of  $100^{\circ}\text{C min}^{-1}$ .

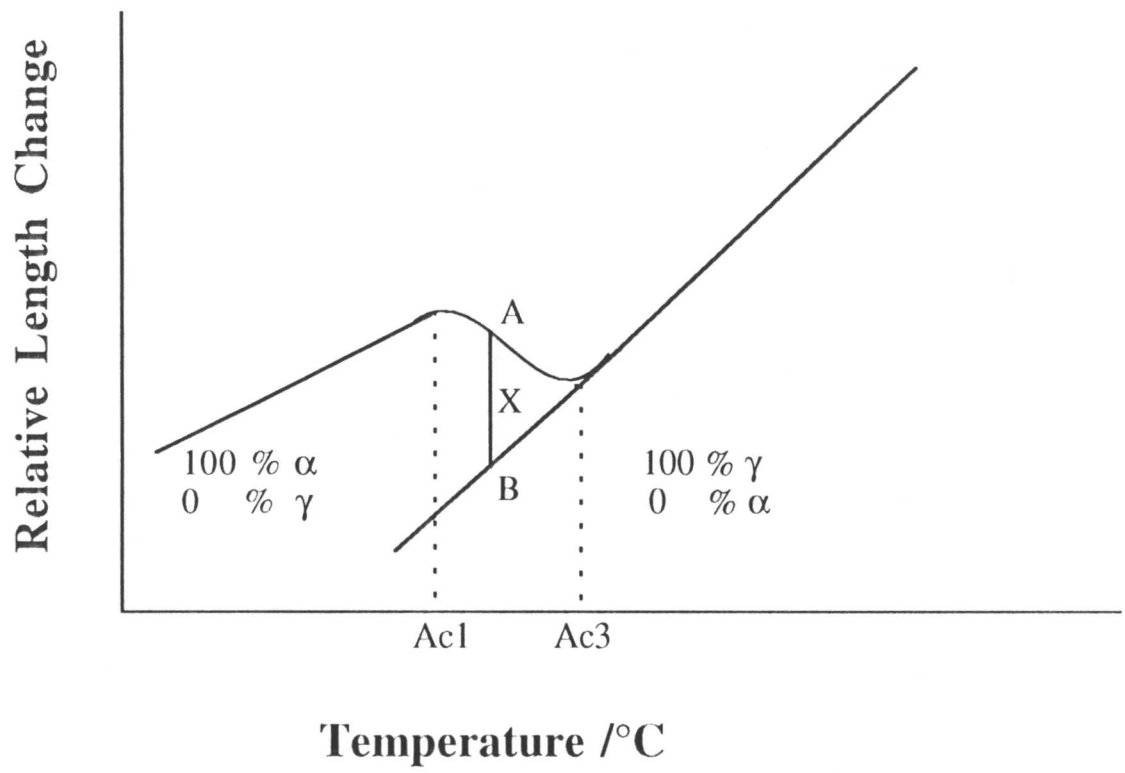


Fig. 4.7: Schematic diagram showing the relative length change as a function of temperature.

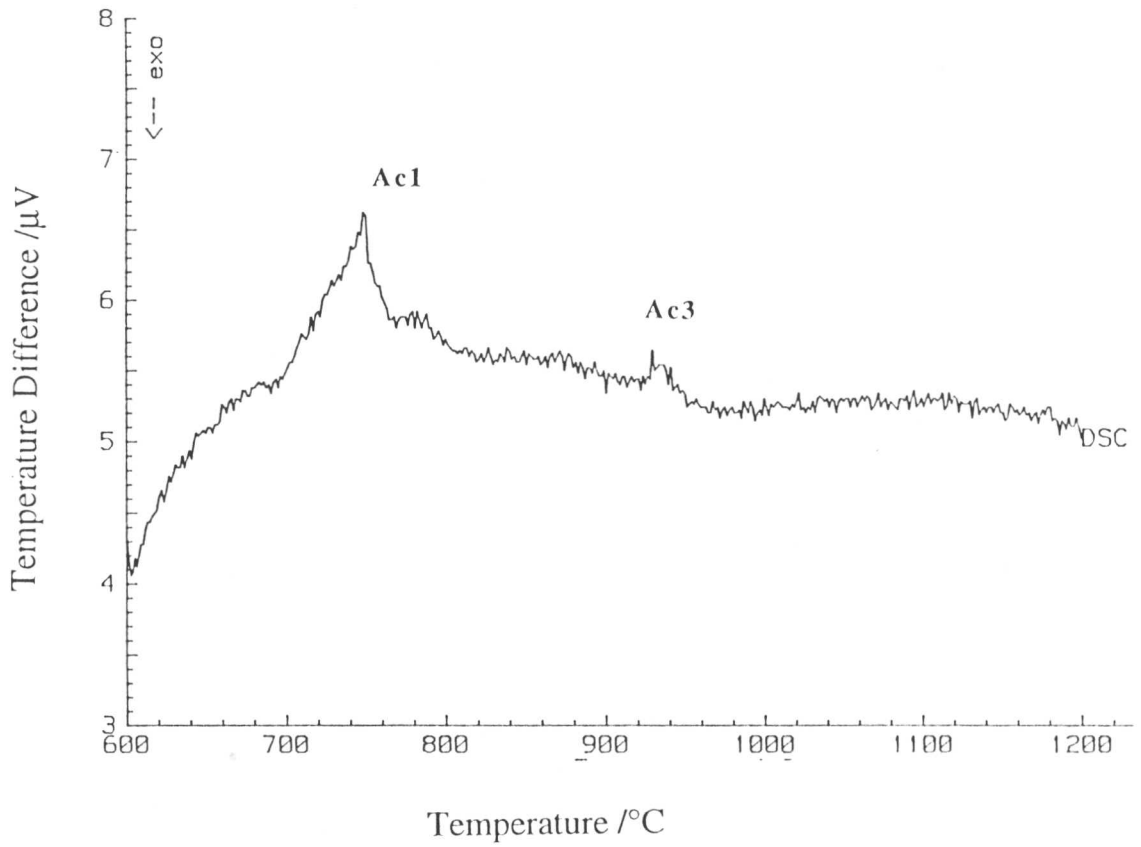


Fig. 4.8: Temperature difference vs temperature for the alloy Fe-1Mo wt.%, tempered at 650°C for 60 minutes, heating rate 2°C min<sup>-1</sup> followed by continuous heating at 1200°C .

---

## Chapter 5

# THE EXCESS STRENGTH AND TEMPERING RESISTANCE OF MOLYBDENUM-CONTAINING STEEL WELDS

---

### 5.1 Introduction

The strength of a steel weld can be estimated fairly accurately from a knowledge of the properties of pure iron, solid solution strengthening and microstructural strengthening terms [Smith and Nutting, 1957; Seal and Honeycombe, 1958; Baker, and Nutting, 1959] This method has revealed a significant discrepancy between the calculated and measured strengths of molybdenum-containing steel welds. The measured strength is found to be larger than that estimated, the discrepancy increasing with the concentration of molybdenum, as shown in Chapter 4 (Fig. 4.2). Molybdenum is a strong carbide forming element so it is natural to associate the excess strength with secondary hardening [Irvine and Pickering, 1960; Woodhead and Quarrel, 1965; Klueh, 1974a; Wada and Biss, 1983; Pilling *et al.*, 1983] due to alloy carbide formation. However, as will be seen below, such carbides have not been detected using transmission electron microscopy.

There is a further peculiarity associated with molybdenum containing steel welds which are fabricated by depositing many layers (*i.e.* multirun welds). The microstructure that is generated after solidification and cooling to ambient temperature is called the *primary* or *as-deposited* microstructure. A distinctive feature of the primary microstructure is that it consists of columnar grains of austenite, which have transformed to a variety of ferritic phases. The deposition of a further quantity of molten metal in the vicinity, during the fabrication of a multirun weld, causes the surrounding solid metal to be reheated. Some of the reheated regions become austenite with an equiaxed grain structure, others are only partially austenitised and the remainder tempered without transformation. This reheated or *secondary* microstructure consists of equiaxed grain structures and is therefore quite different

from the primary structure. A typical multirun weld might consist of about 30% of primary regions and 70% of secondary microstructure. Molybdenum-containing multirun welds, on the other hand, can contain more than 80% of the columnar regions. It therefore appears that the primary microstructure of molybdenum containing welds is extremely resistant to heat treatment, as shown in Chapter 4 (Fig. 4.1).

The purpose of the work presented here was to prove that the inability to predict the strength of molybdenum-containing welds cannot be attributed to inaccurate solid solution strengthening data, but to some submicroscopic secondary hardening effect. It was also intended to demonstrate directly that the molybdenum-containing steel microstructures are much more resistant to tempering heat treatments.

## 5.2 Experimental Procedure

The chemical compositions (wt.%) of the steels used are listed in Chapter 2, but are reiterated here for convenience (Table 5.1). Thin rods of 3 mm diameter and bars 1 × 1 × 4 cm were machined from the original samples. The specimens for heat treatment were sealed in silica tubes containing a partial pressure of argon. The heat treatment studies were carried out using an electric resistance furnace (accuracy ± 5 °C). The tempering was carried out at temperatures in the range 500–800 °C for 3600–86400 seconds, followed by water quenching, for the alloys in the as-deposited condition. The tempering was also carried out at temperatures in the range 400–700 °C for 300–7200 seconds in the as-quenched martensitic condition of the alloys.

The microstructures were observed using optical microscopy, scanning electron microscopy (SEM) and transmission electron microscopy (TEM). The specimen preparation techniques have been described in Chapter 2. Carbon extraction replicas were prepared using the method of Smith and Nutting (1957). The microstructural changes were examined in a Phillips 400T transmission electron microscope operating at 120 kV and some samples of replicas were analysed by energy dispersive X-ray spectroscopy in a TEM. The hardness was measured on a Vicker's hardness machine.

Table 5.1: Chemical compositions (wt.%) of the steels used in the present study.

Alloy	C	Si	Mn	Ni	Mo	Cr	V	Ti	O	N
Fe-0Mo wt.%	0.079	0.30	1.05	0.027	0.005	0.035	0.001	0.0005	0.0435	0.0060
Fe-1Mo wt.%	0.078	0.34	1.09	0.028	1.16	0.036	0.003	0.0005	0.0391	0.0083

## 5.3 Results and Discussion

### 5.3.1 Microstructural Changes

SEM micrographs of the as-deposited microstructures of both of the experimental welds are presented in Fig. 5.1. The microstructure of the molybdenum containing alloy is essentially bainitic with a little acicular ferrite. The molybdenum-free alloy contains in addition some allotriomorphic ferrite and Widmanstätten ferrite. Although these microstructures are different for the two alloys, the microstructural contribution to the strength is almost identical for Widmanstätten ferrite, acicular ferrite and bainite [Sugden and Bhadeshia, 1988], and the amount of allotriomorphic ferrite is very small. Hence, any difference in the strength due to microstructural variation between the two as-deposited regions can be neglected. The microstructural contributions are calculated according to the methodology presented elsewhere [Sugden and Bhadeshia, 1988].

The optical micrographs for the specimens heat treated at 500–800 °C for 1 hour are presented in Fig. 5.2. It is clear from the micrographs that the molybdenum containing alloy is very resistant to tempering. The columnar grain structure is retained, largely unchanged at the low temperatures, and even at the high tempering temperatures for the Fe-1Mo wt.% weld. However the microstructure was found to change completely for the Fe-0Mo wt.% into an equiaxed ferrite structure at a high temperature.

As has been evident from the phase calculations and dilatometric data, presented earlier (Fig. 3.4, Table 4.1–4.2), tempering at 800 °C is above the  $A_{e1}$  temperatures of both of the alloys, so that the heat treatment is not strictly confined to tempering but also to austenite formation. This heat treatment is nevertheless interesting because the tempering and austenite formation processes must compete. A comparison with the sample heat treated at 800 °C (Fig. 5.3) shows clearly that it is the tempering that dominates initially since an equiaxed ferrite structure is

observed after 1 hour at 800 °C. By contrast, it is evident that there is quite a lot of austenite formation on the microstructures which have been annealed for 24 hours at 800 °C.

Transmission electron microscopy for the Fe-1Mo wt.% specimen tempered at 600 °C showed an upper bainitic microstructure, with interplate carbides formed from retained austenite. There is also Mo<sub>2</sub>C precipitation within the plates (Fig. 5.4). The heat treatment at 600 °C for 10800 s, shows the presence of needle like Mo<sub>2</sub>C precipitates (Fig. 5.5).

### 5.3.2 Microanalysis

Carbides were also identified using EDX analysis and electron diffraction on carbon extraction replicas (Fig. 5.6). The results (Table 5.2) show a molybdenum concentration (ignoring carbon) in the range 70 to 90 wt.%, consistent only with Mo<sub>2</sub>C type carbides. Statistical fluctuations are indicated by the standard deviation [Topping, 1961].

Table 5.2: Chemical composition (wt.%) of carbides determined by using energy dispersive X-ray analysis. Specimen tempered at 600 °C for 10800 s. The measurements do not include carbon; the data are normalised to 100%.

Fe	Mn	Mo
9.0 ± 2	2.0 ± 2	89.0 ± 1
6.0 ± 4	3.0 ± 2	91.0 ± 1
22.0 ± 2	0.0	76.0 ± 1
33.0 ± 4	0.0	65.0 ± 2
30.0 ± 4	0.0	68.0 ± 2
17.0 ± 5	0.0	81.0 ± 1

### 5.3.3 Macrohardness Measurements

The alloy containing 1 wt.% molybdenum in the as-deposited weld has a much larger hardness as compared to the alloy without molybdenum. The results of hardness at tempering temperatures 500 to 800 °C for 3600 to 86400 s of both the welds are illustrated in Figs. 5.7–5.8. Tempering the specimens at 500 °C for up to

86400 seconds does not show any significant decrease in hardness, when compared with the hardness changes obtained after tempering at higher temperatures for shorter time periods. Comparison of the two alloys shows that tempering is clearly retarded by molybdenum.

In the as-quenched condition the mean hardness was 304 and 293 for the molybdenum and molybdenum-free welds respectively. Table 5.3 shows the hardness of the samples heated to 1200 °C for 600 s and quenched to martensite. The difference of the hardness of the two alloys due to solid solution strengthening is 11 HV. The difference due to solid solution strengthening by molybdenum is expected to be about 7 hardness points [Sugden and Bhadeshia, 1988]. This result is important because it proves that the large hardness difference for the as-deposited microstructures of the molybdenum and molybdenum-free welds is not due to solid solution strengthening effects.

The effect of tempering time and temperature upon Vickers hardness in the as-quenched specimens is shown in Figs. 5.9–5.10. At 500 °C the hardness decreased slowly with time in the Fe–1Mo wt.%. There was a maximum in the curve at 600 °C corresponding to the precipitation of Mo<sub>2</sub>C. At 700 °C, there was an almost linear decrease in the hardness with the tempering time. The results of tempering from the martensitic condition within the temperature range 500 to 700 °C in Fe–0Mo wt.% show an almost linear decrease of hardness with the tempering time. The retarded softening in the alloys containing 1 wt.% molybdenum is due to the formation of Mo<sub>2</sub>C precipitates. These carbides were identified by TEM. The secondary hardening of the steels containing 2–5 wt.% of molybdenum has been shown by Kuo (1953) and others to be associated with the formation of Mo<sub>2</sub>C. The needle-shaped precipitates have also been observed after 50 hour at 675 °C and after 2 hours at 700 °C for a 0.5 wt.% Mo steel [Smith and Nutting, 1957].

#### 5.3.4 Kinetic Strength

It has been proposed [Holloman and Jaffe, 1945] that for a given isothermal heat treatment (at temperature  $T$  for time  $t$ ), the effectiveness of that treatment should be related to the product

$$t \exp \frac{-Q}{RT}$$

Table 5.3: The hardness (HV5) of the samples heated to 1200 °C for 600 s and quenched to martensite.

Fe-0Mo wt.%	Fe-1Mo wt.%
298	311
283	310
296	312
306	296
304	313
284	284
287	287
292	316
288	298
293	313

where  $Q$  is an effective activation energy. The product of  $\exp\{-Q/RT\}$  versus  $t$  is the kinetic strength of the heat treatment, and can easily be used to estimate the effectiveness of an anisothermal heat treatment. A similar procedure has been used for the prediction of microstructure in welds [Alberry and Jones, 1977; Brown and Ashby, 1980; Ashby and Easterling, 1982; Alberry *et al.*, 1983; Ion *et al.*, 1984; Ashby and Easterling, 1984]. The value of the activation energy  $Q$  was taken to be 240000 J mol<sup>-1</sup>, the activation energy for self diffusion in iron [Weast, 1977]. The real point was to show that for the molybdenum alloys, hardening occurs during the cooling of the solidified weld.

The kinetic strength corresponding to the heat treatment that occurs during the cooling of the weld in the temperature range from 775 to 500 °C was calculated using cooling curves estimated from the work of Svensson *et al.* (1986). The hardnesses of the as-deposited welds are consequently plotted in Fig. 5.11. There are two points to note. Firstly, the kinetic strength of the weld cooling process occurs in the vicinity of the peak hardening due to molybdenum, and hence explains why the molybdenum containing weld is much harder. The prediction is that a faster weld cooling rate should reduce the difference in as-deposited hardness for the two

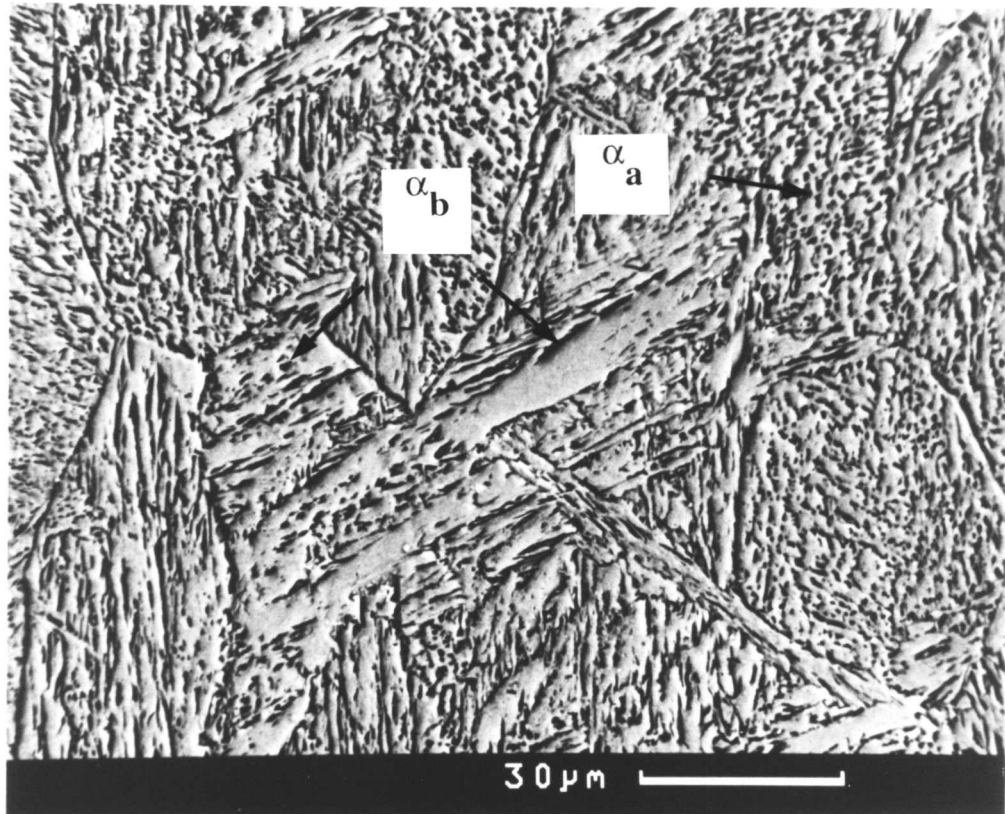
alloys. This is to some extent verified by the fact that the martensitic samples of the two alloys have a much smaller difference in hardness, corresponding to just a solid solution effect. The second point is that the absolute hardnesses of the as-deposited structures are not well predicted by the kinetic strength analysis when compared with the martensitic tempering data. The reason why the weld data lie off the martensite tempering curves is probably because a martensitic microstructure is much finer and therefore, stronger than the as-deposited weld microstructure which consists of higher temperature transformation products.

The hardness data as obtained from large variety of the tempering of the as-deposited and as-quenched specimens, as a function of kinetic strength, are shown in Figs. 5.11. For the isothermal heat treatments the kinetic strength has been calculated in the temperature range from 500–800 °C and 500–700 °C for the as-deposited and as-quenched tempered specimens respectively. To account for the heat treatment experienced by the weld during cooling to ambient temperature, the kinetic strength was calculated from the weld cooling curve over the temperature range 775–500 °C. The higher temperature corresponds to the point where the ferrite begins to form. Fig. 5.11 illustrates that the kinetic strength concept is very useful in that it shows the hardening occurs only in molybdenum alloys which corresponds to the precipitation of  $\text{Mo}_2\text{C}$ .

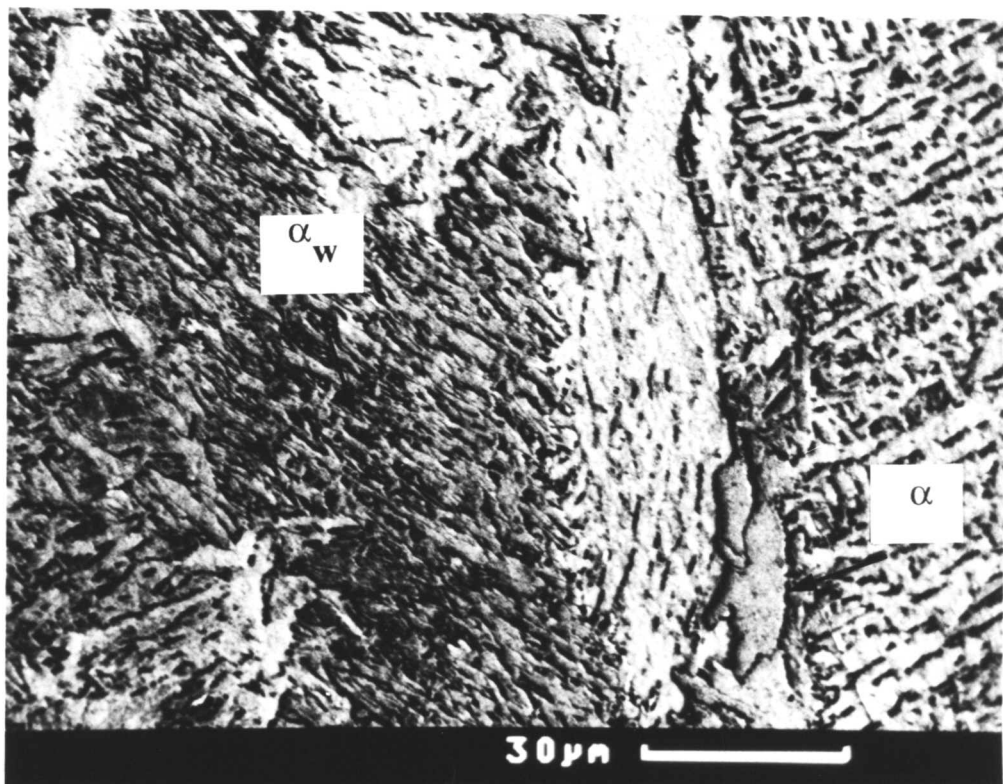
## 5.4 Summary and Conclusions

It has been established that the substantially higher strength of molybdenum containing welds cannot in general be attributed to solid solution strengthening by molybdenum, which makes a rather small contribution at the concentrations of interest. Differences in microstructure, caused by the addition of molybdenum, also do not account for the much higher strength of molybdenum-containing welds. Instead, the heat treatment that the weld experiences as it cools after solidification, causes the early stages of a secondary hardening reaction involving molybdenum.

It is further found that the microstructures of molybdenum containing welds are more resistant to tempering heat treatments. This in turn preserves the strength of the reheated regions in a multipass weld, so that the strength of the weld as a whole is maintained in spite of the heat input as successive layers are deposited.

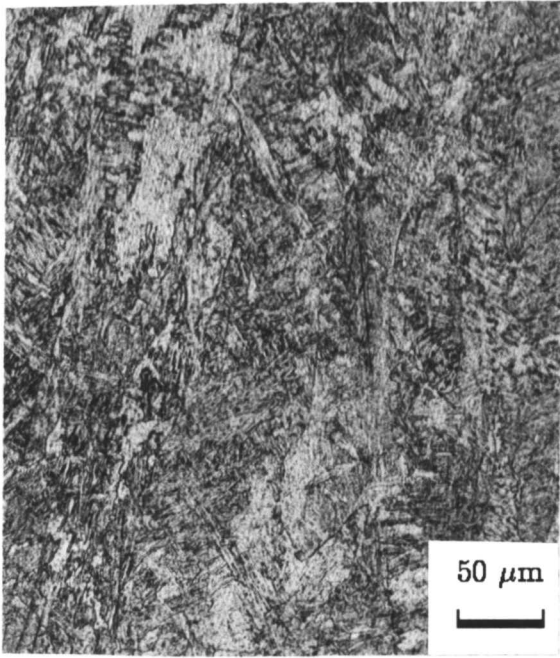


(a)

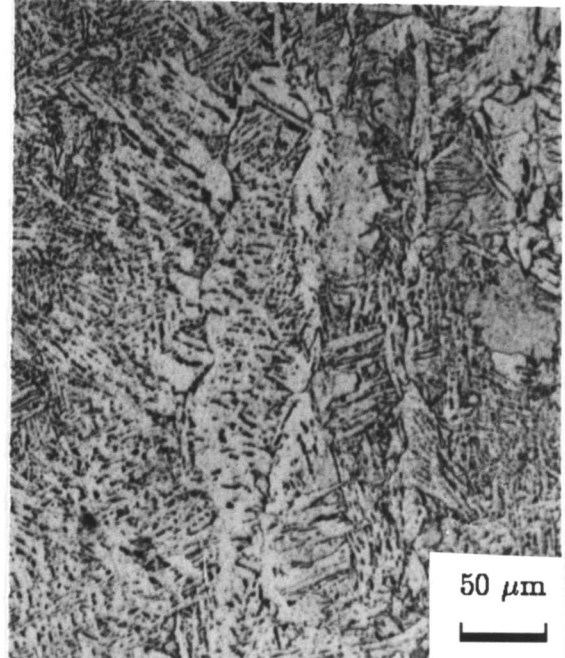


(b)

Fig. 5.1: SEM micrographs from the as-deposited microstructure. (a) Illustrates a mixture of bainite and a little acicular ferrite in the Fe-1Mo wt.%. (b) Shows allotriomorphic ferrite and Widmanstätten ferrite in the Fe-0Mo wt.% alloy.

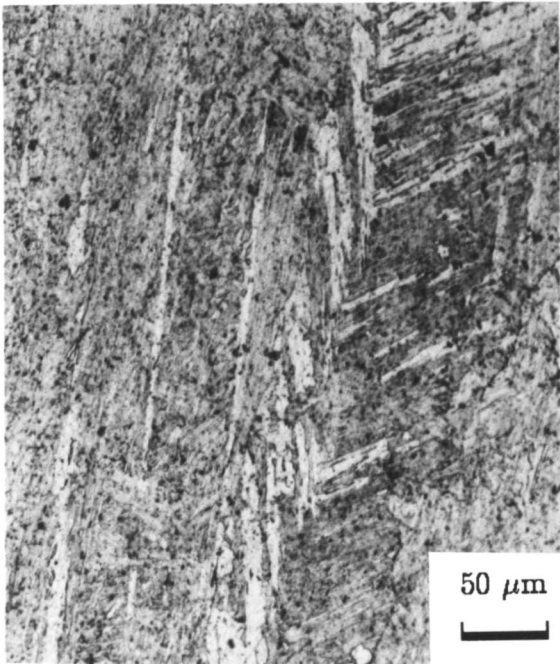


Fe-1Mo wt.%

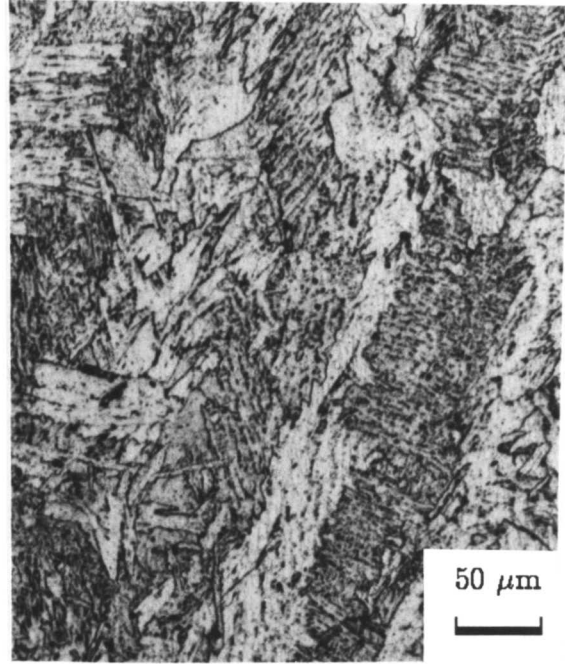


Fe-0Mo wt.%

(a) Specimen tempered at 500 °C for 1hour.



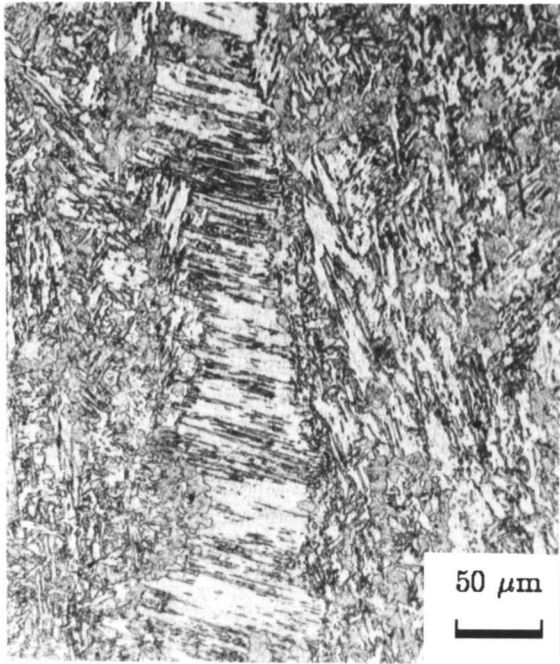
Fe-1Mo wt.%



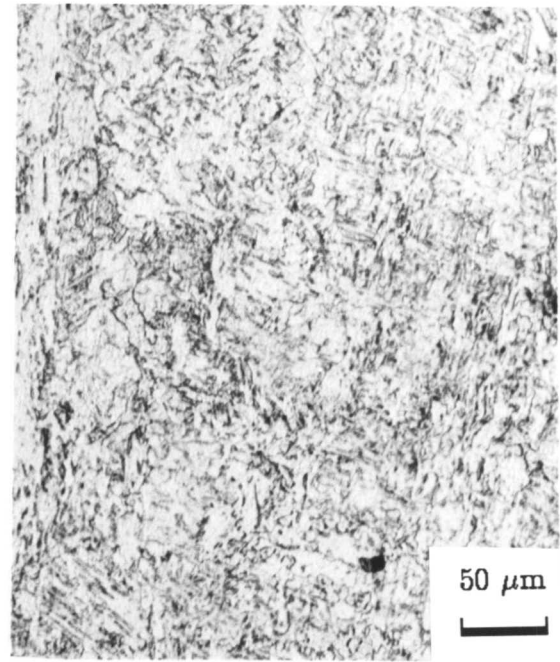
Fe-0Mo wt.%

(b) Specimen tempered at 600 °C for 1hour.

Fig. 5.2: Continued.....

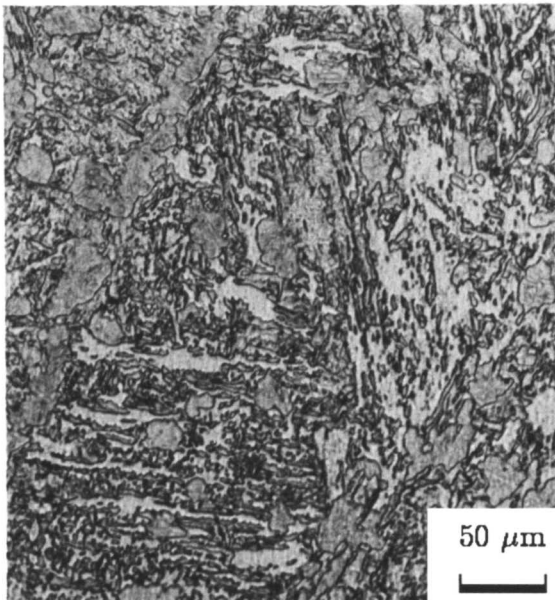


Fe-1Mo wt.%

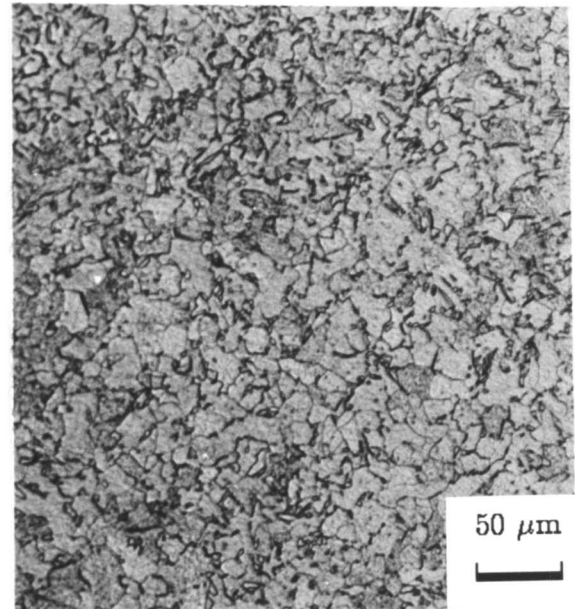


Fe-0Mo wt.%

(c) Specimen tempered at 700 °C for 1 hour.



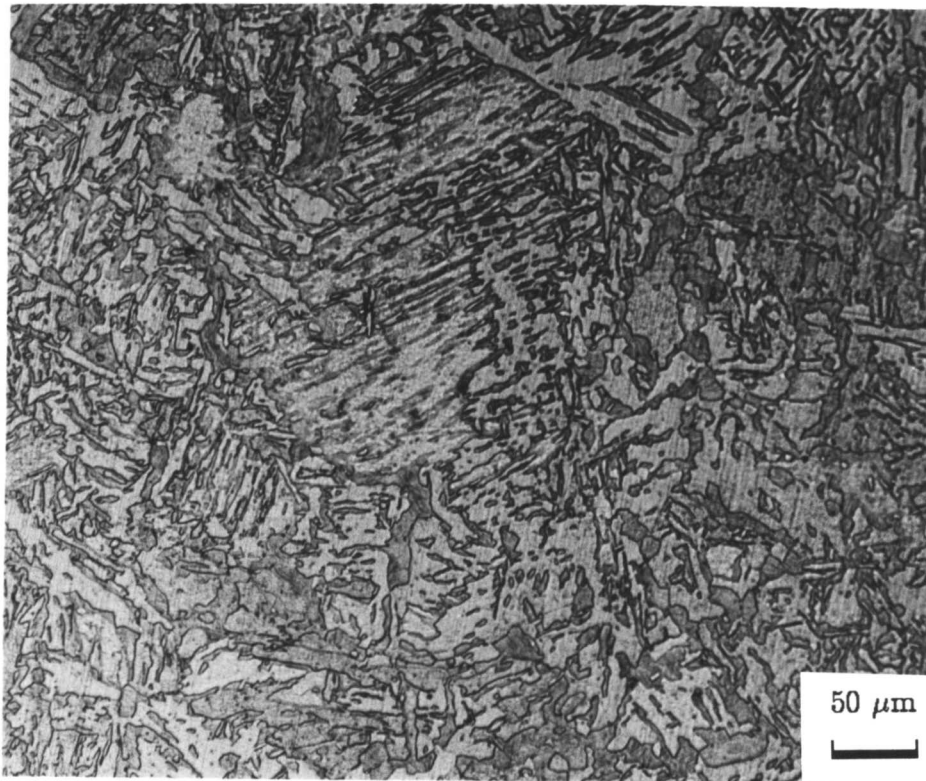
Fe-1Mo wt.%



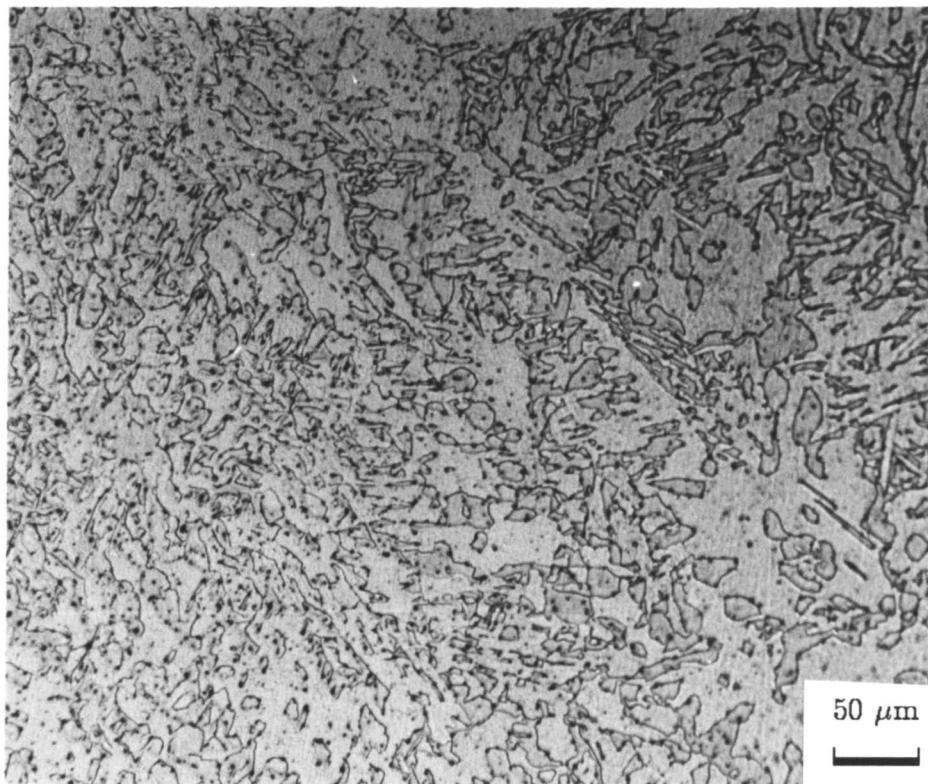
Fe-0Mo wt.%

(d) Specimen tempered at 800 °C for 1 hour.

Fig. 5.2: Optical micrographs after tempering of the as-deposited microstructure.



(a)



(b)

Fig. 5.3: Optical micrographs after tempering. (a) Specimen tempered at 800 °C for 24 hours, the Fe-1Mo wt.%. (b) Specimen tempered at 800 °C for 24 hours, the Fe-0Mo wt.%.

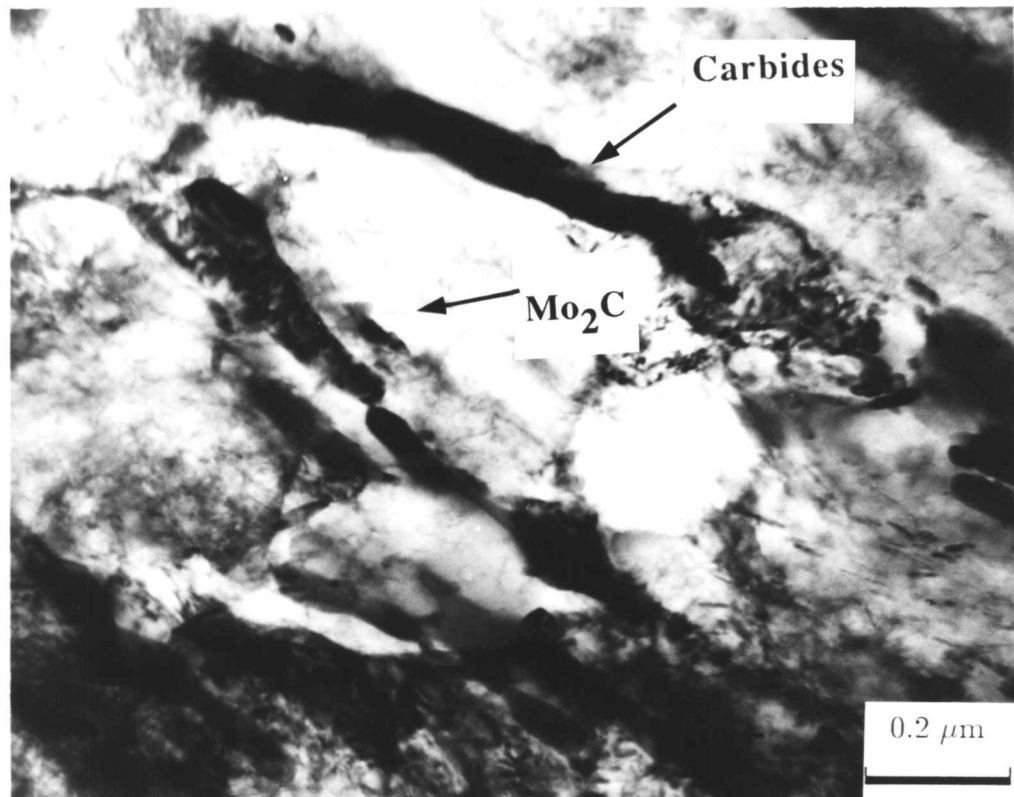
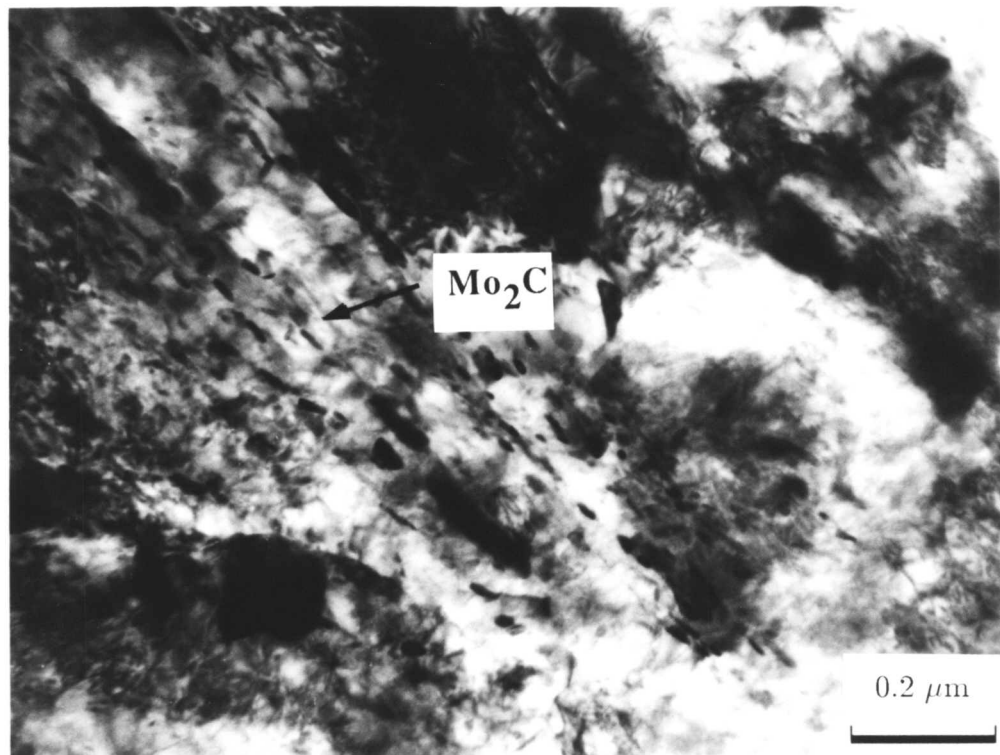
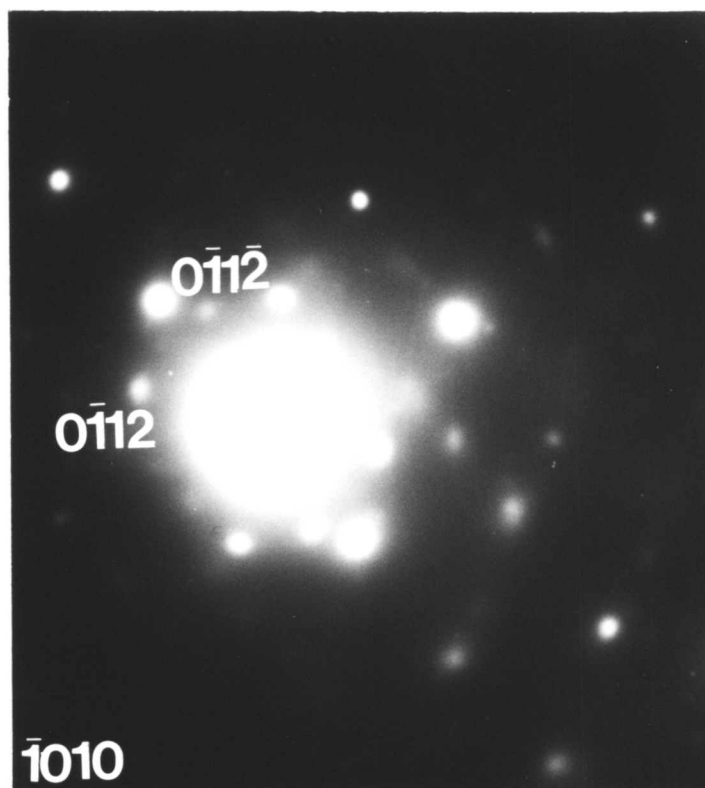


Fig. 5.4: Transmission electron micrograph of a specimen tempered at 600 °C for 10800 s upper bainitic microstructure, with interplate carbides formed from retained austenite. There is also Mo<sub>2</sub>C precipitation within the plates.



(a)



(b)

Fig. 5.5: Micrographs showing  $\text{Mo}_2\text{C}$  precipitates in specimen tempered at  $600^\circ\text{C}$  for 10800 s. (a) Bright field. (b) Corresponding diffraction pattern of  $\text{Mo}_2\text{C}$  carbides.

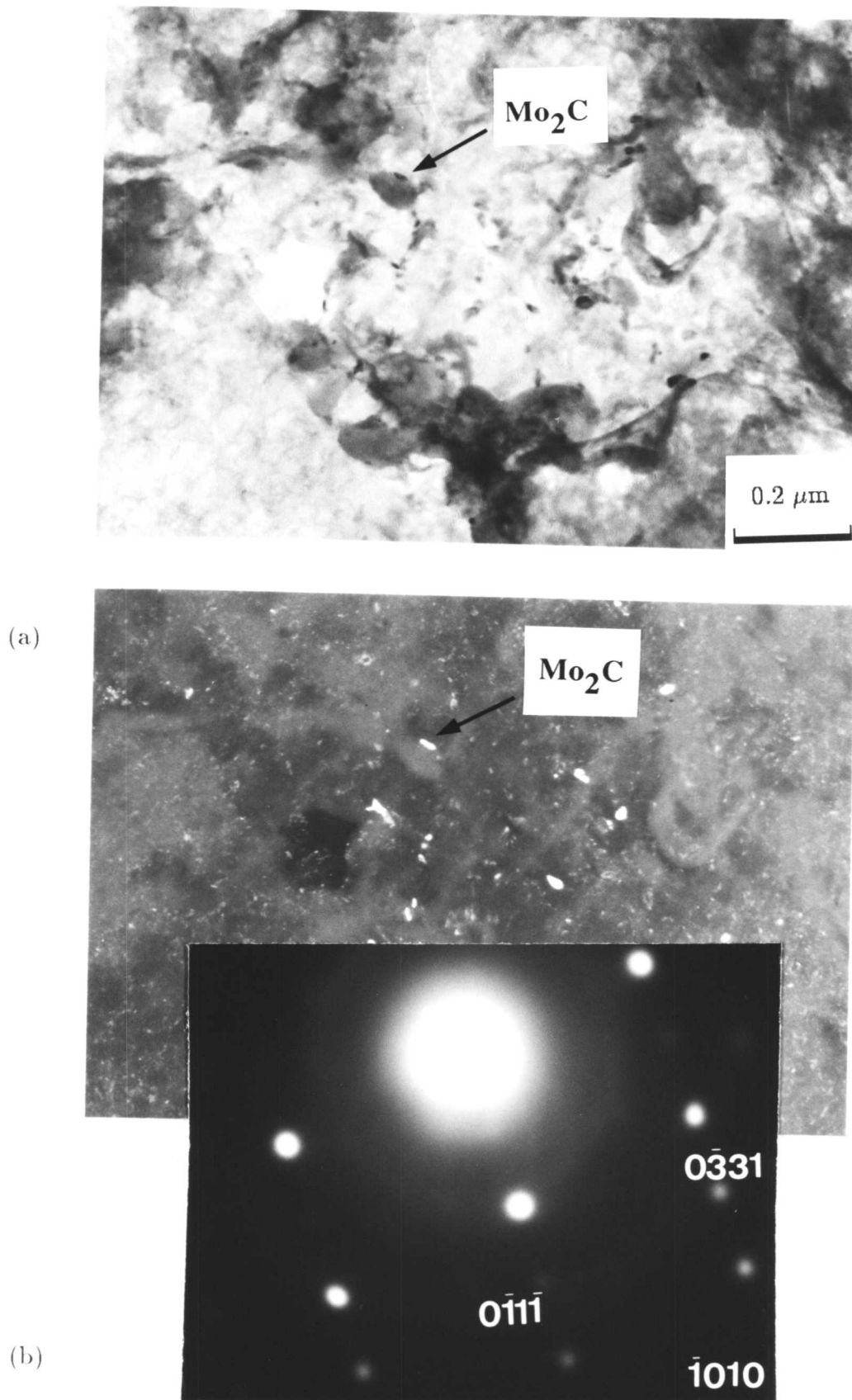


Fig. 5.6: Carbon extraction replica micrographs showing Mo<sub>2</sub>C precipitates in specimen tempered at 600 °C for 10800 s. (a) Bright field. (b) Dark field and the corresponding electron diffraction pattern of Mo<sub>2</sub>C carbides.

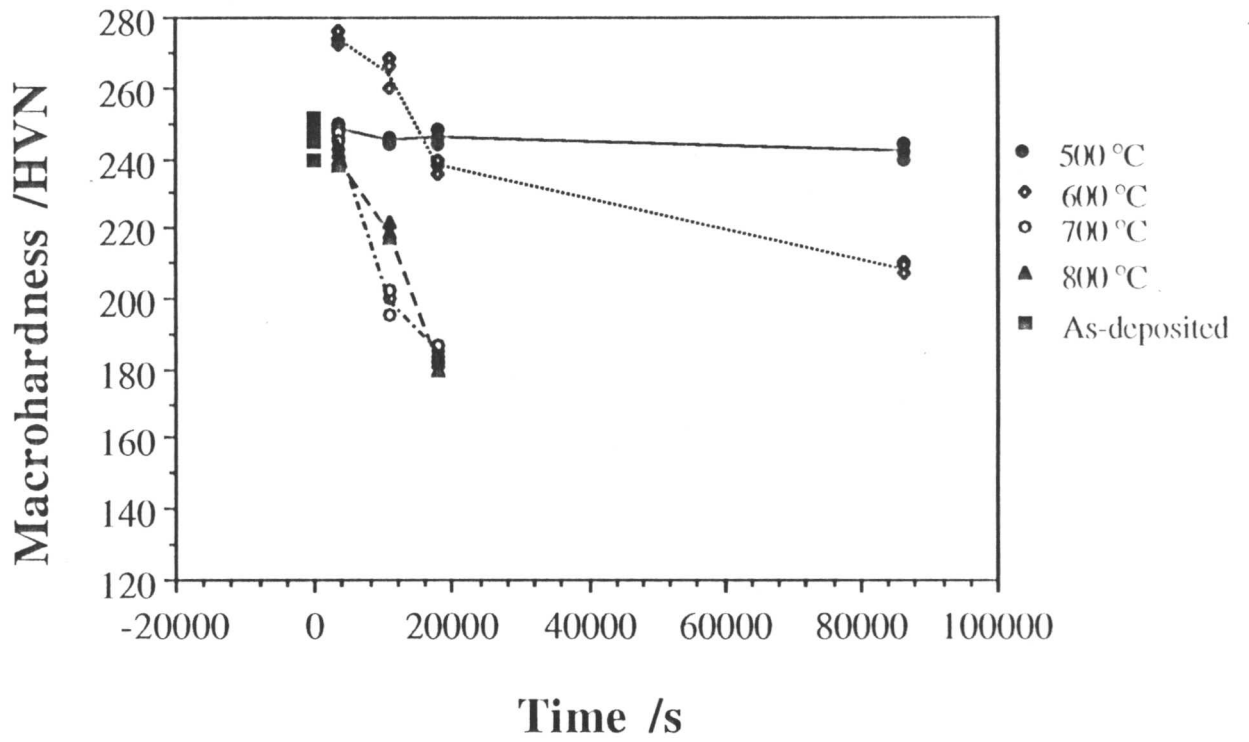


Fig. 5.7: The variation in the hardness of the as-deposited welds at tempering temperatures in the range 500–800 °C for 3600–86400 s, the Fe-1Mo wt.%.

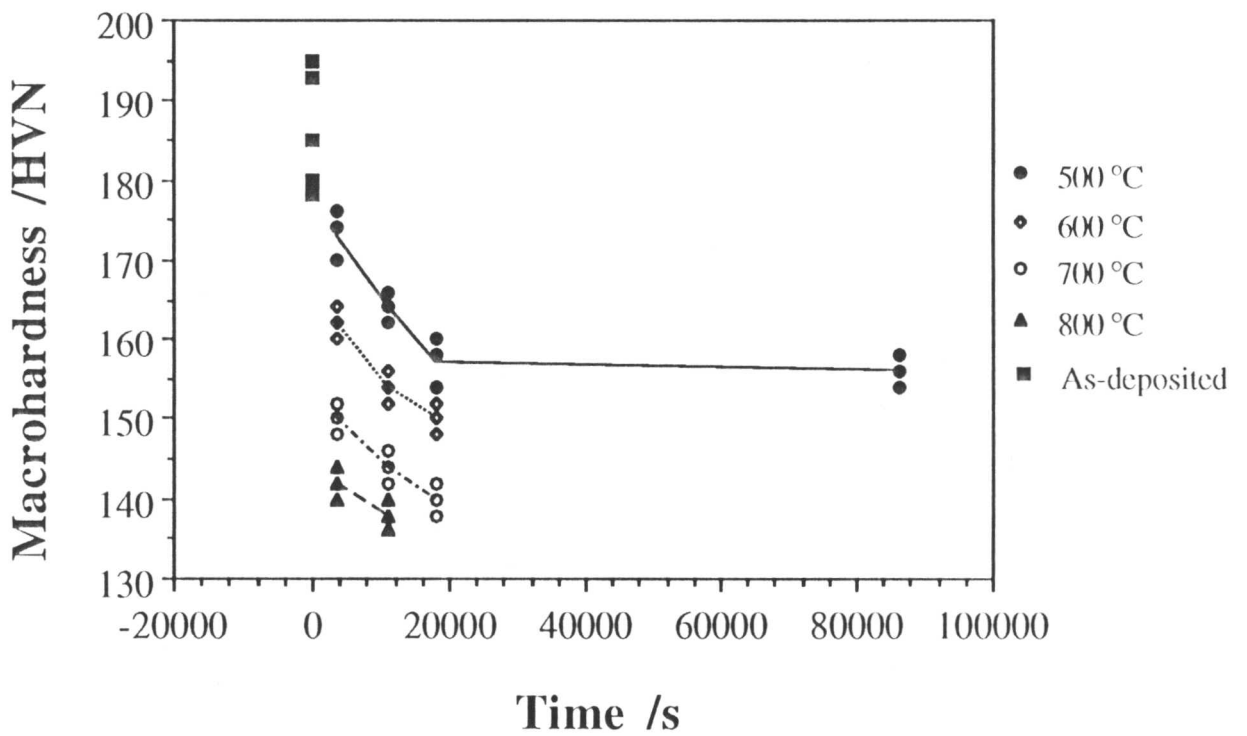


Fig. 5.8: The variation in the hardness of the as-deposited welds at tempering temperatures in the range 500–800 °C for 3600–86400 s, the Fe-0Mo wt.%.

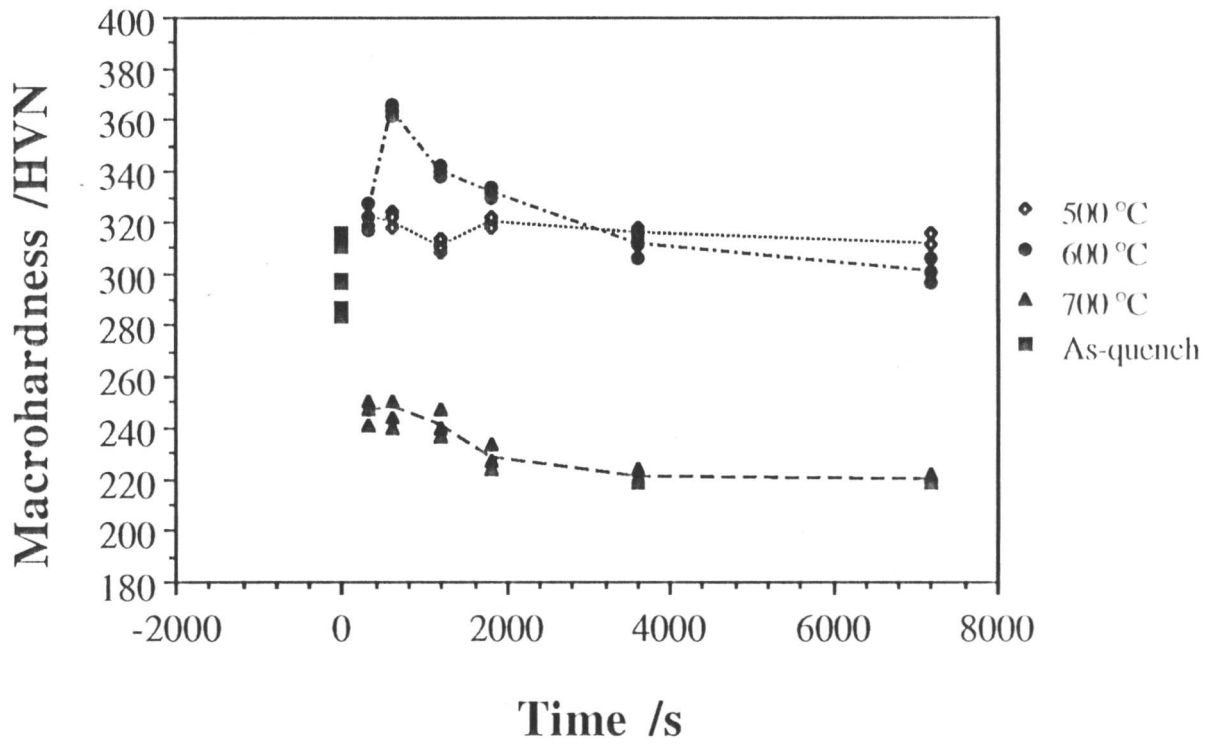


Fig. 5.9: The variation in the hardness, after the tempering of martensite at tempering temperatures in the range 500–700 °C, the Fe-1Mo wt.%.

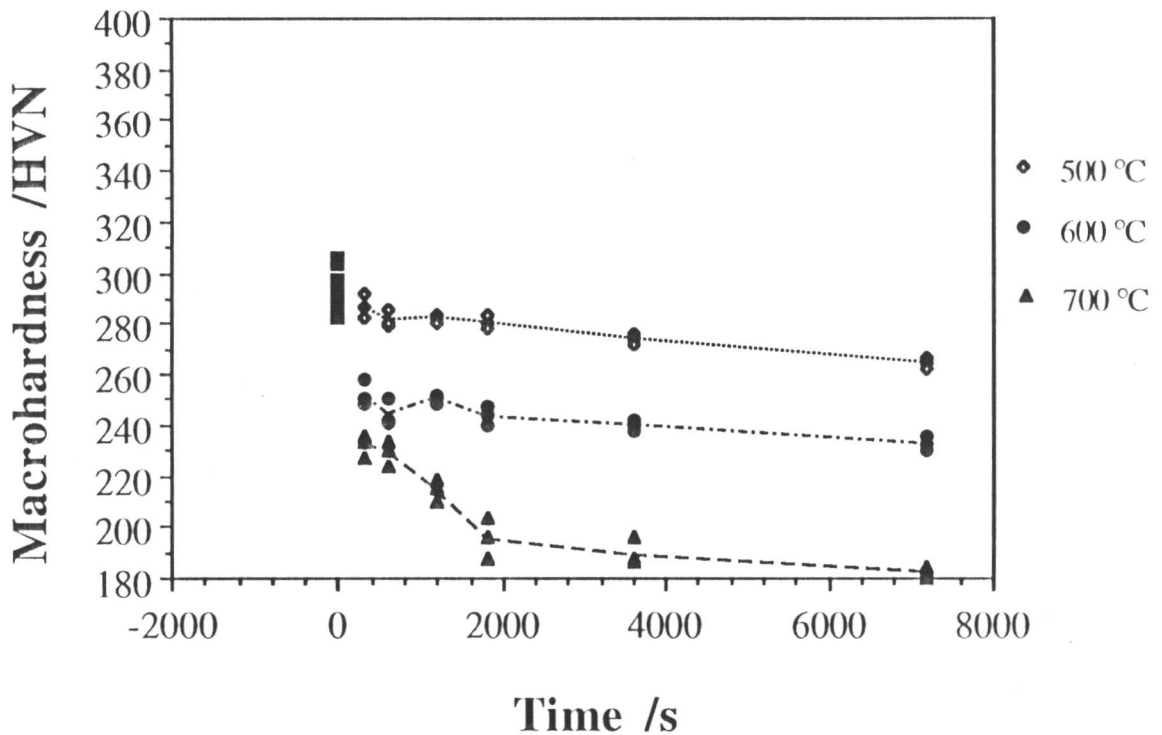
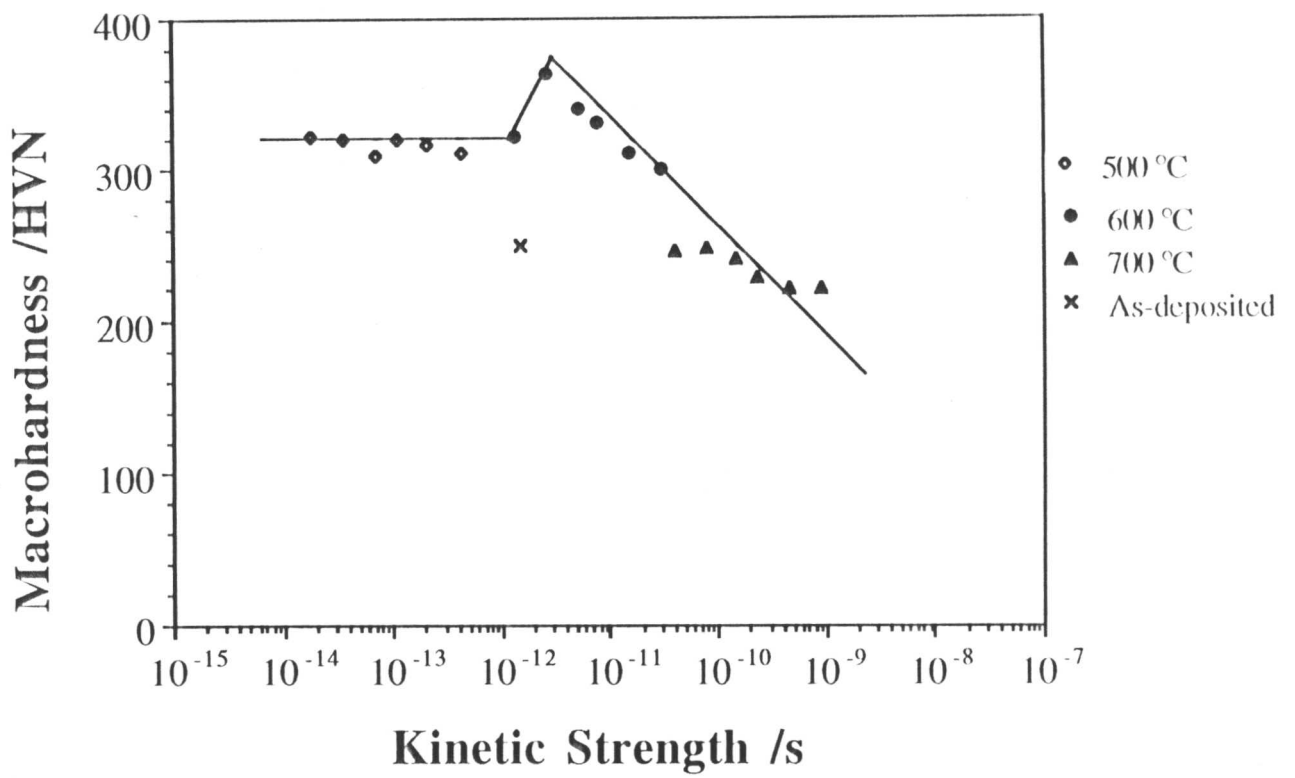
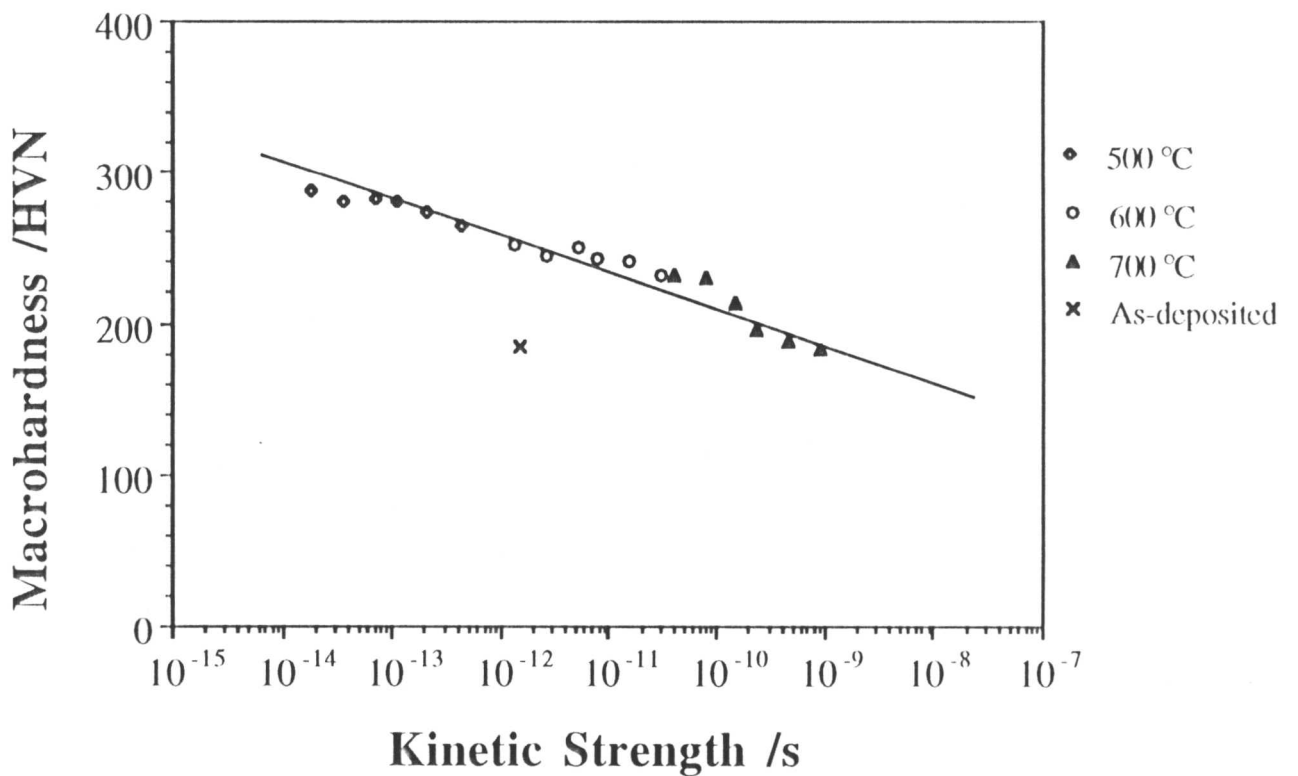


Fig. 5.10: The variation in the hardness, after the tempering of martensite at tempering temperatures in the range 500–700 °C, the Fe-0Mo wt.%.

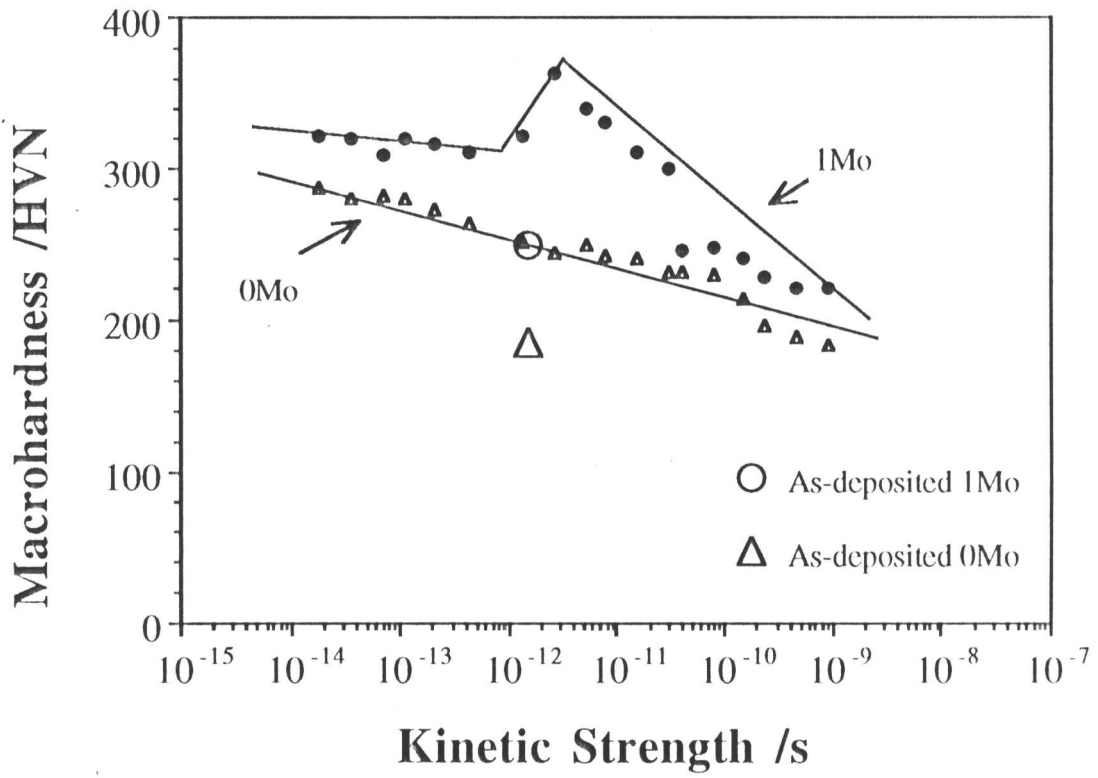


(a) The hardness of the tempered martensite as a function of kinetic strength, the Fe-1Mo wt.%.

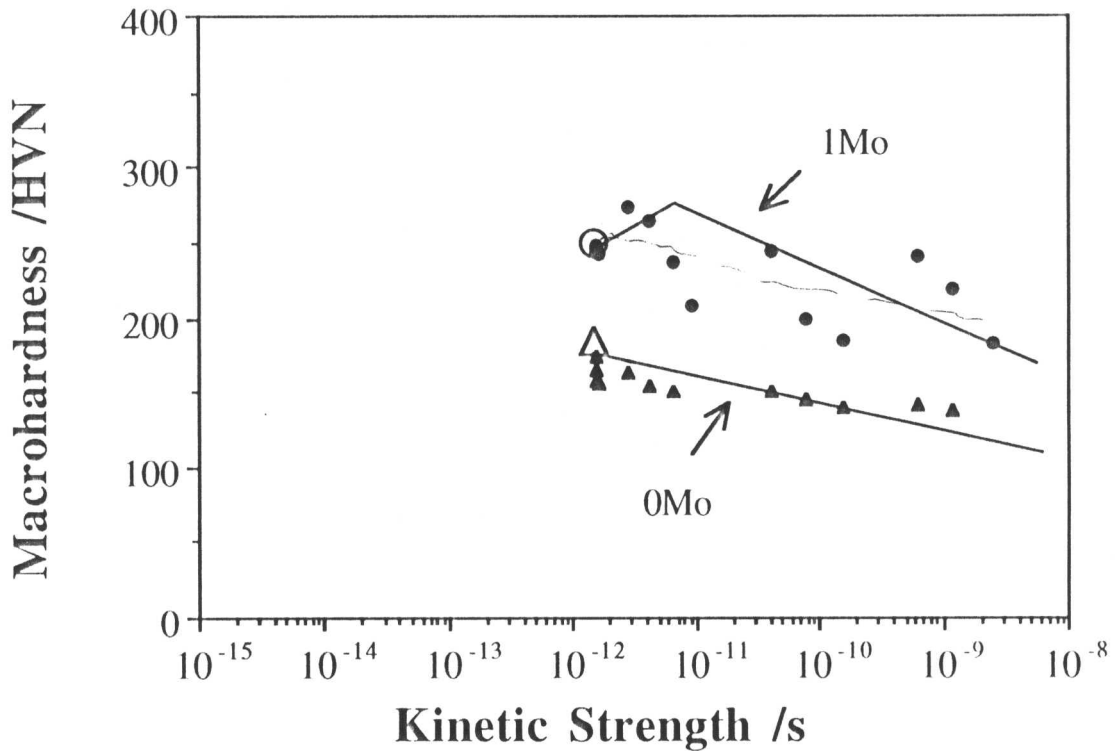


(b) The hardness of the tempered martensite as a function of kinetic strength, the Fe-0Mo wt.%.

Fig. 5.11: Continued.....



(c) Comparison of the hardness of the tempered martensite as a function of kinetic strength of the two alloys



(d) Comparison of the hardness of the tempered as-deposited microstructure as a function of kinetic strength of the two alloys

Fig. 5.11: Comparison of the hardness as a function of kinetic strength of the two alloys.

---

## Chapter 6

# AN ATOM PROBE STUDY OF THE EARLY STAGES OF PRECIPITATION

---

### 6.1 Introduction

An investigation has been carried out to study the possible existence of the early stages of precipitation/clustering of molybdenum atoms, using the atomic resolution method known as APFIM (Atom Probe Field Ion Microscopy). The reason for the relatively large strength of molybdenum-containing welds in the as-deposited condition, compared with molybdenum-free welds is not clear. It was established in Chapter 5 that this large difference cannot be attributed to solid solution strengthening. It was concluded that as a weld cools, it tempers to some extent so that the as-deposited molybdenum containing weld is much harder than expected from solid solution effects alone. It was therefore speculated that the enhanced hardness in the as-deposited molybdenum-containing welds is due to the early stages of molybdenum precipitation/clustering, on a very fine scale since transmission electron microscopy did not reveal any direct evidence for precipitation effects.

APFIM has a sufficiently high resolution to give an accurate composition and spatial determination on the nanometre scale. Atom probe techniques, their operation and applications have been described elsewhere [Miller, 1987; Miller and Smith, 1989; Stark *et al.*, 1990; Waugh *et al.*, 1992]. The particular apparatus used here consists of the APFIM200 field ion microscope combined with a reflectron time-of-flight mass spectrometer, an instrument capable of both spatial and chemical resolution on an atomic scale. The chemical analysis can be carried out on atoms which are induced to evaporate from the sample using voltage pulses. A number of APFIM studies have been recently conducted to investigate the morphology, size and composition of different precipitates [Sha *et al.*, 1990, 1992; Thomson and Bhadeshia, 1991].

## 6.2 Experimental Procedure

The composition of the alloy studied is shown in Table 6.1. Samples with dimensions  $0.35 \times 0.35 \times 20$  mm were machined from the as-deposited weld metal regions. A two stage electropolishing technique was used to prepare fine tips for field ion microscopy. The electropolishing solutions were 25% perchloric acid in acetic acid, floated on carbon tetrachloride at  $\simeq 30$  V for the first stage, and 2% perchloric acid in butoxyethanol at  $\simeq 20$  V for the second stage. Atom probe analyses were performed with the sample at 60 K with background pressure of neon gas of  $1 \times 10^{-5}$  mbar and  $1 \times 10^{-8}$  mbar for imaging and analysis respectively. The voltage pulse fraction used was 0.2.

Table 6.1: Bulk composition, and atom probe measured data for the as-deposited specimens. The atom-probe data represent a sample size of 5207 atoms.

Composition	C	Si	Mn	Mo
Bulk wt.%	0.078	0.340	1.090	1.160
Bulk at.%	0.362	0.675	1.107	0.675
Atom probe wt.%	$0.099 \pm 0.019$	$0.547 \pm 0.070$	$0.550 \pm 0.098$	$2.640 \pm 0.29$
Atom probe at.%	$0.460 \pm 0.090$	$1.090 \pm 0.14$	$0.560 \pm 0.10$	$1.540 \pm 0.17$

## 6.3 Results and Discussion

The possible existence of very small molybdenum-rich clusters in the as-deposited alloy has been examined in the current work. Representative field ion micrographs are presented in Fig. 6.1. The image shows small clusters of very bright atoms; subsequent atom probe analysis showed that these might be attributed to very small molybdenum carbides. It has been observed that molybdenum atoms

in iron image very brightly [Papazian, 1972]. Molybdenum carbides had not been observed in previous TEM investigations in the as-deposited specimens. A typical mass spectrum is illustrated in Fig. 6.2.

The composition depth profile obtained from atom probe analysis, illustrates the variation in the molybdenum concentration in fifty atom blocks from the ferrite phase (Fig. 6.3). Corresponding data for carbon are presented in Fig. 6.4. Statistical fluctuations due to the fine scale of the analysis are given by the standard deviations [Miller and Smith, 1989; Blavette and Buchon, 1989]. This suggests there are very small particles of molybdenum carbide in the early stages of formation within the matrix, but further analysis is needed to establish the significance of this result. There appear to be two molybdenum-rich clusters in the depth profile illustrated in Fig. 6.3, but only one has carbon enrichment associated with it.

The frequency distribution is obtained by plotting the total number of composition blocks with a given number of atoms of a specified element against the concentration. Frequency distributions for iron and molybdenum are shown in Fig. 6.5. For a random solution, the distribution of concentrations should be binomial since the fluctuations are random; any significant deviation from the binomial distribution would indicate the clustering of like or the ordering of unlike pairs. More data are needed to observe any significant deviations from the binomial distribution.

A number of authors have discussed treating the sequence of data as a Markov chain [Hetherington and Miller, 1987, 1988; Tsong *et al.*, 1982]. If clustering is present, the ordering parameter,  $\theta$ , is larger than 1 and for short range ordering,  $\theta$ , should lie between 0 and 1 [Miller and Smith, 1989]. A Markov chain analysis for the molybdenum atoms indicates that there could be clusters of molybdenum atoms, although many more ions are needed to establish the significance of this result. Further work is therefore needed to examine the early stages of molybdenum carbides.

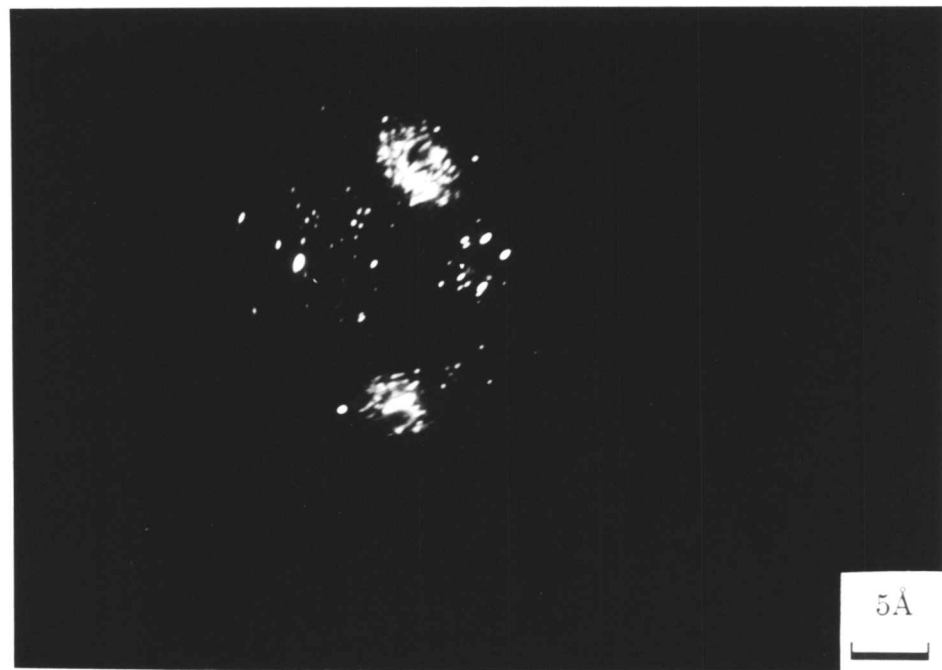
## 6.4 Summary and Conclusions

A preliminary atom probe investigation has been carried out to study the early stages of clustering /precipitation of molybdenum. Field ion micrographs illustrate that very fine scale effects could indeed be present. This is also consistent with the

fine scale chemical measurements. However, the work clearly requires confirmation with much larger data sets.



(a)



(b)

Fig. 6.1: FIM micrograph of the as-deposited specimens. (a) From the matrix (b) Indicates very fine clusters /precipitates. The pictures were taken at a tip voltage of 9, 11 kV respectively, a tip temperature of 60 K.

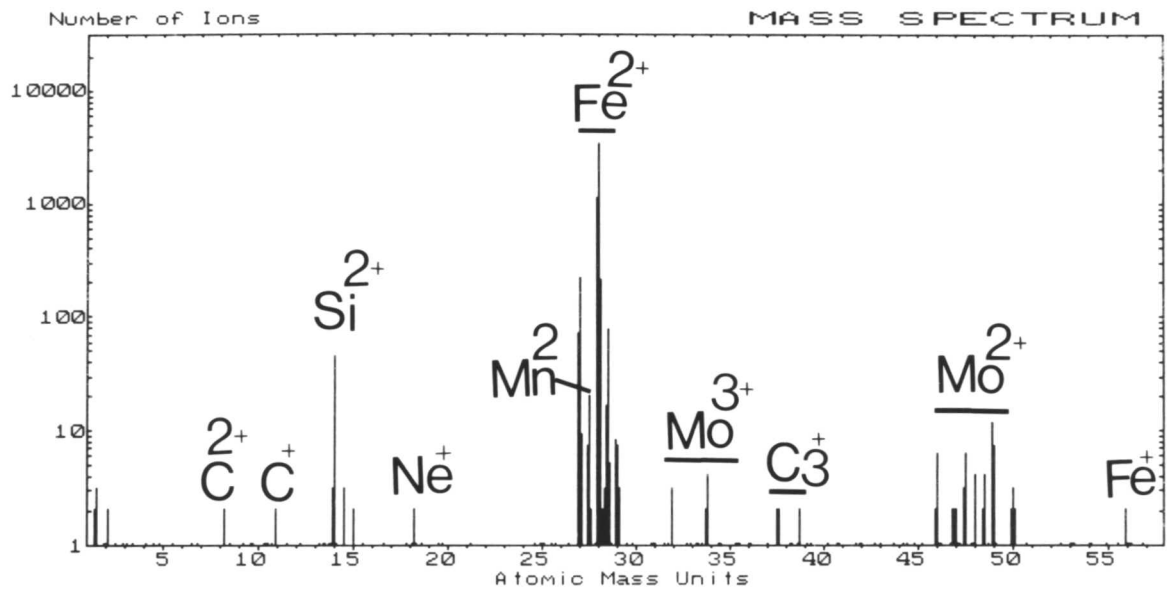


Fig. 6.2: A typical mass spectrum from the as-deposited specimen.

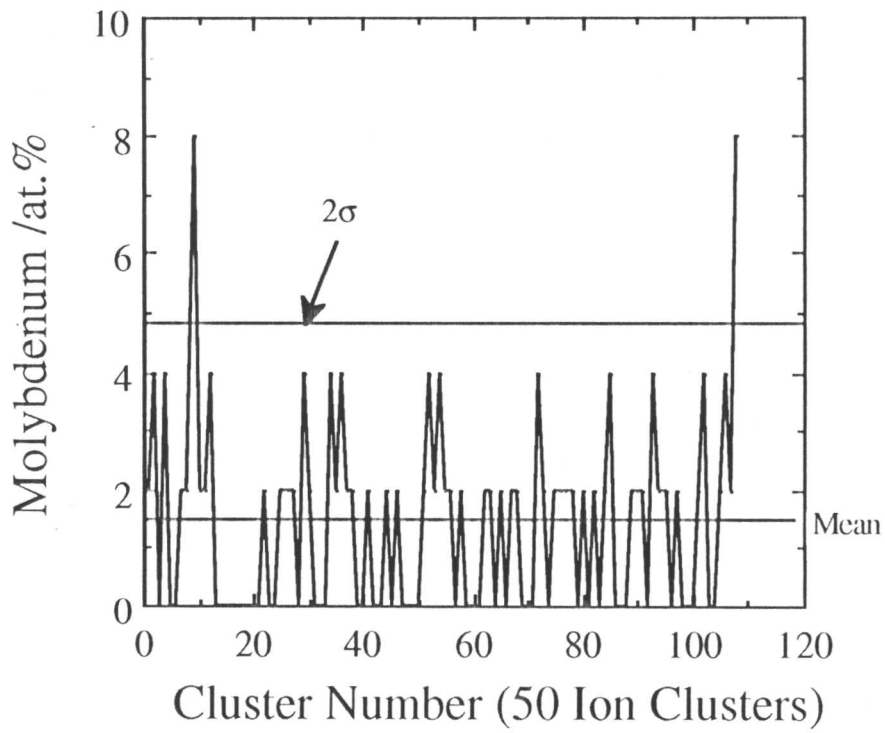


Fig. 6.3: The composition profile of molybdenum as a function of depth.

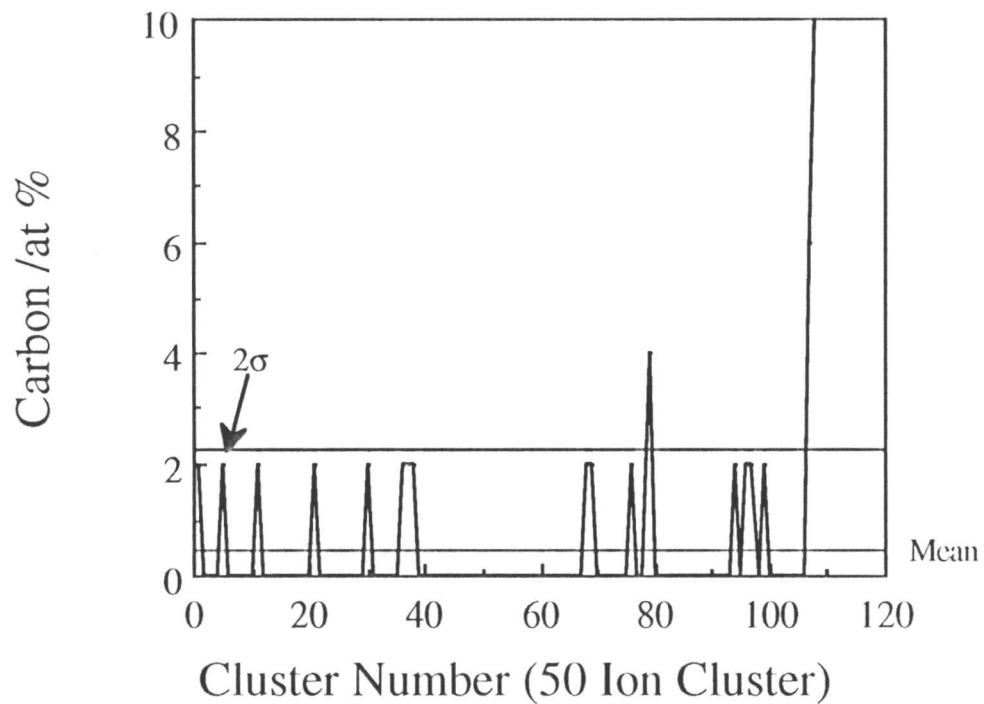


Fig. 6.4: The composition profile of carbon as a function of depth.

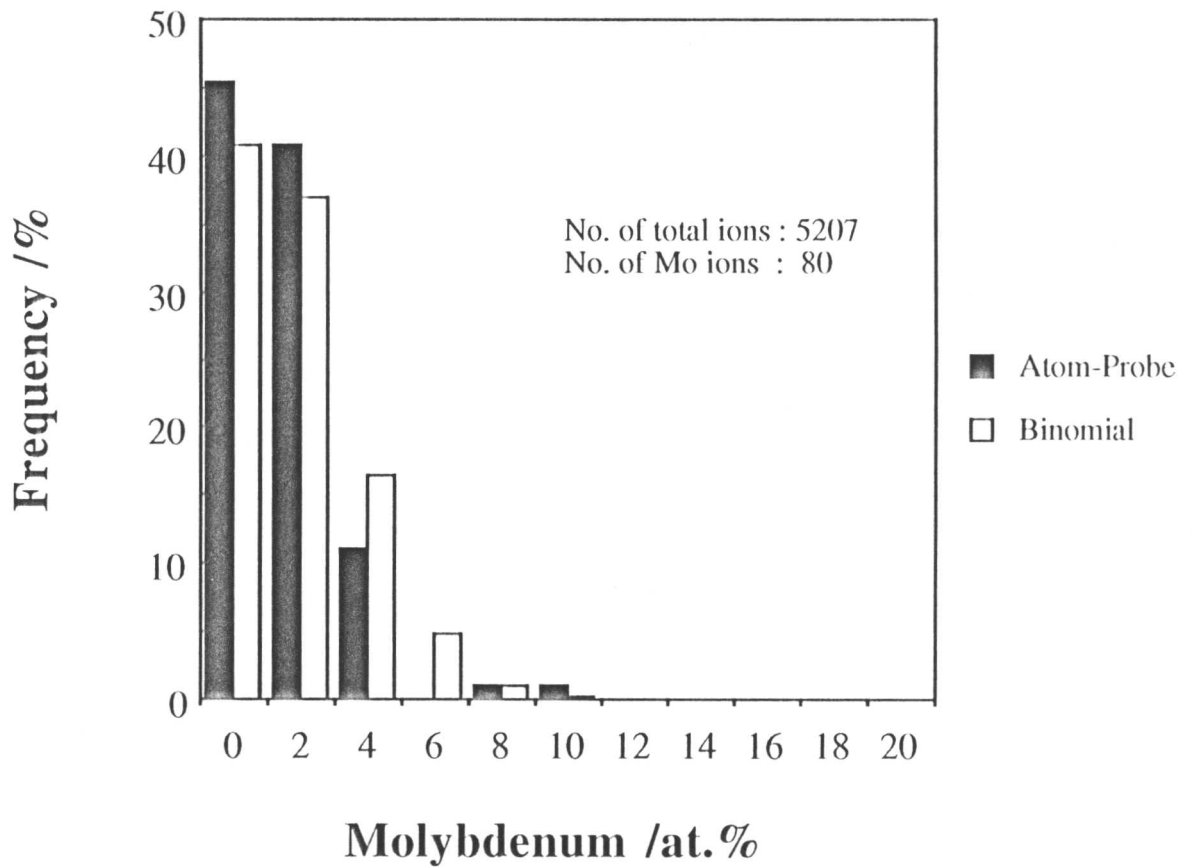
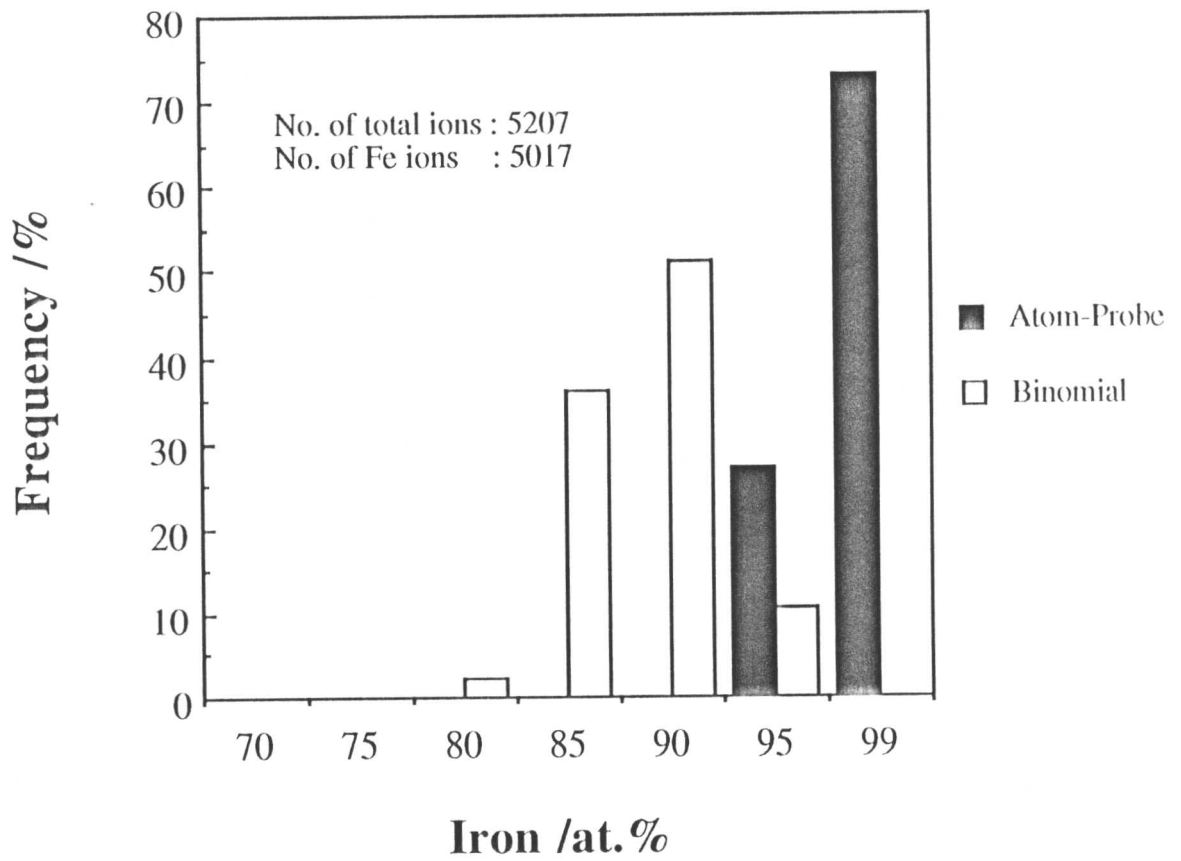


Fig. 6.5: Frequency distribution curves for iron and molybdenum.

---

## Chapter 7

# THE EFFECT OF TITANIUM ON THE MICROSTRUCTURE OF STEEL WELDS

---

### 7.1 Introduction

This investigation describes the possible role of titanium on the microstructure and mechanical properties of multipass steel weld deposits which in some cases also contain molybdenum. Many researchers have found that a microstructure which initially contains little acicular ferrite, can on the addition of titanium in the flux or welding wire, become acicular ferrite dominated [Tarashima and Hart, 1980; Pargeter 1981; Bialy, 1983; Suzuki *et al.*, 1985; Es-Souni *et al.*, 1991]. It is well known that acicular ferrite is generally tougher than other constituents such as allotriomorphic ferrite and Widmanstätten ferrite [Levine *et al.*, 1977; Grong and Matlock, 1986; Abson and Pargeter, 1986].

It has been claimed that X-ray analysis of inclusions in welds showed peaks characteristic of TiN [Thewlis, 1989; Watanabe *et al.*, 1983]. Lau *et al.* (1987) assumed that the titanium is in the form of  $\text{TiO}_2$  whereas Klucken and Grong (1989) assumed it to be combined as  $\text{Ti}_2\text{O}_3$ . Abson (1987) on the other hand, assumes that in weld deposits, the titanium oxide is TiO. Whatever the actual case, it is found that steel containing the titanium rich oxide particles is also rich in acicular ferrite, while the steel containing nitride particles can be devoid of any acicular ferrite [Homma *et al.*, 1986].

The purpose of the work presented here was to confirm the titanium effect in the presence of a large concentration of molybdenum. Experiments like these are difficult in practice, so four alloys which are permutations of titanium and molybdenum have been studied in order to ensure the titanium effect with and without molybdenum.

## 7.2 Experimental Procedure

Optical and SEM microstructural analysis were performed on polished specimens etched in nital, before examining the inclusions using transmission electron microscopy. The chemical compositions of the experimental alloys are shown in Table 7.1. A thermomechanical simulator was also used to study the austenitization behaviour for the Fe-1Mo-Ti wt.%. The specimen preparation techniques have been discussed in Chapter 2. Transmission electron microscopy was employed to examine the morphology and compositions of the inclusions in the weld metals, using carbon extraction replicas. The carbon extraction replicas were examined in a Phillips EM 400T transmission electron microscope operated at 120 kV, using a beryllium specimen holder. X-ray chemical data of inclusions were analysed using the LINK RTS2 FLS program. The hardness was measured on a Vicker's hardness machine. The welding procedure has been discussed in Chapter 2.

Table 7.1: Weld metal composition in wt.%.

Alloy	C	Si	Mn	Ni	Mo	Cr	V	Ti	O	N
Fe-1Mo-Ti wt.%	0.072	0.29	1.06	0.03	1.18	0.035	0.004	0.0025	0.0396	0.0073
Fe-1Mo wt.%	0.078	0.34	1.09	0.028	1.16	0.036	0.003	0.0005	0.0391	0.0083
Fe-0Mo-Ti wt.%	0.084	0.26	1.10	0.03	0.005	0.036	0.001	0.0025	0.0432	0.0075
Fe-0Mo wt.%	0.079	0.30	1.05	0.027	0.005	0.035	0.001	0.0005	0.0435	0.0060

## 7.3 Results and Discussion

### 7.3.1 Microstructural Observations

The results of the metallographic quantitative analysis of the phases present in the weld metals are summarised in Table 7.2. A point count method was used as discussed in chapter 3. The error in the determination of volume fractions is approximately  $\pm 4\%$ . Experiments to confirm or deny a titanium effect are difficult in arc welds because they usually contain so many other impurities. In addition, the minimum level of titanium needed to induce acicular ferrite is not known. However, Fig. 7.1 compares the Fe-0Mo wt.% and Fe-0Mo-Ti wt.% samples; it is clear

that there is substantially more of acicular ferrite in the titanium containing weld. The design of the welds has clearly worked in demonstrating a perceptible titanium effect. These observations are confirmed by the quantitative data presented in Table 7.2.

A further interesting observation is that in the absence of titanium, both allotriomorphic ferrite and Widmanstätten ferrite are able to grow to larger fractions. This shows a positive role of titanium in the sense that the intragranular formation of acicular ferrite prevents the further formation of allotriomorphic ferrite and Widmanstätten ferrite. It is not simply the case that the acicular ferrite forms in the austenite that remains untransformed after the allotriomorphic ferrite and Widmanstätten ferrite have stopped growing.

Fig. 7.2 shows what titanium can do in the presence of molybdenum. It is clear that molybdenum has drastically reduced the grain boundary nucleated phases allotriomorphic ferrite and Widmanstätten ferrite, but that this reduction is larger in the presence of titanium. This is exactly the effect observed in the molybdenum-free welds. Thus, titanium in very small quantities can virtually eliminate the bainitic microstructure. The microstructure in the reheated zones also show similar trends (Fig. 7.3).

An important point to note is that the titanium can only be effective in its competition with grain boundary nucleated bainite if the latter can not nucleate easily [Babu and Bhadeshia, 1991]. In Cr–Mo welds where allotriomorphic ferrite and Widmanstätten ferrite are completely absent, only bainite forms even in the presence of inclusions. However, if grain boundary nucleation is suppressed then acicular ferrite forms [Babu and Bhadeshia, 1991]. The fact that there is some allotriomorphic ferrite and Widmanstätten ferrite in the Fe–0Mo wt.% alloy means that bainite nucleation is difficult, so that a small addition of titanium permits acicular ferrite to form intragranularly without being swamped by grain boundary nucleated bainite.

### *7.3.2 Austenite Formation*

A thermomechanical simulator was used to study the austenitization behaviour for the Fe–1Mo–Ti wt.%. The specimens were heated to 1200 °C and quenched

Table 7.2: Microstructural constituents in the welds containing molybdenum.

ALLOY	Microstructural component in %			
	$\alpha$	$\alpha_w$	$\alpha_a$	$\alpha_b$
Fe-0Mo-Ti wt.%	20	30	45	5
Fe-0Mo wt.%	35	40	20	5
Fe-1Mo wt.%	5	5	30	60
Fe-1Mo-Ti wt.%	< 1	< 1	95	5

to ambient temperature. After this, they were first tempered at 650 °C for 60 minutes at the reaction temperature and then quenched to ambient temperature using helium gas. This was followed by continuous heating to 1200 °C at a variety of heating rates. The heating rates chosen were respectively 2, 8, 20, and 30 °C s<sup>-1</sup>. The specimens were again quenched to ambient temperature. The relative length change as a function of temperature at a heating rate of 2 °C s<sup>-1</sup> is shown in Fig. 7.4. The results (Table 7.3) show that there is at most a 30 °C difference in the  $Ac_1$  and  $Ac_3$  temperatures with increasing heating rates.

Table 7.3: Transformation temperatures observed during continuous heating experiments on the tempered martensite specimens.

Alloy	Tempering °C	Heating Rate °C s <sup>-1</sup>	$Ac_1$ °C	$Ac_3$ °C
Fe-1Mo-Ti wt.%	650	2	760	860
		8	780	880
		20	790	890
		30	790	890

### 7.3.3 Macrohardness Measurements

Macrohardness measurements on the as-deposited specimens of the experimental alloys are presented in Fig. 7.5. The Fe-1Mo-Ti wt.% has a lower hardness as compared to the Fe-1Mo wt.%. This small difference is difficult to explain but it is

speculated that bainite may be slightly harder than acicular ferrite since platelets growing in packets are constrained by each other and therefore may be finer. As expected, the hardness of the molybdenum-free welds was always lower than the alloys containing 1 wt.% molybdenum. The molybdenum additions produced a hardness difference of 50–60 HV5 in the top bead, and this occurred also in the upper half. In the lower part, a divergence occurred, repeated thermal cycling causing softening in the molybdenum free weld and hardening in the weld containing 1 wt.% molybdenum. All these effects are consistent with the work presented in Chapter 5. The hardness of the different zones of the weld deposits are presented in Fig. 7.6. The results show that the hardness of the reheated zones also show similar trends.

#### 7.3.4 Microanalysis

Two of the four welds [Fe–1Mo wt.% (Ti < 0.0005 wt.%) and Fe–1Mo–Ti wt.% (Ti ~ 0.0025 wt.%)] were studied further to check for any obvious differences in the inclusions. Transmission electron microscopy for inclusions of both the alloys are shown in Fig. 7.7. Comparison of inclusion compositions determined by TEM–EDX on the primary weld metal deposits are shown in Fig. 7.8. The low atomic number elements carbon, nitrogen and oxygen could not be determined. An overall increase in titanium content within the inclusions was observed with increasing titanium content of the weld metals. In the high titanium welds the majority of inclusions had a large fraction of titanium when compared against the titanium-free welds. The main elements in the inclusions were Al, Mn, Si, Ti. The results illustrate that all inclusions contain significant quantities of each element examined. Therefore it is found that the inclusions must be complex multiphase. Inclusions of varying shape and size were examined. Inclusions from the same area generally had the same main elements representing one type of inclusion composition, whereas inclusions from a different area of the weld could have different main elements.

## 7.4 Summary and Conclusions

The effect of titanium has been investigated on the as-deposited weld metals which in some cases also contain molybdenum. It is confirmed that molybdenum drastically reduces the grain boundary nucleated phases allotriomorphic ferrite and Widmanstätten ferrite, but that this reduction is larger in the presence of titanium.

A further interesting observation is that in the absence of titanium, both allotriomorphic ferrite and Widmanstätten ferrite are able to grow to larger fractions. This shows a positive role of titanium in the sense that the intragranular formation of acicular ferrite *prevents* the further formation of allotriomorphic ferrite and Widmanstätten ferrite by hard impingement.

An important point to note is that titanium in very small quantities in the presence of molybdenum can virtually eliminate the bainitic microstructure. The microstructure in the reheated zones also show similar trends.

Inclusion chemistry has also been examined. It is found that in the high titanium welds the majority of inclusions had a large fraction of titanium when compared against the titanium-free welds. However, the inclusions contain significant quantities of each element examined; therefore it is found that the inclusions must be complex multiphase.

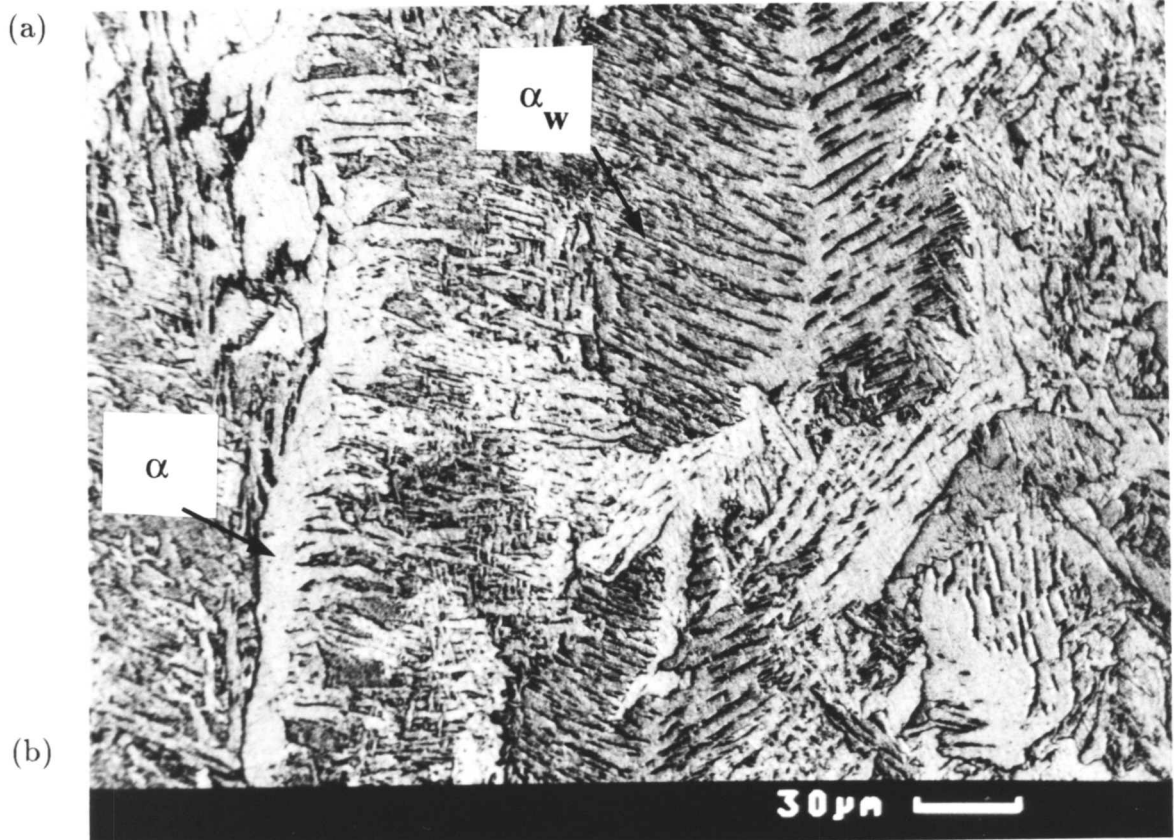
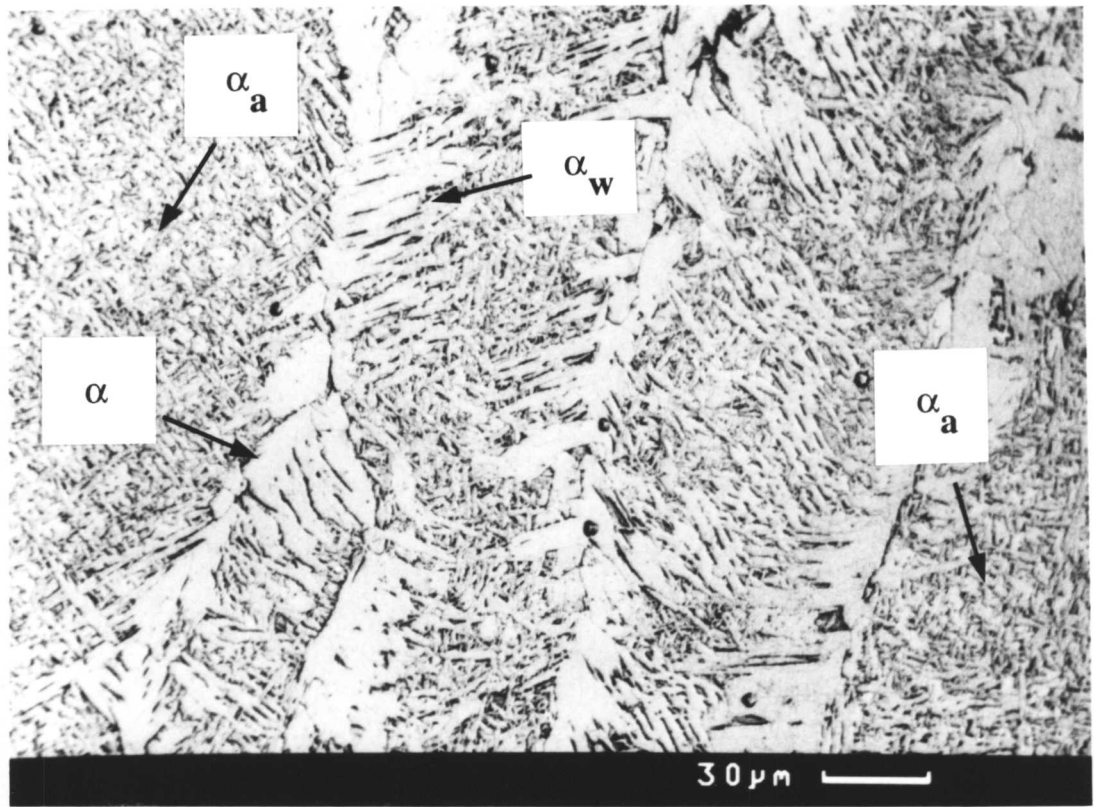
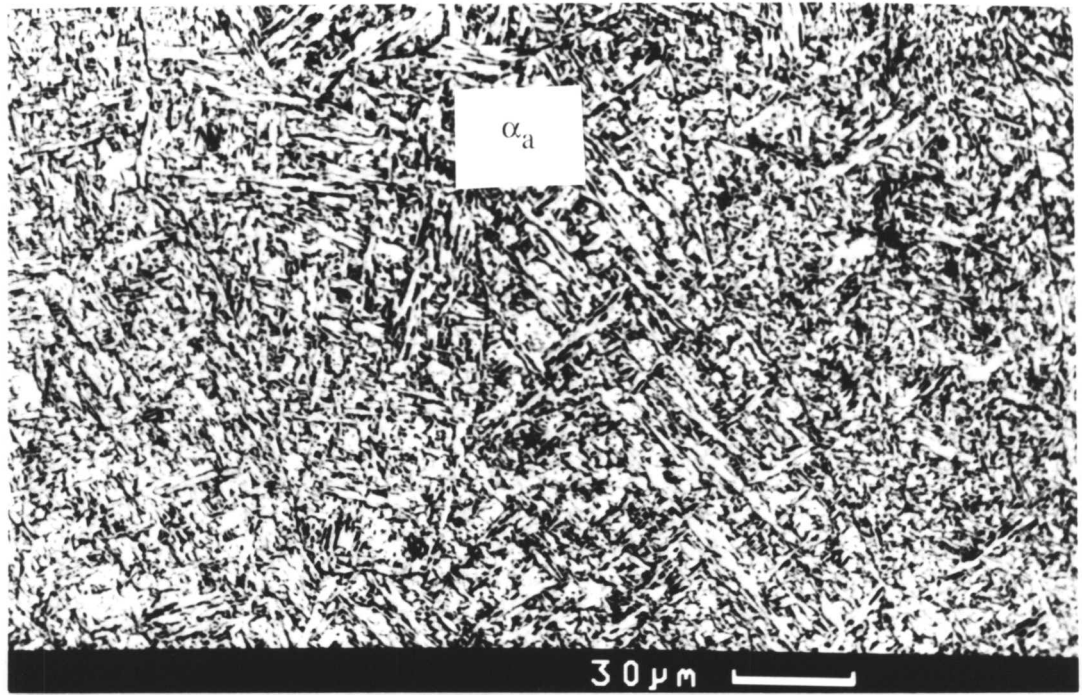
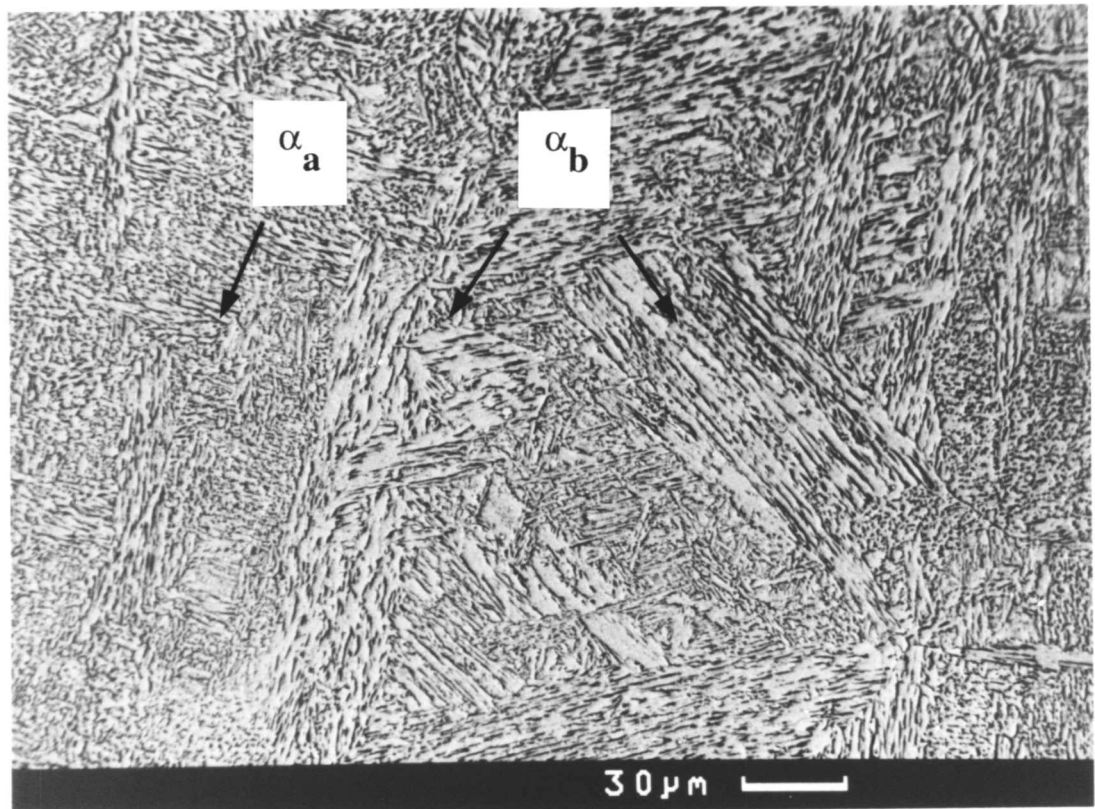


Fig. 7.1: SEM micrographs from the as-deposited microstructure. (a) Shows a mixture of allotriomorphic ferrite, Widmanstätten ferrite and acicular ferrite in the Fe-0Mo-Ti wt.%. (b) Illustrates a mixture of Widmanstätten ferrite and allotriomorphic ferrite in the Fe-0Mo wt.%.

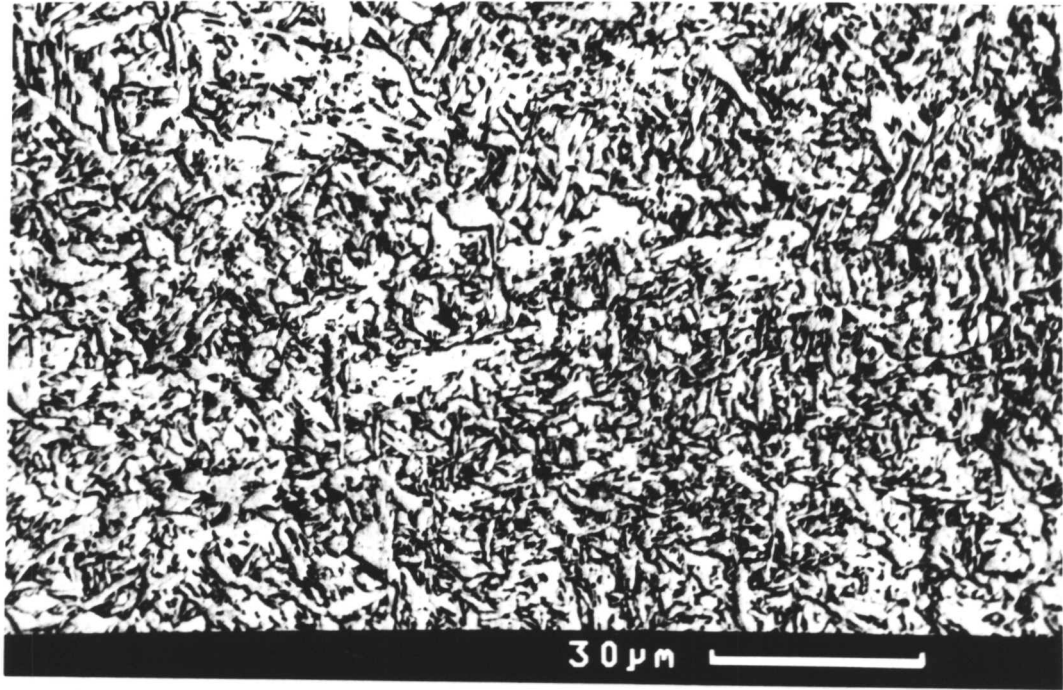


(a)

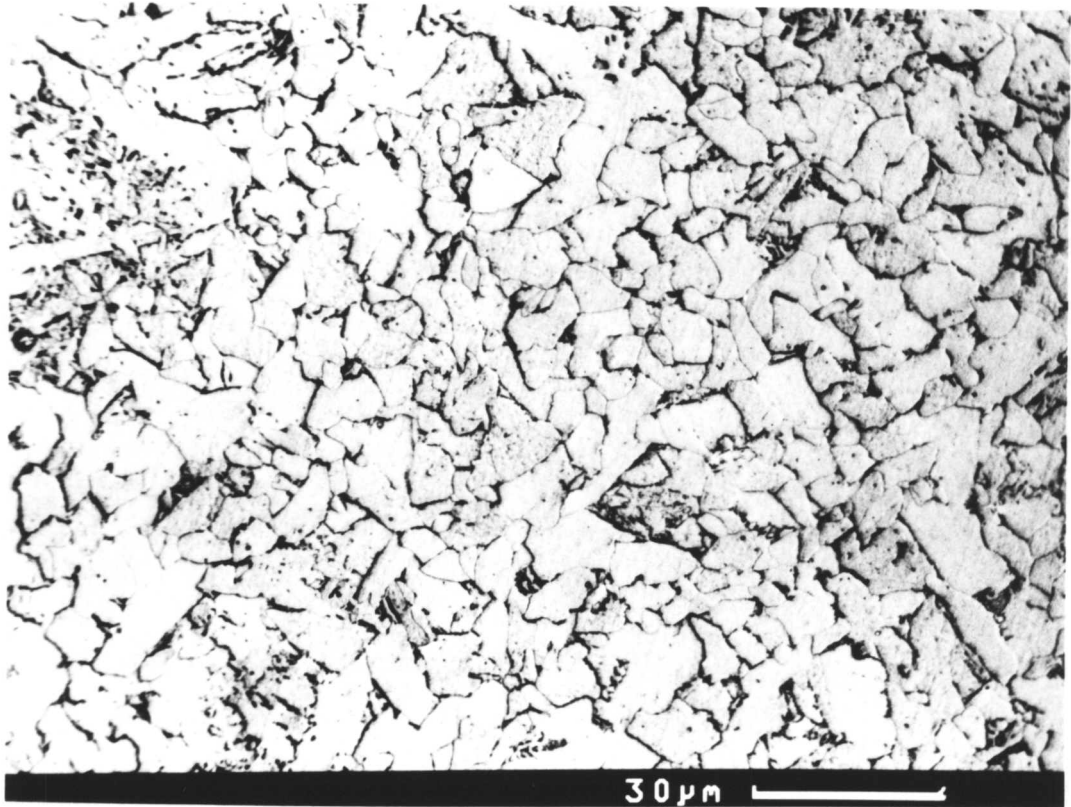


(b)

Fig. 7.2: SEM micrographs from the as-deposited microstructure. (a) Shows acicular ferrite in the Fe-1Mo-Ti wt.%. (b) Illustrates a mixture of bainite and a little acicular ferrite in the Fe-1Mo wt.%.



(a)



(b)

Fig. 7.3: SEM micrographs showing microstructure of the reheated zone in weld metal deposits. (a) Fe-1Mo-Ti wt.% (b) Fe-0Mo-Ti wt.%.

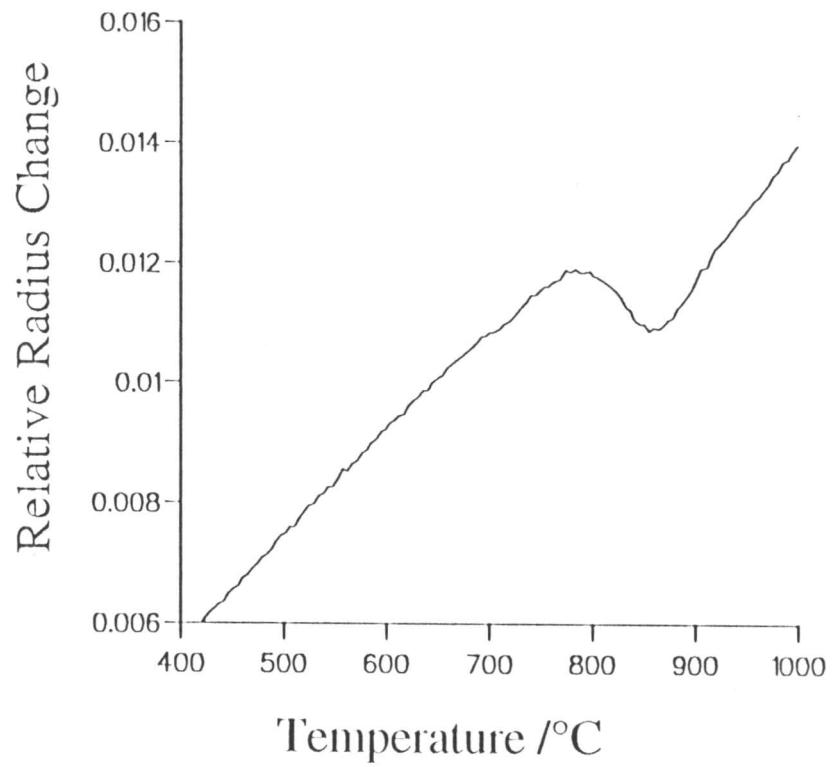


Fig. 7.4: The relative length change vs temperature at a heating rate of  $2^{\circ}\text{C s}^{-1}$ .

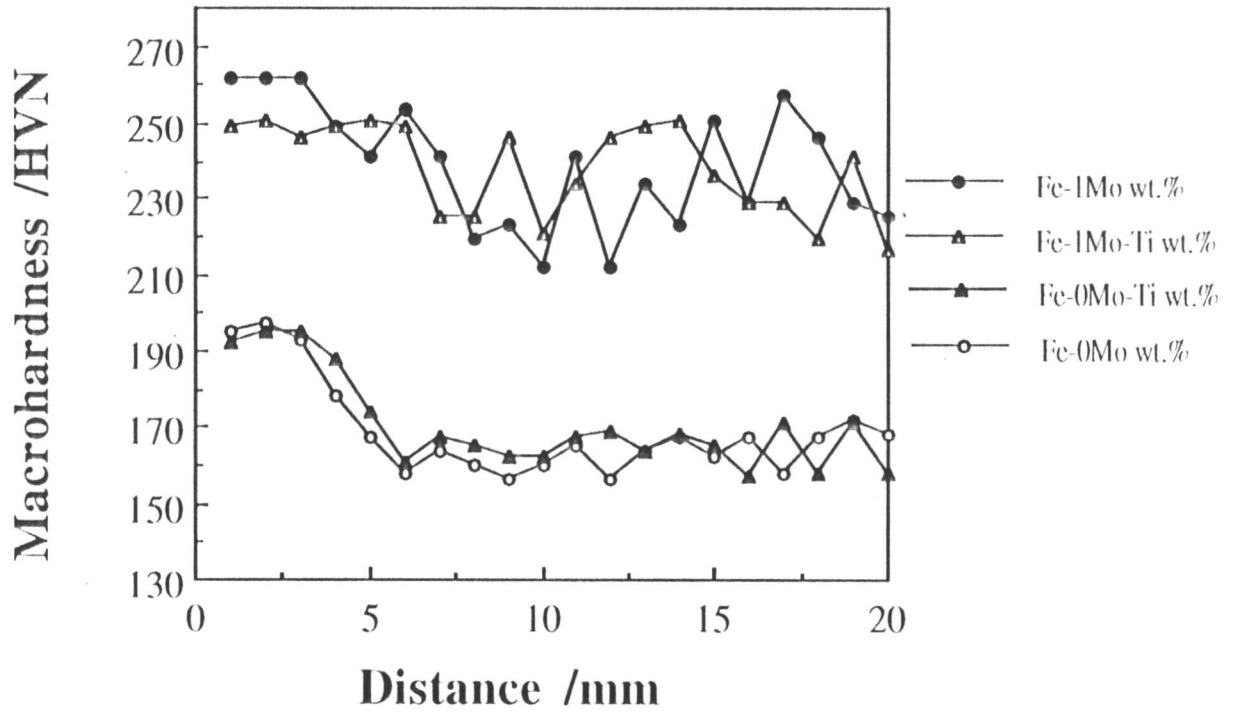


Fig. 7.5: Typical hardness variations across a multipass weld metal regions.

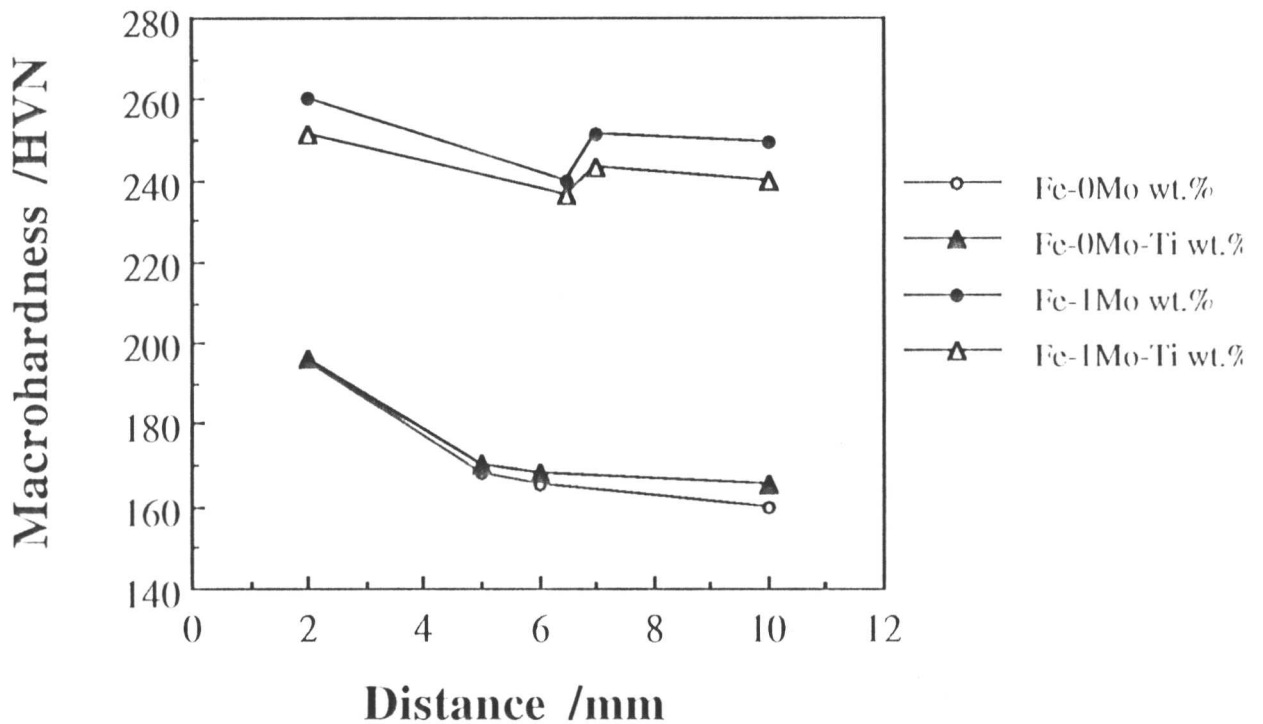
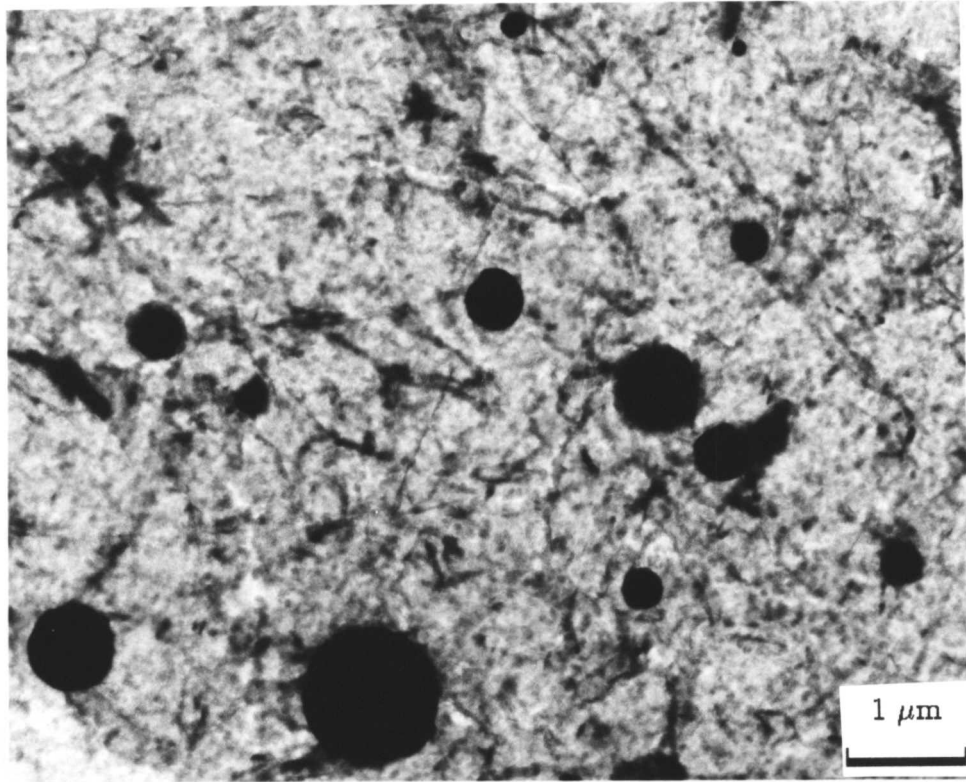
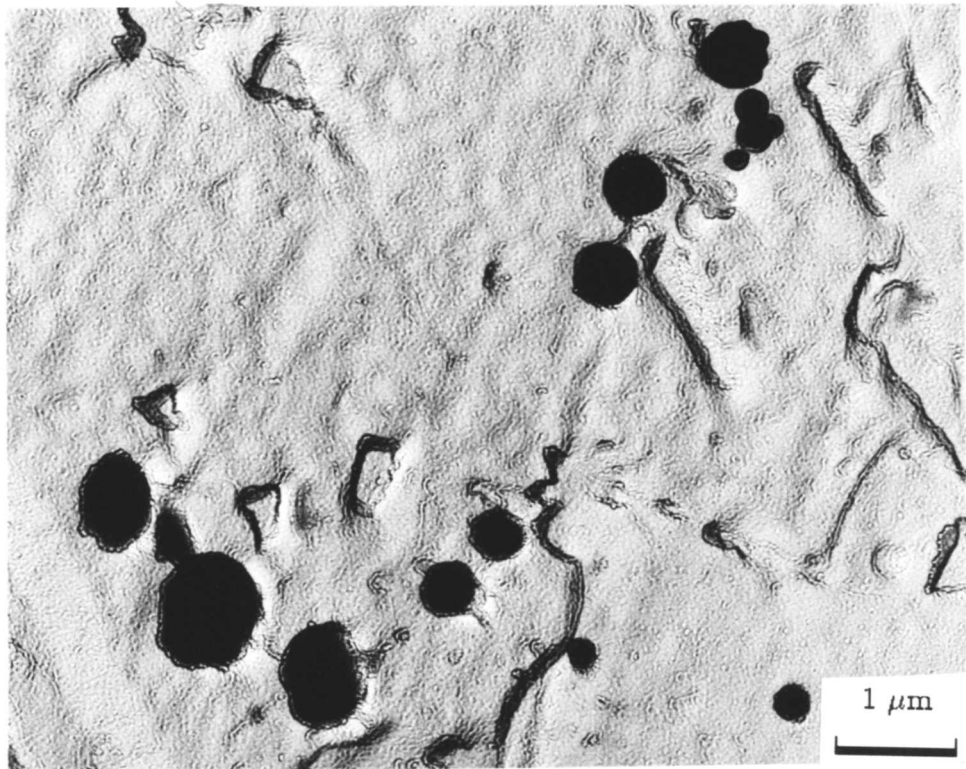


Fig. 7.6: The hardness of the different zones of the weld metal deposits.

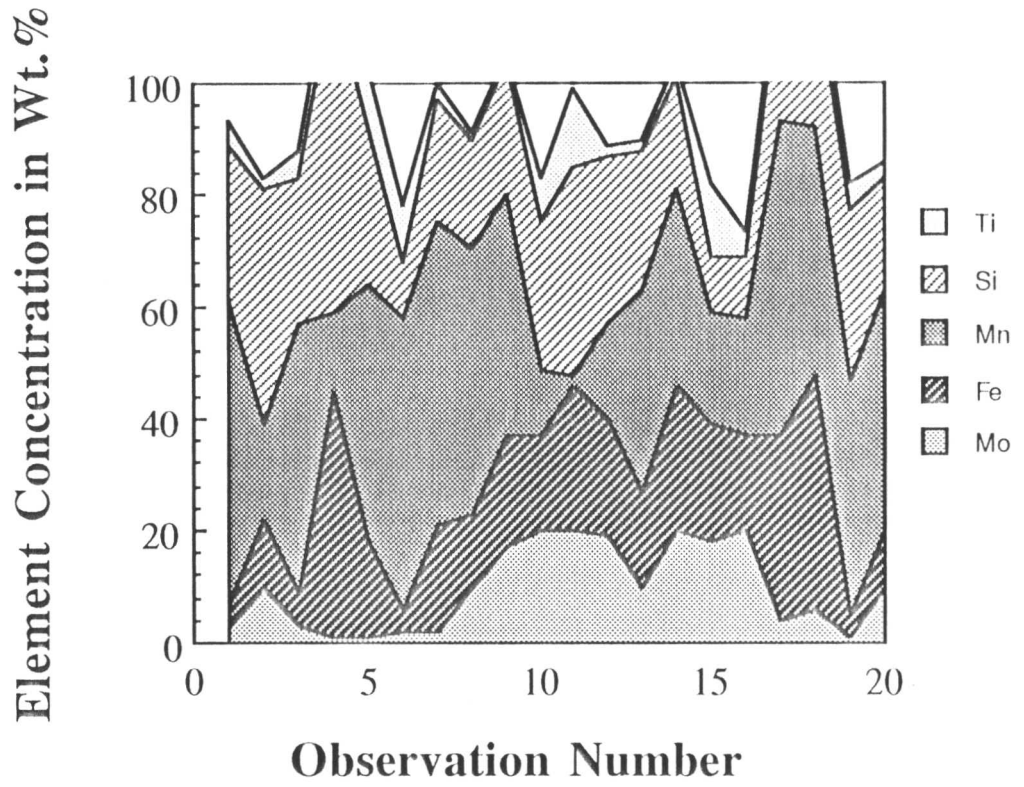


(a)

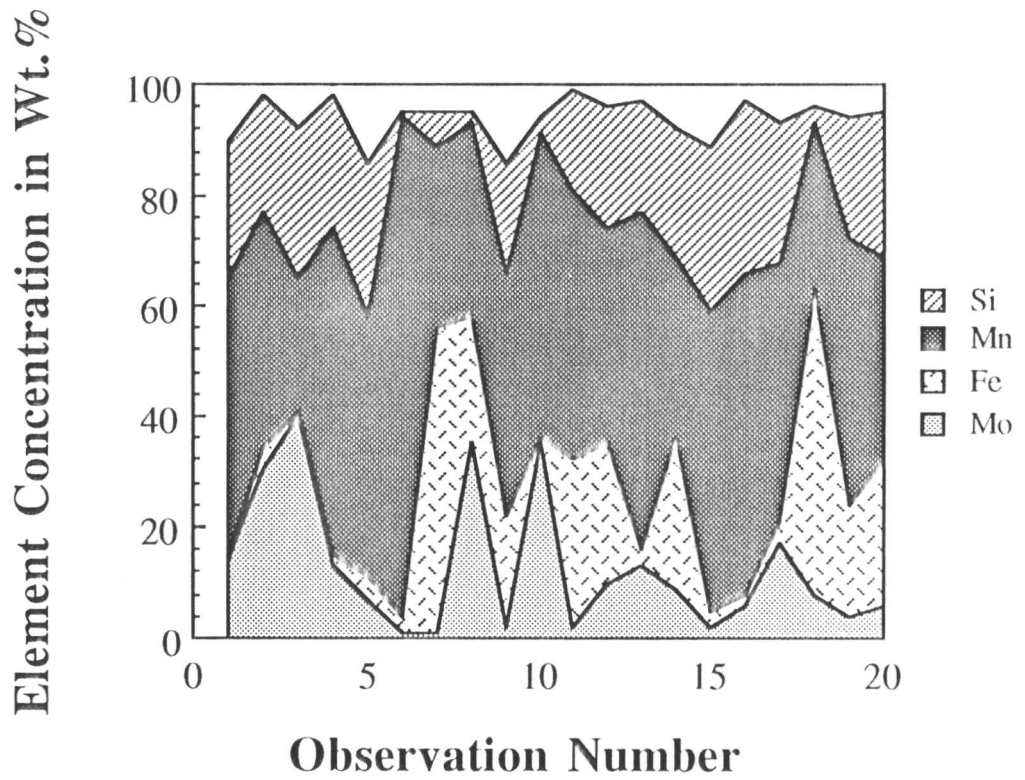


(b)

Fig. 7.7: Transmission electron micrographs showing different types of inclusions of the as-deposited weld metals. (a) Fe-1Mo-Ti wt.% (b) Fe-1Mo wt.%.



(a)



(b)

Fig. 7.8: Microanalytic data on inclusions of as-deposited weld metals. (a) Fe-1Mo-Ti wt.% (b) Fe-1Mo wt.%.

---

## Chapter 8

### SUGGESTIONS FOR FUTURE WORK

---

The effects that have been observed for molybdenum probably also exist for other strong carbide forming elements in steel welds, such as vanadium or to a lesser extent, chromium. There is some evidence (for example in the extensive characterisation experiments of Evans) to suggest that this is indeed the case.

Since secondary hardening depends both on the carbide former and the carbon, there is a need to systematically study the role of carbon so that a quantitative model can be developed for the enhanced strength and tempering resistance of such materials.

The atomic resolution experiments reported in this thesis are limited in scope and data. Further more extensive work needs to be carried out, not only to confirm the present observations in a more rigorous way, but also to study the time evolution of the clustering/precipitation phenomena.

## REFERENCES

- Abson, D. J., (1987)  
*Nonmetallic Inclusions in Ferritic Steel Weld Metals*, IIW-Doc. IX, pp. 1486–1487.
- Abson, D. J. and Pargeter, R. J., (1986)  
*Int. Met. Reviews*, **31**, pp. 141–194.
- Alberry, P. J. and Jones, W. K. C., (1977)  
*Met. Technol.*, **4**, pp. 557–566.
- Alberry, P. J. and Jones, W. K. C., (1982)  
*Met. Technol.*, **9**, pp. 419.
- Alberry, P. J., Brunstrom, R. R. L. and Jones, K. E., (1983)  
*Met. Technol.*, **10**, pp. 28–38.
- Ashby, M. F. and Easterling, K. E., (1982)  
*Acta Metall.*, **30**, pp. 1969–1978.
- Ashby, M. F. and Easterling, K. E., (1984)  
*Acta Metall.*, **32**, pp. 1935–1948.
- Babu, S. S. and Bhadeshia, H. K. D. H., (1991)  
*Mechanism of the Transition from Bainite to acicular ferrite*, Materials Transactions, Japan Institute of Metals.
- Baily, N., (1983)  
*Welding Inst.*, Res. Rep., 221.
- Bain, E. C. and Paxton, H. W., (1961)  
*The Alloying Elements in Steel, 2nd ed.*, American Society for Metals, Metals Park, Ohio, U.S.A.
- Baker, R. G. and Nutting, J., (1959)  
*Journal of the Iron and Steel Institute*, **192**, pp. 257–268.
- Bhadeshia, H. K. D. H., (1981a)  
*Acta Metallurgica*, **29**, pp. 1117–1130.
- Bhadeshia, H. K. D. H., (1981c)  
*Metal Science*, **15**, pp. 178–180.

- Bhadeshia, H. K. D. H., (1981d)  
*Metal Science*, **15**, pp. 175–177.
- Bhadeshia, H. K. D. H., (1982)  
*Metal Science*, **16**, pp. 159–165.
- Bhadeshia, H. K. D. H., (1987)  
*Bainite in Steel, Phase Transformation*, Institute of Metals, London, pp. 309–314.
- Bhadeshia, H. K. D. H., (1988)  
*CERL Report no. TPRD/L, 3224/R87*, pp. 5.
- Bhadeshia, H. K. D. H., (1989)  
*Int. Conf. on Trends in Welding Research*, Gatlingburg, U.S.A.
- Bhadeshia, H. K. D. H., (1990)  
*Int. Conf. on Metallurgy Welding and Qualification of Microalloyed (HSLA) Steel Weldments*, American Welding Society, pp. 1–35.
- Bhadeshia, H. K. D. H. and Christon, J. W., (1990)  
*Metallurgical Transactions A*, **21A**, pp. 767–797.
- Bhadeshia, H. K. D. H. and Edmonds, D. V., (1980)  
*Acta Metallurgica*, **28**, pp. 1265–1273.
- Bhadeshia, H. K. D. H., Svensson, L. –E. and Gretoft, B., (1985)  
*Acta Metallurgica*, **33**, pp. 1271–1283.
- Bhadeshia, H. K. D. H., Svensson, L. –E. and Gretoft, B., (1986a)  
*Prediction of Microstructure of Submerged–Arc line Pipe Welds.*, *International Conference on Welding and Performance of Pipelines*, Published by the Welding Institute, U.K.
- Bhadeshia, H. K. D. H., Svensson, L. –E. and Gretoft, B., (1986b)  
*Journal of Materials Science*, **21**, pp. 3947–3951.
- Bhadeshia, H. K. D. H. and Waugh, A. R., (1982)  
*Acta Metallurgica*, **30**, 775–784.
- Blavette, D. and Buchon, S., (1989)  
*Advanced Materials and Processes; Proceeding of the First European Conference, EUROMAT 1*, pp. 419–424.
- Brown, A. M. and Ashby, M. F., (1980)  
*Acta Metall.*, **28**, pp. 1085–1101.
- Calvo, F. A., Bently, K. P. and Baker, R. G., (1963)  
*Studies of the Welding Metallurgy of Steels*, BWRA. Abingdon, Cambridge, U.K.

- Cal, X. L., Garratt-Reed, A. J. and Owen, W. S., (1985)  
*Met. Trans.*, **16**, 543–557.
- Cochrane, R. C., (1982)  
*Int. Inst. Welding*, Doc. IX, 1248–1282.
- Christon, J. W. and Edmonds, D. V., (1984)  
*Proc. Int. Conf. on Phase Transformation in Ferrous Alloys*, Metals Park, Ohio, London.
- Davies, G. J. and Garland, J. G., (1975)  
*Int. Met. Reviews*, **20**, pp. 83–104.
- David, S. A. and Vitek, J. M., (1993)  
*Metallurgical Modelling of Weld Phenomena*, Institute of Metals, London, pp. 41–58.
- Dubé, C. A., (1948)  
*Ph.D thesis*, Carnegie inst. of technology, Pittsburgh, U.S.A.
- Easterling, K. E., (1983)  
*Introduction to the Physical Metallurgy of Welding*, Butterworths, London.
- Easterling, K. E., (1993)  
*Metallurgical Modelling of Weld Phenomena*, Institute of Metals, London, pp. 183–200.
- Es-Souni, M., Beaven, P. A. and Evans, G. M., (1991)  
*Orelikon Welding Ind.*, Res. Rep., II-A-Doc, 847.
- Evans, G. M., (1986)  
*The Effect of Molybdenum on the Microstructure and Properties of C-Mn all-Weld Metal Deposits*, IIW-Doc., II-A-666–86.
- Evans, G. M., (1988)  
*The Effect of Chromium on the Microstructure and Properties of C-Mn all-Weld Metal Deposits*, IIW-Doc., II-A-739–88.
- Garcia, C. I. and Deardo, A. J., (1981)  
*Met. Trans.*, **12**, 521–530.
- Grong, G. and Matlock, D. K., (1986)  
*Int. Met. Reviews*, **31**, pp. 27–48.
- Hillert, M., (1952)  
*Jernkontorets Ann*, **136**, pp. 25–37.
- Homma, R., (1974)  
*Trans. I. S. I. J*, **14**, 434–443.

- Homma, H., Ohkita, S., Matsuda, S. and Yamamoto, K., (1986)  
*Nippon Steel Corp.*, Res. rep., Japan.
- Holloman, H. J. and Jaffe, L. D., (1945)  
*Trans. AIME*, **162**, pp. 223–249.
- Hetherington, M. G. and Miller, M. K., (1987)  
*J. de Physique*, **48–C6**, pp. 559.
- Hetherington, M. G. and Miller, M. K., (1988)  
*J. de Physique*, **49–C6**, pp. 427.
- Irvine, K. J. and Pickering, F. B., (1960)  
*Journal of the Iron and Steel Insititute*, **194**, pp. 137–152.
- Ion, J. C., Easterling, K. E. and Ashby, M. F., (1984)  
*Acta Metall.*, **32**, pp. 1949–1962.
- Jaffe, L. D. and Gordon, E., (1957)  
*Trans. ASM*, **49**, pp. 359–371.
- Kar, R. J. and Todd, J. A., (1982)  
*Alloy Modification of Thick-Section  $2\frac{1}{4}$ Cr-1Mo steel*, ASTM Special Technical Publication 755, pp. 208–228.
- Kayali, E. S., Pacey, A. J. and Kerr, H. W., (1983)  
*J. Mat. Science*, **2**, 123–128.
- Kinoshita, S. and Ueda, T., (1974)  
*Trans. I. S. I. J.*, **14**, pp. 411–418.
- Klueh, R. L., (1974a)  
*J. Nucl. Mat.*, **54**, pp. 41–54.
- Klueh, R. L., (1974b)  
*J. Nucl. Mat.*, **54**, pp. 55–63.
- Kou, K., (1956)  
*Journal of the Iron and Steel Insititute*, **184**, pp. 258–268.
- Lau, T. W., Sadowsky, M. M., North, T. H. and Weartherly, G. C., (1987)  
*Welding Metallurgy of Structural Steel*, Metallurgical Society of AIME, 349–365.
- Law, N. C. and Edmonds, D. V., (1980)  
*Metallurgical Transactions*, **11A**, pp. 33–46.
- Lenel, U. R. and Honeycombe, R. W. K., (1984)  
*Metal Science*, **18**, pp. 201–205.

- Levine, E. and Hill, D. C., (1977)  
*Metallurgical Transactions*, **8A**, pp. 1453–1463.
- Lundin, C. D., Kelly, S. C., Menon, R., and Kruse, B. J., (1986)  
*Stress Rupture Behaviour of Post Weld Heat Treated  $2\frac{1}{4}$ Cr-1Mo Steel Weld Metal*,  
 WRC Bulletin, 315.
- Matsuda, S. and Okamura, Y., (1974)  
*Trans. I. S. I. J.*, **14**, 363–368.
- Matas, S. J. and Hehemann, R. F., (1961)  
*Trans. Met. Soc. AIME*, **221**, pp. 179–185.
- Mcgrath, J. T., Chandel, R. S., Orr, R. F. and Gianetto, J. A., (1989)  
*Canadian Metallurgical Quarterly*, **28**, pp. 75–83.
- Miller, M. K., (1987)  
*International Materials Reviews*. **32**, pp. 221–240.
- Miller, M. K. and Smith, G. D. W., (1989)  
*Atom Probe Microanalysis: Principles and Applications to Materials Problems*, Ma-  
 terials Research Society, U.S.A.
- MTDATA, (1988)  
*Metallurgical and Thermochemical Databank*, National Physical Laboratory, Ted-  
 dington, Middlesex, U.K.
- Musgen, B., (1985)  
*Metal Construction*, **17**, pp. 495–500.
- Pacey, A. J., Kayali, S. and Kerr, H. W., (1982)  
*Canadian Metallurgical Quarterly*, **21**, pp. 309–318.
- Pargeter, R. J., (1981)  
*Welding Inst.*, Res. Rep., 151.
- Papazian, J. M., (1972)  
*J. Microsc.*, **95**, pp. 429.
- Plichita, M. R. and Aaronson, H. I., (1974)  
*Metallurgical Transactions*, **5A**, pp. 2611–2613.
- Pilling, J., Ridley, N. and Gooch, D. J., (1983)  
*Metallurgical Transactions*, **14A**, pp. 1443–1449.
- Reed, R. C. and Bhadeshia, H. K. D. H., (1989)  
*Complete Reaustenitisation in Multirun Steel Weld Deposits*, Presented to the 2nd  
 International Conference on Trends in Welding Research, Gatlingburg, Tennessee,  
 U.S.A.

- Reed, R. C., (1990)  
*Ph.D Thesis*, University of Cambridge, U.K.
- Raiter, V. and Gonzalez, J. C., (1988)  
*Canadian Metallurgical Quarterly*, **28**, pp. 179–185.
- Rodrigues, P. and Rogerson, J. H., (1977)  
*Low Carbon Structural Steels for the Eighties*, Institute of Metals, London, pp. 33–40.
- Savage, W. F., (1980)  
*Welding in the World*, **18**, pp. 89–114.
- Savage, W. F. and Aaronson, A. H., (1966)  
*Welding Journal*, **45**, pp. 85–90.
- Savage, W. F., Lundin, C. D. and Aaronson, A. H., (1965)  
*Welding Journal*, **9A**, pp. 999–1008.
- Seal, A. K. and Honeycombe, R. W. K., (1958)  
*Journal of the Iron and Steel Institute*, **188**, pp. 9–15.
- Sha, W., Cerezo, A. and Smith, G. D. W., (1990)  
*Surface Science*, **246**, pp. 457–461.
- Sha, W., Smith, G. D. W. and Cerezo, A., (1992)  
*Surface Science*, **266**, pp. 378–384.
- Shiflet, G. J., Bradley, J. R. and Aaronson, H. I., (1978)  
*Metallurgical Transactions A*, **9A**, pp. 999–1008.
- Smith, E. and Nutting, J., (1957)  
*Journal of the Iron and Steel Institute*, **187**, pp. 314–329.
- Souza, M. M., Guimaraes, J. R. C. and Chawala, K. K., (1982)  
*Met. Trans.*, **13**, 575.
- Speich, G. R. and Szirmai, A., (1969)  
*Trans. of Met. Soc. AIME*, **245**, 1063–1074.
- Speich, G. R., Demarest, V. A. and Miller, R. L., (1981)  
*Met. Trans.*, **12**, 1419–1428.
- Speich, G. R. and Leslie, W. C., (1972)  
*Metallurgical Transactions*, **3**, pp. 1043–1054.
- Stark, I., Smith, G. D. W., (1987)  
*J. Phys.*, **48-C6**, pp. 447–452.

- Stark, I., Smith, G. D. W. and Bhadeshia, H. K. D. H., (1990)  
*Metallurgical Transactions*, **21A**, pp. 837–844.
- Strangwood, M. and Bhadeshia, H. K. D. H., (1987a)  
*The Mechanism of Acicular Ferrite Transformation in Steel Weld Deposits*, Proc. Conf. on Advances in Welding Science and Technology, ASM international, Ohio, U.S.A.
- Strangwood, M. and Bhadeshia, H. K. D. H., (1987c)  
*Proc. Int. Conf. on Welding Metallurgy of Structural Steel*, AIME, Pennsylvania, Edited by J. Y. Koo, pp. 495–504.
- Sugden, A. A. B. and Bhadeshia, H. K. D. H., (1988)  
*Metallurgical Transactions A*, **19A**, pp. 1597–1602.
- Suzuki, M., Kunisada, Y. and Watanabe, I., (1985)  
*Nippon Kokan Res. Cent.*, II W-Doc, 1043–1085.
- Svensson, L. -E. and Bhadeshia, H. K. D. H., (1988)  
*The Design of Submerged Arc Weld Deposits for High Strength Steels*, Proc. of the Vienna Conference of the International Institute for Welding, Published by Pergamon Press, Oxford.
- Svensson, L. -E., Bhadeshia, H. K. D. H. and Greftoft, B., (1986)  
*Scandinavian Journal of Metallurgy*, **15**, pp. 97-103.
- Takahashi, M. and Bhadeshia, H. K. D. H., (1990)  
*Mater. Sci. Technol.*, **6**, pp. 592–603.
- Terashima, H. and Hart, P. H. M., (1980)  
*Welding Inst.*, Res. Rep., 27.
- Thewlis, G., (1989)  
*Joining and Materials*, **1**, pp. 25–31.
- Thomson, R. C., (1990)  
*Ph.D Thesis*, University of Cambridge, U.K.
- Thomson, R. C. and Bhadeshia, H. K. D. H., (1991)  
*Atom Probe and STEM Investigation*, Appl. Surface Science, in Press.
- Topping, J, (1961)  
*Errors of Observation and Their Treatment*, The Institute of Physics and The physical society, U.K.
- Tsong, T. T., Mclane, S. B., Ahmad, M. and Wu, C. S., (1982)  
*J. Appl. Phy.*, **53**, pp. 4180.
- Underwood, E. E., (1970)  
*Scandinavian Journal of Metallurgy*, **2**, pp. 177–182.

- Vitek, J. M., Packan, N. H. and David, S. A., (1986)  
*Proc. Int. Conf. on Trends in Welding Research*, ASM, Ohio, pp. 203–208.
- Wada, T. and Biss, V. A., (1983)  
*Metallurgical Transactions*, **14A**, pp. 845–855.
- Wada, T. and Eldis, G. T., (1982)  
*Transformation Characteristics of  $2\frac{1}{4}$ Cr-1Mo steel*, ASTM, Special Technical Publication 755, pp. 343–360.
- Watanabe, S. and Kunitake, T., (1976)  
*Trans. I. S. I. J.*, **16**, 28–35.
- Watanabe, I. and Kojima, T., (1983)  
*Welding Inst.*, Res. Rep., 1.
- Waugh, A. R., Richardson, C. H. and Jenkins, R., (1992)  
*Surface Science*, **266**, pp. 501–505.
- Weast, R. C., (1976–1977)  
*Hand Book of Chemistry and Physics*, 57 ed., F63–71, Cleveland, OH, CRC Press.
- Widgrey, D. J., (1975)  
*Welding Journal*, **3**, pp. 57.
- Woodhead, J. H. and Quarrel, A. G., (1965)  
*Journal of the Iron and Steel Institute*, **203**, pp. 605–620.
- Yang, J. R. and Bhadeshia, H. K. D. H., (1987a)  
*Thermodynamics of the Acicular Ferrite Transformation in Alloy-Steel Weld Deposits*, Proc. Conf. on Advances in Welding Science and Technology ASM International, pp. 209–213.
- Yang, J. R. and Bhadeshia, H. K. D. H., (1987b)  
*Int. Conf. on Welding of Structural Steel*, The Metallurgical Society of AIME, Warrendale, Pennsylvania, Edited by J. Y. Koo, pp. 549–563.
- Yang, J. R. and Bhadeshia, H. K. D. H., (1989)  
*Materials Science and Technology*, **5**, pp. 93–97.
- Yang, J. R. and Bhadeshia, H. K. D. H., (1990)  
*Materials Science and Engineering*, **A118**, pp. 155–170.
-